1988-09

The sea breeze circulation during the Land Sea Breeze Experiment (LASBEX) in central California.

Fagan, Michael.

https://hdl.handle.net/10945/23384

NAVAL POSTGRADUATE SCHOOL
Monterey, California

THESIS

THE SEA BREEZE CIRCULATION DURING THE LAND SEA BREEZE EXPERIMENT (LASBEX) IN CENTRAL CALIFORNIA

by

Michael Fagan

September 1988

Thesis Advisor William J. Shaw

Unclassified

ecurity classification of this page

REPORT DOCUMENTATION PAGE

1a Report Security Classification Unclassified

1b Restrictive Markings

2a Security Classification Authority

2b Declassification/Downgrading Schedule

3 Distribution/Availability of Report
Approved for public release; distribution is unlimited.

4 Performing Organization Report Number(s)

5 Monitoring Organization Report Number(s)

6a Name of Performing Organization
Naval Postgraduate School

6b Office Symbol *(if applicable)* 35

7a Name of Monitoring Organization
Naval Postgraduate School

6c Address *(city, state, and ZIP code)*
Monterey, CA 93943-5000

7b Address *(city, state, and ZIP code)*
Monterey, CA 93943-5000

8a Name of Funding/Sponsoring Organization

8b Office Symbol *(if applicable)*

9 Procurement Instrument Identification Number

8c Address *(city, state, and ZIP code)*

10 Source of Funding Numbers

Program Element No	Project No	Task No	Work Unit Accession No

11 Title *(include security classification)* THE SEA BREEZE CIRCULATION DURING THE LAND SEA BREEZE EXPERIMENT (LASBEX) IN CENTRAL CALIFORNIA

12 Personal Author(s) Michael Fagan

13a Type of Report	13b Time Covered	14 Date of Report *(year, month, day)*	15 Page Count
Master's Thesis	From To	September 1988	140

16 Supplementary Notation The views expressed in this thesis are those of the author and do not reflect the official policy or position of the Department of Defense or the U.S. Government.

17 Cosati Codes

Field	Group	Subgroup

18 Subject Terms *(continue on reverse if necessary and identify by block number)* Land-Sea Breeze, LASBEX, Lidar, Sodar.

19 Abstract *(continue on reverse if necessary and identify by block number)*

The sea breeze circulation was investigated using a combination of acoustic doppler sodar, doppler lidar and conventional observations in central California on the coast of Monterey Bay in September 1987. The study was called LASBEX (Land Sea Breeze EXperiment) and used the combined effort and resources of the Naval Postgraduate School (NPS), NOAA Wave Propagation Lab (WPL) and Naval Environmental Prediction Research Facility (NEPRF).

A monostatic three-axis phased-array doppler sodar was able to detect the various features of the sea breeze front, which has many of the characteristics of a gravity head current produced in laboratory experiments, such as the longitudinal vortex, lobe and cleft structure, and strong regions of turbulence and convergence. Profiles of the wind field and its component variances were generated every five minutes. Vertical velocities up to 1.0 m/s were detected in the updraft region at the front. Vertical velocity fields were used to derive the horizontal divergence associated with the sea breeze and values of convergence in the range of $4 \times 10^{-3} s^{-1}$ and greater were calculated. These are believed to be more accurate values than any found in previous sea breeze studies.

Doppler lidar radial velocity information was useful in mapping the various layers and wind structure of the sea breeze. The wind field of the sea breeze seen by the lidar was compared with the sodar. The results of this comparison showed that the sodar was well suited to investigate features under 600 meters in height, such as the updraft region behind the front and the variance of the wind, whereas the lidar was better at describing the larger scale flow, such as the return flow of the sea breeze, the convergence zone along the sea breeze front and prevailing synoptic winds. Together, these instruments gave a comprehensive and complete description of the sea breeze frontal structure, evolution and movement.

20 Distribution/Availability of Abstract
☒ unclassified/unlimited ☐ same as report ☐ DTIC users

21 Abstract Security Classification
Unclassified

22a Name of Responsible Individual	22b Telephone *(include Area code)*	22c Office Symbol
William J. Shaw	(408) 646-3430/2044	63SR

DD FORM 1473.84 MAR

83 APR edition may be used until exhausted
All other editions are obsolete

security classification of this page

Unclassified

The Sea Breeze Circulation during the Land Sea Breeze Experiment (LASBEX) in Central California

by

Michael Fagan
Lieutenant, United States Navy
B.S., United States Naval Academy, 1981

Submitted in partial fulfillment of the
requirements for the degree of

MASTER OF SCIENCE IN METEOROLOGY AND OCEANOGRAPHY

from the

NAVAL POSTGRADUATE SCHOOL
September 1988

ABSTRACT

The sea breeze circulation was investigated using a combination of acoustic doppler sodar, doppler lidar and conventional observations in central California on the coast of Monterey Bay in September 1987. The study was called LASBEX (Land Sea Breeze EXperiment) and used the combined effort and resources of the Naval Postgraduate School (NPS), NOAA Wave Propagation Lab (WPL) and Naval Environmental Prediction Research Facility (NEPRF).

A monostatic three-axis phased-array doppler sodar was able to detect the various features of the sea breeze front, which has many of the characteristics of a gravity head current produced in laboratory experiments, such as the longitudinal vortex, lobe and cleft structure, and strong regions of turbulence and convergence. Profiles of the wind field and its component variances were generated every five minutes. Vertical velocities up to 1.0 m/s were detected in the updraft region at the front. Vertical velocity fields were used to derive the horizontal divergence associated with the sea breeze and values of convergence in the range of $4 \times 10^{-3} s^{-1}$ and greater were calculated. These are believed to be more accurate values than any found in previous sea breeze studies.

Doppler lidar radial velocity information was useful in mapping the various layers and wind structure of the sea breeze. The wind field of the sea breeze seen by the lidar was compared with the sodar. The results of this comparison showed that the sodar was well suited to investigate features under 600 meters in height, such as the updraft region behind the front and the variance of the wind, whereas the lidar was better at describing the larger scale flow, such as the return flow of the sea breeze, the convergence zone along the sea breeze front and prevailing synoptic winds. Together, these instruments gave a comprehensive and complete description of the sea breeze frontal structure, evolution and movement.

TABLE OF CONTENTS

I. INTRODUCTION 1

A. GENERAL DESCRIPTION 1

B. MOTIVATION FOR THE STUDY OF LAND-SEA BREEZE 2

C. PREVIOUS STUDIES 3

D. LAND-SEA BREEZE EXPERIMENT (LASBEX) 4

II. DESCRIPTION OF EXPERIMENT 6

A. LOCATION OF THE EXPERIMENT 6

B. ACOUSTIC DOPPLER SODAR 8

C. DOPPLER LIDAR 8

D. SURFACE MEAUREMENTS 9

E. SYNOPTIC SITUATION BETWEEN 16-30 SEPTEMBER 1987 9

III. DATA AND ANALYSIS 13

A. SODAR THEORY 13

1. Basic Sodar Theory and Turbulence in the Inertial Subrange 13

a. Thermal Structure 14

b. Velocity Structure 15

B. LIDAR THEORY 17

C. SODAR CROSS SECTIONS 18

1. Time-Height Cross Sections 18

D. DERIVED DATA 18

E. ANALYSIS OF TIME-HEIGHT CROSS SECTIONS 19

1. Wind Direction 19

a. Wind Direction Gradients and Onset of Sea Breeze 19

b. Height and Duration of the Sea Breeze 23

c. Slope of Sea Breeze Fronts 24

2. Wind Speed 27

a. Synopsis of Wind Speed Data During LASBEX 27

3. Wind speed after frontal passage 28

4. Vertical Velocity Structure 29

a. Vertical Velocity Maxima and Location of the Updraft Region . . . 29
5. Variations of the Vertical Velocity 32
F. DERIVED DATA TIME-HEIGHT CROSS SECTIONS 32
1. Horizontal Divergence 32
2. Turbulent Kinetic Energy (TKE) 34

IV. CASE STUDY OF THE SEA BREEZE ON 16 SEPTEMBER 1987 37
A. MOTIVATION FOR STUDY 37
B. SYNOPTIC CONDITIONS 37
C. WIND FIELD DATA AND ANALYSIS 37
1. Wind Direction and the Onset of the Sea Breeze 37
2. Wind Speed 39
3. Vertical Velocity 41
4. Standard Deviation of Vertical Velocity 44
5. Horizontal Divergence 49
6. Turbulent Kinetic Energy 50
D. LIDAR DATA 50
1. Color Coding 50
2. RHI Plots 50
3. PPI Plots 52

V. SUMMARY AND CONCLUSIONS 60
A. MAPPING THE SEA BREEZE CIRCULATION 60
1. Accuracy of the Sodar and Lidar 60
2. General Characteristics of the Sea Breeze Circulation 60
3. Tracking of the Sea Breeze Front 61
B. RECOMMENDATIONS 61

APPENDIX A. TWO-HOUR WIND DIRECTION CROSS SECTIONS 63

APPENDIX B. TWO-HOUR WIND SPEED CROSS SECTIONS 73

APPENDIX C. TWO-HOUR VERTICAL VELOCITY CROSS SECTIONS . . . 83

APPENDIX D. TWO-HOUR STANDARD DEVIATION CROSS SECTIONS . 93

APPENDIX E. 24-HOUR WIND DIRECTION CROSS SECTIONS 103
A. NOTES 103

APPENDIX F. 24-HOUR WIND SPEED CROSS SECTIONS 113
A. NOTES 113

LIST OF REFERENCES 123

INITIAL DISTRIBUTION LIST 126

LIST OF TABLES

Table 1. WPL DOPPLER RADAR CAPABILITIES 9
Table 2. GRADIENTS OF WIND DIRECTION AT THE SEA BREEZE FRONT 20
Table 3. TIMES OF ONSET FOR THE SEA BREEZE 22
Table 4. MAXIMUM HEIGHT AND DURATION OF THE SEA BREEZE . . 24
Table 5. SPEED OF ADVANCE OF THE SEA BREEZE FRONT 26
Table 6. SLOPE OF THE SEA BREEZE FRONT 27
Table 7. GRADIENTS OF WIND SPEED AT THE SEA BREEZE FRONT . . 28
Table 8. MAXIMUM WIND SPEEDS DURING THE SEA BREEZE AND MAXIMUM OFFSHORE FLOW 29
Table 9. VERTICAL MOTION CHARACTERISTICS OF THE SEA BREEZE 30
Table 10. STANDARD DEVIATION OF VERTICAL VELOCITY ACROSS THE SEA BREEZE FRONT 33

LIST OF FIGURES

Fig. 1. Typical Lake Breeze Circulation. (from Keen and Lyons, 1978). 2
Fig. 2. Location of Silver Prince, Lidar and Sodar 7
Fig. 3. Typical Surface Synoptic Situation 17-30 September 1987 11
Fig. 4. 850mb Synoptic Situation 25 September 1987 12
Fig. 5. Photographs of a Laboratory Gravity Head Structure in Prevailing 21
Fig. 6. Surface Data Record from 29 September 1987 at the Sodar Site 23
Fig. 7. 24 Hour Directional Plot for 16 September 1987 25
Fig. 8. Flow regions of the Gravity Head 31
Fig. 9. Divergence values of the Chicago Lake Breeze Study 35
Fig. 10. Divergence values of the LASBEX Study 36
Fig. 11. Synoptic Situation on 16 September 38
Fig. 12. Three Dimensional View of a Gravity Current Head 40
Fig. 13. Two-Hour Cross-Section of Wind Direction (16 September 1987) 41
Fig. 14. Two-Hour Cross-Section of Wind Speed (16 September 1987) 42
Fig. 15. 24-Hour Cross Section of Wind Speed (16 September 1987) 43
Fig. 16. Two-Hour Cross-Section of Vertical Velocity (16 September 1987) 45
Fig. 17. Two-Hour Cross-Section - Standard Deviation of w 46
Fig. 18. Standard Deviation of w on 16 September 47
Fig. 19. Standard Deviation of w on 16 September 48
Fig. 20. Standard Deviation of w normalized 49
Fig. 21. Two-Hour Cross-Section of Horizontal Divergence 51
Fig. 22. Two-Hour Cross-Section of Turbulent Kinetic Energy 52
Fig. 23. RHI Lidar Display at 1722 UTC, 16 September 1987 53
Fig. 24. RHI Lidar Display at 1805 UTC, 16 September 1987 54
Fig. 25. PPI Lidar Display at 1716 UTC, 16 September 1987 56
Fig. 26. PPI Lidar Display for 1719 UTC, 16 September 57
Fig. 27. PPI Lidar Display for 1747 UTC, 16 September 1987 58
Fig. 28. PPI Lidar Display for 1827 UTC, 16 September 1987 59
Fig. 29. Two-Hour Wind Direction Cross Section - 17 September 1987 64
Fig. 30. Two-Hour Wind Direction Cross Section - 18 September 1987 65
Fig. 31. Two-Hour Wind Direction Cross Section - 19 September 1987 66

Fig. 32. Two-Hour Wind Direction Cross Section - 20 September 1987 67
Fig. 33. Two-Hour Wind Direction Cross Section - 21 September 1987 68
Fig. 34. Two-Hour Wind Direction Cross Section - 22 September 1987 69
Fig. 35. Two-Hour Wind Direction Cross Section - 23 September 1987 70
Fig. 36. Two-Hour Wind Direction Cross Section - 27 September 1987 71
Fig. 37. Two-Hour Wind Direction Cross Section - 29 September 1987 72
Fig. 38. Two-Hour Wind Speed Cross Section - 17 September 1987 74
Fig. 39. Two-Hour Wind Speed Cross Section - 18 September 1987 75
Fig. 40. Two-Hour Wind Speed Cross Section - 19 September 1987 76
Fig. 41. Two-Hour Wind Speed Cross Section - 20 September 1987 77
Fig. 42. Two-Hour Wind Speed Cross Section - 21 September 1987 78
Fig. 43. Two-Hour Wind Speed Cross Section - 22 September 1987 79
Fig. 44. Two-Hour Wind Speed Cross Section - 23 September 1987 80
Fig. 45. Two-Hour Wind Speed Cross Section - 27 September 1987 81
Fig. 46. Two-Hour Wind Speed Cross Section - 29 September 1987 82
Fig. 47. Two-Hour Vertical Velocity Cross Section - 17 September 1987 84
Fig. 48. Two-Hour Vertical Velocity Cross Section - 18 September 1987 85
Fig. 49. Two-Hour Vertical Velocity Cross Section - 19 September 1987 86
Fig. 50. Two-Hour Vertical Velocity Cross Section - 20 September 1987 87
Fig. 51. Two-Hour Vertical Velocity Cross Section - 21 September 1987 88
Fig. 52. Two-Hour Vertical Velocity Cross Section - 22 September 1987 89
Fig. 53. Two-Hour Vertical Velocity Cross Section - 23 September 1987 90
Fig. 54. Two-Hour Vertical Velocity Cross Section - 27 September 1987 91
Fig. 55. Two-Hour Vertical Velocity Cross Section - 29 September 1987 92
Fig. 56. Two-Hour Standard Deviation Cross Section - 17 September 1987 94
Fig. 57. Two-Hour Standard Deviation Cross Section - 18 September 1987 95
Fig. 58. Two-Hour Standard Deviation Cross Section - 19 September 1987 96
Fig. 59. Two-Hour Standard Deviation Cross Section - 20 September 1987 97
Fig. 60. Two-Hour Standard Deviation Cross Section - 21 September 1987 98
Fig. 61. Two-Hour Standard Deviation Cross Section - 22 September 1987 99
Fig. 62. Two-Hour Standard Deviation Cross Section - 23 September 1987 100
Fig. 63. Two-Hour Standard Deviation Cross Section - 27 September 1987 101
Fig. 64. Two-Hour Standard Deviation Cross Section - 29 September 1987 102
Fig. 65. 24-Hour Wind Direction Cross Section - 17 September 1987 104

Fig. 66. 24-Hour Wind Direction Cross Section - 18 September 1987 105
Fig. 67. 24-Hour Wind Direction Cross Section - 19 September 1987 106
Fig. 68. 24-Hour Wind Direction Cross Section - 20 September 1987 107
Fig. 69. 24-Hour Wind Direction Cross Section - 21 September 1987 108
Fig. 70. 24-Hour Wind Direction Cross Section - 22 September 1987 109
Fig. 71. 24-Hour Wind Direction Cross Section - 23 September 1987 110
Fig. 72. 24-Hour Wind Direction Cross Section - 27 September 1987 111
Fig. 73. 24-Hour Wind Direction Cross Section - 29 September 1987 112
Fig. 74. 24-Hour Wind Speed Cross Section - 17 September 1987 114
Fig. 75. 24-Hour Wind Speed Cross Section - 18 September 1987 115
Fig. 76. 24-Hour Wind Speed Cross Section - 19 September 1987 116
Fig. 77. 24-Hour Wind Speed Cross Section - 20 September 1987 117
Fig. 78. 24-Hour Wind Speed Cross Section - 21 September 1987 118
Fig. 79. 24-Hour Wind Speed Cross Section - 22 September 1987 119
Fig. 80. 24-Hour Wind Speed Cross Section - 23 September 1987 120
Fig. 81. 24-Hour Wind Speed Cross Section - 27 September 1987 121
Fig. 82. 24-Hour Wind Speed Cross Section - 29 September 1987 122

ACKNOWLEDGEMENTS

I wish to thank the Naval Environmental Prediction Research Facility for providing the funds necessary to carry out LASBEX. The field measurements were supported by the Naval Environmental Prediction Research Facility with work request N685687WR67635-12 AUG 87.

I wish to thank Dr. Dennis Thomson at Pennsylvania State University for arranging the use of the doppler sodar system during this experiment. Many thanks go to the NOAA Wave Propagation Laboratory for the use of the information and data from their doppler lidar, which made this study a success, with special thanks to Janet Intrieri, who provided the lidar pictures for the case study.

I would like to thank Dr. William J. Shaw for his encouragement and support during the research and writing of this thesis and to Dr. John W. Glendening for his insight and advice. I would like to acknowledge Tamar Neta, Gail Vaucher and Neil Harvey for their assistance with the computer programming necessary to make the process of data compilation and assimilation an easy and swift effort. Many thanks go out to my wife, Nellie, for her enduring patience and understanding.

I. INTRODUCTION

A. GENERAL DESCRIPTION

The land-sea breeze is a diurnal mesoscale circulation that occurs on sea coasts due to the differences in surface temperatures between the land and sea. A typical horizontal temperature gradient is 1°C/20 km (Atkinson, 1981). This situation induces a thermally direct circulation that alternates between onshore or sea breeze and offshore or land breeze. The circulation occurs during the day due to solar heating of the land which warms faster that the sea. This results in a horizontal pressure gradient with slightly higher pressure over the land. The pressure differential causes air to flow at higher levels towards the sea, thereby leading to convergence aloft. The resulting counter-flow at the surface is the sea breeze. Fig. 1. shows a lake breeze circulation, which has a similar structure as the sea breeze circulation.

The land breeze is due to the same thermal structure except it is reversed. At night, the land loses heat quicker than the sea and, therefore, sets up a circulation opposite to the sea breeze. In both cases, the flow at the surface is from the cooler region toward the warmer region. By comparison, the sea breeze is the stronger circulation, since the heating of the land provides for a more intense heat source to drive the flow.

The sea breeze occurs more frequently given a weak horizontal pressure field (Estoque, 1962; Simpson et al., 1977). This is because the thermal effects have to alter any existing conditions. If the existing pressure field is strong enough, the resulting gradient winds can overwelm the land-sea breeze effect.

Under some conditions, an offshore gradient wind will generate a frontal zone at the leading edge of a sea breeze (Atkinson, 1981). Estoque (1962) notes in his model that an offshore flow counter to the sea breeze will enhance the horizontal temperature gradient. The sea breeze front is also characterized by gradients in humidity, wind speed and wind direction. This sea breeze front is similar in form to a synoptic scale cold front, because the cooler moist marine air is advancing into the warmer dry land regime. Passage of such a front is a measurable feature and can induce significant mesoscale meteorological phenomena such as showers, thunderstorms and gusty winds (Pielke, 1974; John, 1980; Richiardone and Pearson, 1983). The horizontal extent of the sea breeze is large enough that it can develop a component parallel to the coast due to coriolis deflection (Defant, 1951; Walsh, 1974).

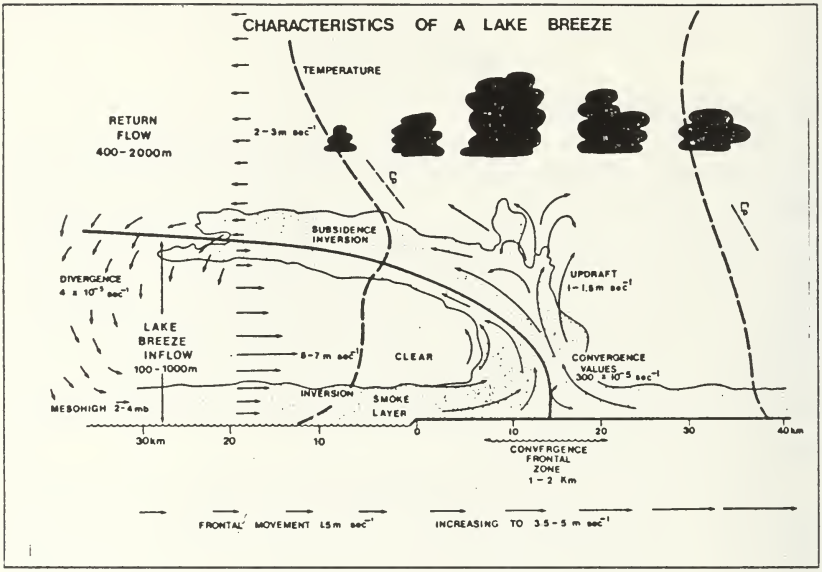

Fig. 1. Typical Lake Breeze Circulation. (from Keen and Lyons, 1978).

B. MOTIVATION FOR THE STUDY OF LAND-SEA BREEZE

The land-sea breeze circulation and sea breeze front can affect the dispersion of aerosols and pollutants over a wide area. This effect has been observed and modelled many times (Lyons, 1972; Lyons and Olsson, 1973; Anthes, 1978; Kondo and Gambo, 1979; Kitada et al., 1986; Ogawa et al., 1986). In a sea breeze, particulates and gases can be carried inland over long distances. Collis and Russell (1976) summarized some of the important effects that particle pollutants have on climate, such as cloud formation, precipitation and transfer of solar radition. Pollutants can enhance cloud formation and result in acidic rainfall. Particulates and gases can block incoming solar radiation and trap outgoing long-wave radiation.

In the case of lidar (light detection and ranging) sensors, concentrations of pollutants such as NO_2 and SO_2 can attenuate or distort the return signal so that information may be misinterpreted (Measures, 1984).

Measuring the intensity and mapping the structure of the sea breeze can give a better understanding of how particles are transported and dispersed. Satellite data could be used to detect a sea breeze occurrence. In addition, forecasts of pollution events may be feasible. Surface data also can be used to evaluate satellite observations of the planetary boundary layer and the mesoscale features that occur during the sea breeze.

C. PREVIOUS STUDIES

A study was conducted by Johnson and O'Brien (1973) of the sea breeze along the Oregon coast. In their study, the sea breeze was found to have a maximum depth of 700 meters, with a maximum speed of 7.5 m/s at the surface. The zonal wind was utilized to describe the variability of the sea breeze because of the north-south orientation of the Oregon coast. The inland penetration of the sea breeze front was up to 60 km. A return flow was found between 1000 and 1500 meters. Johnson and O'Brien made the following observations: the low-level onshore flow of the land-sea circulation was located entirely within the marine layer; the marine layer tends to deepen briefly at the onset of sea breeze due to the low level convergence ahead of the sea breeze front; the return flow above the inversion appears to be in the form of surges, probably in response to the surges observed in the sea breeze; and a distinct wind maximum follows the sea breeze front inland.

Simpson, et al. (1977) observed sea-breeze fronts that penetrated over 45 km inland with some fronts moving as far as 80 km. These fronts had an average advance speed of 3 m/s. They also showed that the structure of the sea breeze front is similar in structure to gravity currents produced in laboratory water-tanks.

Mitsumoto et al. (1983) conducted a laboratory experiment which used a water-tank to simulate the sea breeze. This experiment reproduced many of the characteristics of the sea breeze flow, such as strong vertical motion at the leading edge of the sea breeze, compensating flow aloft and production of longitudinal convective vortices within the sea breeze flow.

Ogawa et al. (1986) observed the gravity head structure reproduced by Mitsumoto's laboratory experiment during a lake breeze. Ogawa's experiment utilized a kytoon-mounted ultrasonic anemometer-thermometer to measure instantaneous wind and temperature in order to observe the turbulent structure of the lake breeze. He found that the penetration of a lake breeze produced an upward rolling motion within the head of the front. He recorded upward flow velocities around 3 m/s. Ogawa found that the temperature profile had peaks indicating the frontal passage. These peaks were due to the boundary between the offshore wind aloft and the lake air below. Another feature that was observed was the development of the Thermal Internal Boundary Layer (TIBL). The TIBL develops due to the temperature discontinuity between the land and the water (Stunder and Sethurman, 1985). The TIBL plays a significant role in the fumigation of coastal pollution that is advected into it.

Estoque's (1962) model had a maximum penetration of sea-breeze front of 32 km and a minimum penetration of 18 km. The maximum penetration occurred during calm initial conditions and the minimum penetration occurred during offshore counter-flow.

Pearson et al. (1983) used a model and found that with a mean flow perpendicular to the coast, the speed of the sea breeze front is a linear function of the onshore component of the mean flow. He found that the maximum vertical velocity in the front at any given time was not affected by the mean flow. Another characteristic that Pearson found was that in a negative shear case (upper flow is from land to sea), there was an increase in the vertical extent of the sea-breeze front.

For a general descriptive summary of sea breeze studies, Atkinson (1981) provides a comprehensive review from many locations and experiments.

D. LAND-SEA BREEZE EXPERIMENT (LASBEX)

A measurement program was conducted in the Monterey Bay area in September 1987, to understand the structure of the land-sea breeze effect and generate data to evaluate many of the models which have been used to demonstrate the behavior of the air flow. This experiment was unique because it utilized a varied array of instruments including doppler acoustic sounder (sodar), a doppler lidar, rawinsonde launches over the the sea, radiosonde launches over land, conventional surface recordings of temperature, humidity and wind and corresponding observations by the NOAA 9,10 and GOES satellites. This combined instrument analysis allowed for comparison of the data among many sources. The final result will be a comprehensive view of the land-sea breeze intensity and structure. This study focuses on data from one sodar supplemented by lidar observations.

The products obtained from the sodar data were the height of the marine boundary layer and time-height cross sections of wind direction, wind speed, vertical velocity and the standard deviation of the vertical velocity. From these it was possible to compute time-height cross sections of horizontal divergence and turbulent kinetic energy. The time-height cross sections will be compared with conventional data obtained from radiosonde, rawinsonde and surface observations. The boundary layer height observations will be compared with the time-height and conventional data.

The lidar provided pictures of the radial wind field in the sea breeze front. The lidar observations will be compared with the sodar to find differences between the instruments ability to map the sea breeze front and measure the associated wind field.

The combination of lidar and sodar has been applied before to analyzing the atmosphere. However, the two instruments have not been used to study the sea breeze circulation. Russell et al. (1974) used the combination to observe the atmospheric boundary layer in an urban environment. One comparison in Russell's study was the ability of either instrument to detect subsidence. In the case of the lidar, detection was degraded because aerosols tend to be excluded from descending air. For the sodar, the temperature gradient associated with a large-scale subsidence inversion is easily detectable. Lopez (1977) used the combination to study the properties of convective activity and small cumulus formation. This combination is effective since either instrument can detect different features to give a better overall picture of the atmosphere.

The objective of this thesis is to evaluate the effectiveness of the sodar in the detection and mapping of sea breeze events and to compare its measured wind field with that of the lidar. A case study on 16 September 1987 is presented. An overall look at typical characteristics of the sea breeze in the Monterey Bay Salinas Valley will be generated for use in other studies, such as aerosol transport or the evaluation of satellite imagery.

II. DESCRIPTION OF EXPERIMENT

A. LOCATION OF THE EXPERIMENT

LASBEX was conducted from between 15 and 30 September 1987 on the Monterey Bay coast. The collection of data started at 1200 Pacific Standard Time (PST) on 15 September and ended at 1300 PST on 30 September. All instruments were operated continuously except the contracted research vessel Silver Prince, which was stationed in Monterey Bay to monitor surface wind, temperature, humidity and pressure as well as launch rawinsondes. The ship collected data from 1000 PST until 1600 PST on various days throughout the experiment. The instruments evaluated in this paper were the Pennylvania State University (PSU) sodar and the NOAA Wave Propagtion Laboratory (WPL) lidar. The sodar was located southeast of Castroville at the mouth of the Salinas Valley. The lidar was located on a flat knoll approximately 1.5 km from the coast, southeast of Moss Landing. It was on a line of 310° with the sodar, which approximated the orientation of the Salinas Valley. The separation between the sodar and the lidar was 5.5 km. The Silver Prince was stationed in Monterey Bay approximately 16 km from the lidar location. The three main instrument locations are shown in Fig. 2.

The terrain around the sodar site was at elevations of less than 30 meters, with elevations greater than 30 meters northeast, starting 2.5 km away. The interference caused by the town of Castroville was considered minimal for the experiment. The terrain surrounding the lidar was generally flat with higher elevations to the north and east. To the east the terrain rose to levels of 100 meters and greater, up to 400 meters. To the north, the terrain generally had a maximum elevation of 150 meters. North-northeast of the lidar, Elkhorn Slough, a brackish inlet, interruped the elevated terrain.

At the lidar, sodar and ship, twenty-second averages of vector wind velocity, air temperature, relative humidity and surface pressure were collected at the stations during the experiment. Radiosondes were launched at the sodar station at the discretion of the research team, coinciding with significant changes in the environment.

Satellite AVHRR imagery during LASBEX was available from the Scripps Institution of Oceanography.

B. ACOUSTIC DOPPLER SODAR

During LASBEX, the doppler sodar was used to monitor the acoustic backscattered energy of turbulent fluctuations in the atmosphere. The sodar is a 3-axis monostatic

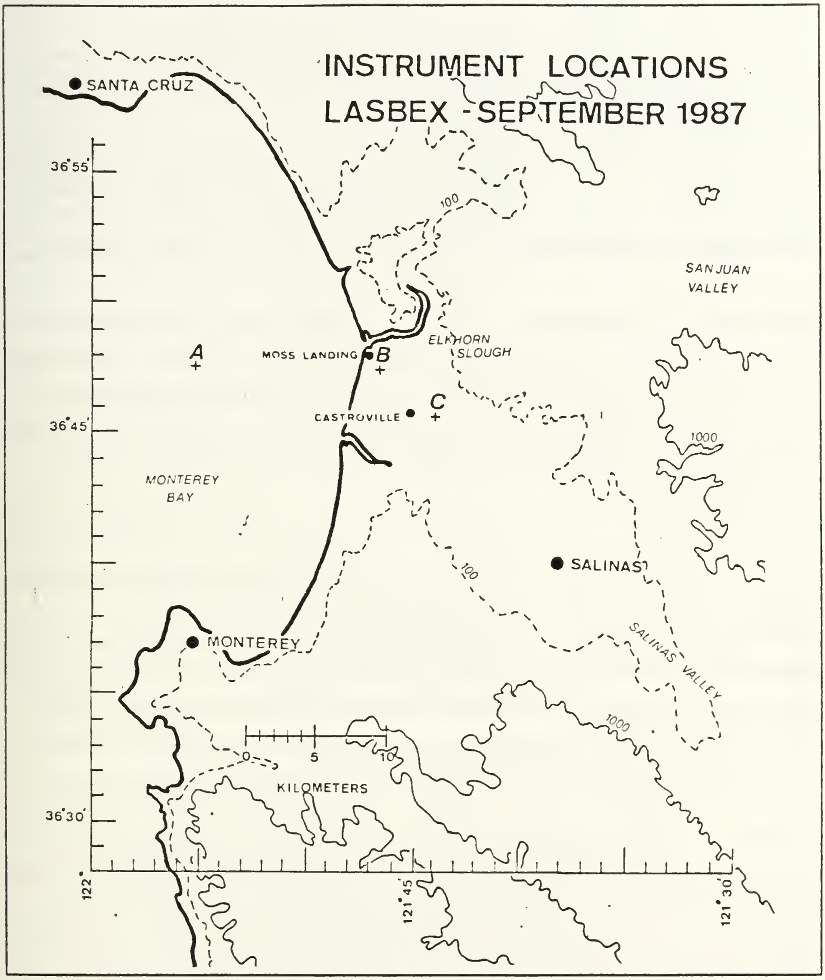

Fig. 2. **Location of Silver Prince, Lidar and Sodar:** The Silver Prince was at location A. The Lidar was at location B. The Sodar was at location C. Elevations are in feet. Distances are in kilometers.

doppler system manufactured by Xontech and consists of a phased array of 25 transducers which operated at a frequency of 1600 hertz. The pulse repetition interval is 10 seconds per beam, giving a cycle time of 30 seconds between the 3 acoustic beams. Two cycles were integrated per minute. A wind profile was sampled every five minutes, giving an effective number of 10 cycles per record.

The sodar uses sound energy to detect the small-scale temperature fluctuations and discontinuities in the mean temperature profile (Crease et.al., 1977; Koracin and Berkowicz, 1988). The addition of doppler capabilities allows for the recording of wind speed and direction (Kaimal and Haugen, 1977). The backscattered energy provides information about the height of the marine boundary layer, wind speed, wind direction, vertical velocity and vector winds. Neff and King (1988) demonstrated that the sodar can give indirect spatial and temporal information on both the location and thickness of turbulent layers. In addition, Neff was able to identify mixing processes in the boundary layer. Small mixing processes could be attributed to turbulence, where as large processes could be associated with effects such as Kevin-Helmholtz instabilities.

C. DOPPLER LIDAR

The lidar used during LASBEX was the WPL 10.6 micron doppler system. The lidar operated under computer control and had real-time data processing and color display capabilites. The system could compute the zero, first and second moment of the echo spectrum for each range gate. For LASBEX, the lidar was operated in the range-height indicator (RHI) and plan postion indicator (PPI) modes. In RHI, the beam of the lidar sweeps in a 180° arc from foward to overhead and then behind the instrument. In PPI, the beam sweeps at a fixed angle of elevation from the horizon in a 360° circle around the lidar, the path describing an inverted cone. In both modes, the display of information is of the radial velocity relative to the lidar. Familiarity with a doppler presentation is required to analyze the PPI display. This analysis is similar to a doppler radar PPI and is described in Wood and Brown (1983). In RHI, the lidar beam was aligned parallel to the axis of the Salinas Valley with an orientation angle of 140°, or east-west with an angle of 90°, with the preferred orientation being east-west. This was because climatological records indicated that the sea breeze blew from due west in the Moss Landing area. In PPI, the elevation of the lidar beam was 1° and 5°. The 1° beam shows the low level structure below 200 meters, whereas the 5° beam gives structure above 300 meters. These values were determined triginometrically. Table 1 lists some of the clear-air radial velocity parameters of this instrument:

Table 1. WPL DOPPLER RADAR CAPABILITIES

Expected range	10-15 km
Range resolution	140-400 m
Beam width	< 0.1 degree
Pointing accuracy	0.1 degree
Accuracy of radial velocity measurment	> 1.0 m s
Operation modes	PPI, VAD, RHI, range-time, raster-scan

The lidar uses the backscattered energy of a laser from gas molecules and particulates to detect atmospheric features such as clouds or aerosol layers. Collis and Russell (1976) cited an example of how lidar was used to find the depth of the mixed layer or determine the heights of inversions, which can affect the dispersion of pollutants. Noonkester et al. (1974) was able to detect Kelvin-Helmholtz instabilities in the boundary-layer. In clear air, a lidar can detect the stratification associated with a deep stable boundary layer.

D. SURFACE MEAUREMENTS

A portable coastal meteorological station was used to take 20-second averages of wind direction, wind speed, air temperature, relative humidity and barometric pressure at the surface. This instrument used a propeller anemometer to measure wind speed. A self-aspirated thermometer and hygrometer measured air temperature and relative humidity. Wind direction was taken from a vane that gave angles with respect to true north. The ranges of the instrument errors were: ± 5° for wind direction; ± 0.3 m s for wind speed; ± 0.3° for air temperature; and ± 5% for relative humidity.

E. SYNOPTIC SITUATION BETWEEN 16-30 SEPTEMBER 1987

On 16 September, California was under the influence of a surface high pressure system off the coast and a local thermal trough in the center of the state. The winds were northerly to northwesterly between 5 and 10 knots. This configuration continued to influence the west coast from 17 to 24 September. Fig. 3shows the synoptic situation during this period. Around the 25th, a short wave which was detectable at the 850 mb level began to pass through northern California from the northwest. This wave built up a strong thermal gradient off the coast of California, providing an increase of cold thermal advection. This was the most significant feature associated with an actual synoptic frontal passage during LASBEX. Fig. 4 shows the short wave location. Winds during this wave passage were mainly northerly with speeds averaging 7 m/s or more. After the passage of the wave on the 26th, high pressure off the coast and the thermal trough in the center of the state were reestablished. This weather pattern persisted for the remainder of the experiment.

The combination of a high pressure system over the eastern North Pacific Ocean and a thermal trough in central California is the typical summmer and early autumn synoptic pattern. This situation accounts for the common Monterey Bay pattern of low clouds and fog with light and variable winds during the night and morning. A tropical disturbance named 'Otis' formed west of the Baja Peninsula during the 23rd but did not significantly affect surface and lower level flow during that part of the experiment.

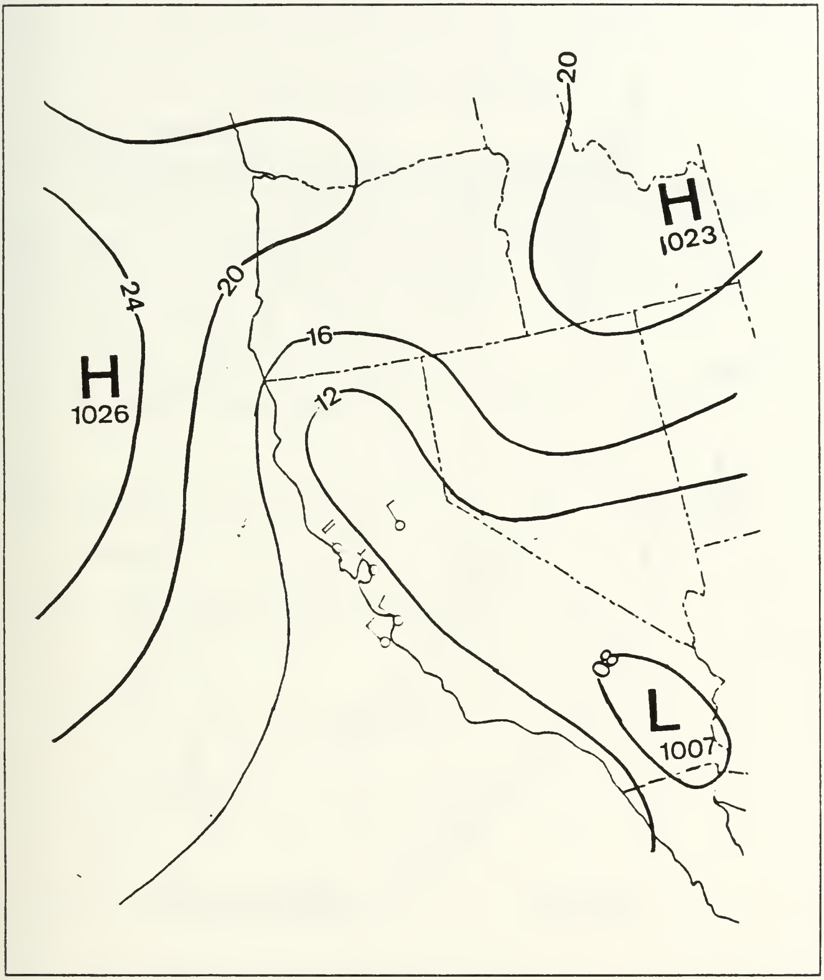

Fig. 3. Typical Surface Synoptic Situation 17-30 September 1987: Solid lines are sea level isobars. Values are + 1000 mb.

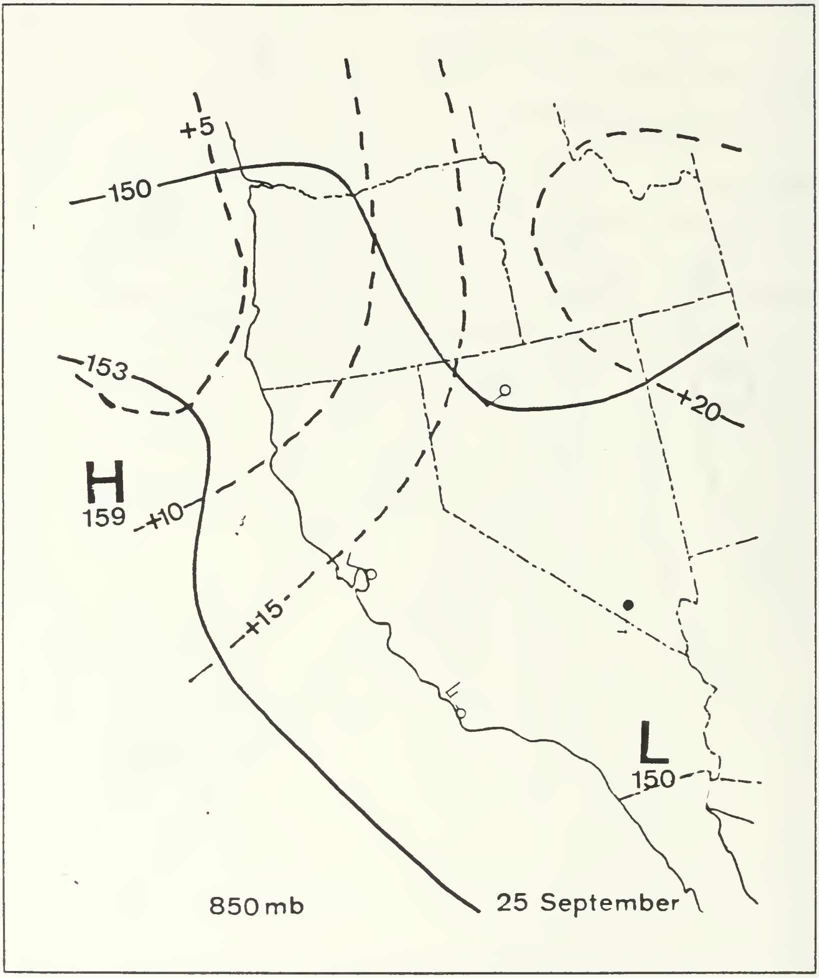

Fig. 4. 850mb Synoptic Situation 25 September 1987: Solid lines are isoheights. Values are + 1000 meters. Dashed lines are isotherms. Temperatures are in degrees Celsius.

III. DATA AND ANALYSIS

A. SODAR THEORY

1. Basic Sodar Theory and Turbulence in the Inertial Subrange

This discussion of sodar theory and operation follows Underwood (1981). The sodar utilizes the backscatter of acoustic energy to determine certain parameters in the atmosphere. The relationship between the acoustic power emitted and the backscattering cross section is defined by the sodar equation.

$$P(R) = P_o \frac{AG}{R^2} L_v e^{-2\bar{\alpha}R} \left(\frac{A_o}{A_o + A_T} \right) \sigma(\pi), \tag{3.1}$$

where

$P(R)$ = received acoustic power (watts),

P_o = transmitted acoustic power (watts),

A = cross sectional area of the receiver antenna (m^2),

G = antenna gain factor,

L_v = length of the acoustic pulse in space (m),

$\bar{\alpha}$ = path averaged molecular attenuation coefficient (m^{-1}),

R = distance from the scatterer to the receiver (m),

$\frac{A_o}{A_o + A_T}$ = "excess" attenuation and

$\sigma(\pi)$ = backscattering cross section (m^{-1}).

The backscattering cross section can be related to the temperature structure parameter C_T^2, and the velocity structure parameter C_v^2, as shown by Little (1969). These structure parameters indicate the intensity of high frequency variations of temperature or velocity. Explicitly, the backscatter cross-section is

$$\sigma(\pi) = 0.03k^{1/2}\cos^2(\theta)\left[\frac{C_v^2}{c^2}\cos^2\left(\frac{\theta}{2}\right) + 0.13\frac{C_T^2}{T^2}\right]\left(\sin\frac{\theta}{2}\right)^{-11/3}, \tag{3.2}$$

where

$\sigma(\pi)$ = backscattered acoustic energy,

c = speed of sound,

T = absolute air temperature,

C_v^2 = velocity structure parameter and

C_T^2 = temperature structure parameter.

Turbulent mixing in clear air causes fluctuations in potential temperature and water vapor which scatter and attenuate the acoustic energy in the sodar signal. The backscattering cross section determines how much energy is returned to the sodar antenna after attenuation by the turbulence. Turbulent eddies with a size equal to one half the wavelength of the emitted acoustic energy $\lambda_{a/2}$, (Russell et al., 1974) are detectable with a sodar. Eddies of this size fall within the inertial subrange of turbulence and are assumed to be isotropic. Energy relationships in the inertial subrange follow the Kolmogoroff description of isotropic turbulence. The backscattered data are processed using Fast Fourier Transforms (FFT) to establish the frequency shift due to the radial components. The two main fields which the monostatic doppler sodar can map are the thermal structure and the mean velocity field along with its variances.

a. *Thermal Structure*

Molecular attenuation is described by Sutherland (1975) and Piercy et al. (1977) as those effects at the molecular scale which influence the propagation of energy through a medium such as air. The factors which cause molecular attenuation of sound energy are due to thermal, viscous and diffusive effects as well as rotational and vibrational losses on the molecular scale. The molecular attenuation increases with frequency and is the limiting factor in the maximum usable frequency in a sodar. The lower limit is based on antenna size. "Excess" attenuation is due to turbulent spreading of the beam pattern (Brown and Clifford, 1976). Any of the sodar signal that is not attenuated can be scattered back to the receiver by turbulent eddies according to (3.2).

As the lapse rate changes in the atmosphere, any mechanical turbulence will create small eddies that backscatter the acoustic energy. The monostatic sodar (θ = 180°) gives an indication of the changes in the lapse rate along the beam path, which can be related to thermal structure (Wyckoff et al., 1973). In a monostatic sodar, only temperature fluctuations contribute to received power according to (3.2).

b. Velocity Structure

Doppler processing is used to derive the velocity structure. This discussion follows Peterson (1988) in a handbook on doppler wind profilers.

(1) Basic Setup of A Doppler Sodar. The sodar emits sound energy at a narrow band of frequencies and is reflected by turbulent eddies and temperature fluctuations. A frequency shift (doppler shift) is caused by any motion on the same axis as the sodar beam and is proportional to the speed of that motion. By measuring the doppler shift, the radial velocity of the scattering volume can be calculated. In order to obtain a wind velocity, Doppler shifts from three axes are required. The configuration of the sodar is to have one beam directed overhead, with the other two at perpendicular cardinal headings (i.e. north and east). The beams are typically pointed at high elevations, so that they are sampling nearly the same flow. The vertical velocity from the beam directed upwards can be subtracted from the other two, leaving the horizontal components of the wind vector.

The sodar used during LASBEX consists of 25 separate transducers. Using electronic phasing, these transducers were fired at different times in order to direct the acoustic beam. If there was no phasing between all the transducers, the beam would travel directly overhead. By delaying the time that each transducer emitted, the beam of acoustic energy can be directed at different angles.

(2) Range Aliasing. The signal from the sodar must be of a pulse repetition frequency (PRF) that precludes aliasing. Aliasing occurs when the the signal from the current pulse is overlapped by return signals from the previous pulse. These overlapping signals will be erroneously interpreted. This type of aliasing is called range aliasing because a return from a distant scatterer could be mistaken for a closer one. The time between pulses must be long enough to prevent this effect. The effective height that the sodar can function without range aliasing is determined by the following equation:

$$R_{\max} = \frac{c}{2 \times PRF}, \tag{3.3}$$

where

$R_{\max}$ = maximum range, (m)

c = speed of sound in air (m/s)and

PRF = pulse repetition frequency (s^{-1}).

The maximum height that the PSU sodar was set to detect is 750 meters, which is about half its maximum range, and only information starting 50 meters above the surface was recorded. These settings effectively avoided any range aliasing during the experiment.

(3) Velocity Aliasing. Only doppler shifts of certain frequencies can be determined without error. Doppler shifts that are either too large or too small will be incorrectly mistaken for other velocities. This is called velocity aliasing. The frequency limits for which a doppler shift can be interpreted correctly rely upon the sampling rate. The optimum selection is to have a sampling rate as high as possible. However, there must be balance between velocity aliasing which requires a high PRF and range aliasing which requires a small PRF. The wind speed data during LASBEX showed no extreme values and therefore velocity aliasing was negligible.

(4) Data Processing. For each detection cycle, many samples are gathered and converted into a frequency spectrum using the Fast Fourier Transform technique. Doppler shifts in a frequency spectrum show up as peaks offset from 0 or the no shift position. Motion towards the sodar is indicated by a positive doppler shift. A negative shift indicates motion away from the receiver. The doppler shift is converted into a radial velocity component of the wind. The height of the frequency peak is a measure of received power and the width of the peak a measure of spread of the acoustic energy over frequency. The spread of energy is directly related to the standard deviation of radial velocity. Using deviations of radial velocities among the three beams, the standard deviations of each velocity component (σ_u, σ_v, σ_w) can be calculated.

The preferred method is to sample in the time domain, so that several consecutive samples can be gathered and averaged before conversion into the frequency domain with an FFT. A mean frequency spectrum is calculated from several consecutive frequency domains to generate a spectral average, which gives a better indication of a doppler shift in the signal. The background noise is filtered out to better refine the frequency peak. This cycle of sampling, conversion, averaging and filtering is set by the user and typically lasts one or two minutes per beam. The PSU sodar integration occurred over 60 seconds, with each beam sampled every 10 seconds.

B. LIDAR THEORY

The lidar uses the same principal as the sodar to analyze the backscatter from a pulse of energy. The lidar utilizes a laser beam to emit pulses of high intensity light that will be reflected from gases, aerosols and particulates. A general form of the lidar equation is given (Russell et al.,1974):

$$P_r(R) = P_t \frac{c\tau}{2} \frac{A}{R^2} \beta(R) t^2(R), \tag{3.4}$$

where

$P_r(R)$ = received power from range, (R)

P_t = transmitted optical power,

c = speed of light in air,

τ = duration of laser pulse,

A = effective telescope aperature,

$\beta(R)$ = Optical volume backscattering coefficient and

$t(R)$ = Optical transmittance of atmosphere.

This equation is similar in form to the sodar equation (3.1), except that the lidar equation is dealing with electromagnetic energy, whereas the sodar equation deals with acoustic energy. The received signal from the lidar is a function of the optical properties and concentration of the backscattering volume. Since gases and aerosols have different effects on the attenuation of light, the received energy can be analyzed to determine what causes the scatter.

Aerosols and gases are distributed by the winds and are trapped in layers due to the stratification of the atmosphere. The detection of these gases and aerosols gives an indication of the mean wind field and the degree of stratification. The doppler lidar uses the same principle of operation to deduce radial velocities as the doppler sodar.

C. SODAR CROSS SECTIONS

1. Time-Height Cross Sections

The wind vector data at the sodar were collected and stored on floppy disk files in tabular form, with a header indicating the date and time of the record. The data were recorded every 25 meters in the vertical, beginning 50 meters from the surface up to and including 750 meters. These files were transferred to the mainframe computer at the Naval Postgraduate School on mass-storage for consolidation into separate files of wind speed, wind direction, vertical speed, and σ_u, σ_v and σ_w. These consolidated files were plotted in time-height cross sections. Time for the records was in Universal Time Coordinates (UTC), but converted to decimal days for plotting. The conversion from UTC to Pacific Standard Time (PST) is to subtract 8 hours from UTC. Plots were generated in the following formats: 24 hours up to 750 meters, four hours up to 350 meters and two hours up to 550 meters. The two and four hour plots were centered as close to possible to the passage of the sea breeze front. The 24-hour plots started and ended at 0600 local time (1400 UTC or 0.5833 decimal day). The raw data from mass-storage were read and set to a standard grid with a resolution of five minutes on the abscissa and 25 meters on the ordinate. The density of the grid depended on the time and height resolution of the desired field (i.e. 24-hour plots with 750 meter heights were 29 by 288, whereas two hour plots with 550 meter heights were 19 by 24). Contours were fitted to the standard grid using a rational spline interpolation scheme. Plots were generated and checked for bad data, which showed up as unusually strong gradients surrounding a single point. Vertical records were manually checked for consistency and errant readings were removed by comparison to adjacent values. The two hour cross-sections of wind direction, wind speed, vertical velocity and σ_w are included as appendices A, B, C and D. The 24-hour cross-sections of wind direction and wind speed are included as appendices E and F.

D. DERIVED DATA

Horizontal divergence and turbulent kinetic energy were derived from the velocity and σ_u, σ_v and σ_w fields respectively and plotted in the same format as the velocity fields.

Horizontal divergence was determined from the continuity equation for incompressible flow:

$$\left(\frac{\partial u}{\partial x} + \frac{\partial v}{\partial y} + \frac{\partial w}{\partial z}\right) = 0. \tag{3.5}$$

The divergence was calculated from the vertical velocity field such that

$$\frac{\partial w}{\partial z} = -\nabla_H \cdot \vec{V}. \tag{3.6}$$

This calculation was simple, since the vertical velocity component of the wind with respect to height was readily available from the sodar data.

The turbulent kinetic was determined using the values of σ_u, σ_v and σ_w as follows:

$$\bar{e} = \frac{1}{2}(\sigma_u^2 + \sigma_v^2 + \sigma_w^2), \tag{3.7}$$

where $\bar{e}$ equals turbulent kinetic energy.

E. ANALYSIS OF TIME-HEIGHT CROSS SECTIONS

1. Wind Direction

a. Wind Direction Gradients and Onset of Sea Breeze

The criteria that mark the onset of the sea breeze typically are the change in wind direction and increase of wind speed. The wind data from the sodar were analyzed to determine the degree of the wind speed change. A sharp change in wind direction with time which indicated sea breeze frontal passage was present in 10 plots during LASBEX. Wind direction was contoured with an interval of 30°. Onshore wind was considered 270° ± 60° and offshore 90° ± 60°. Up valley was 330 ± 20°. Down valley was considered 150 ± 20°. Frontal passage and the onset of the sea breeze was evident when the wind direction showed a strong temporal gradient. The mean temporal gradient for sea breezes during LASBEX was on the order of a 90° clockwise shift over 44 minutes for a strong offshore flow and over 42 minutes for a weak offshore flow. The fastest change occurred over 10 minutes during strong offshore flow, while the slowest change occurred over 104 minutes during weak offshore flow. 90° was selected as the criterion to define sea breeze onset, when the wind turned through alongshore to onshore flow, because the observed temporal wind shift was greatest over this interval. The relative strength of the offshore flows was divided into strong and weak flows based on the preexisting winds below 400 meters before the onset of the sea breeze. The 400-meter level was selected since it was the average depth of the established offshore flow. Strong flows were considered 3 m/s or greater and weak flows less than 3 m/s. There was no correlation between the sharpness of the front based on the temporal gradient and the strength of the previous offshore flow. This agrees with the model result of Pearson et al. (1983) that the intensity of the sea breeze circulation is unaltered by the mean flow. Table 2 on page 20 lists the various gradients for sea breeze fronts that were detected during LASBEX.

Table 2. **GRADIENTS OF WIND DIRECTION AT THE SEA BREEZE FRONT:** μ_s = mean of strong offshore flows, μ_w = mean of weak offshore flows

Date	Temporal Directional ∇(°/min)	Vert. Directional ∇(°/m)	Offshore Flow (Strong or Weak)
16	90/24	180/45	Strong
17	90/14	180/25	Weak
18	90/70	180/37	Weak
19	90/10	180/50	Strong
20	90/60	180/105	Strong
21	90/34	180/45	Strong
22	90/30	180/90	Weak
23	90/104	180/180	Weak
27	90/82	180/50	Strong
29	90/56	180/50	Strong
μ_s	90/44	180/58	n/a
μ_w	90/42	180/83	n/a

A shear layer was evident in the direction plots as a strong gradient in the vertical. This shear zone indicates the boundary between the offshore flow and the sea breeze. These gradients are shown in Table 2. The mean wind shift in the vertical was 180° over 58 meters and 83 meters for the strong and weak offshore cases, respectively. It does appear that a strong offshore flow limited the vertical extent of the shear zone and that a weak flow allowed a deeper region of directional shear, which agrees with the results produced by Simpson and Britter (1980) in a laboratory experiment, as shown in Fig. 5 on page 21.

In the majority of the frontal passages, the wind direction change preceeded a change in wind speed or vertical velocity. In all cases, the direction of the breeze after the direction shift was 300° ± 20°,which was onshore and up valley.

The average onset times for the sea breeze determined at the sodar site by the change in wind direction was 1742 UTC. The earliest onset time was at 1644 UTC

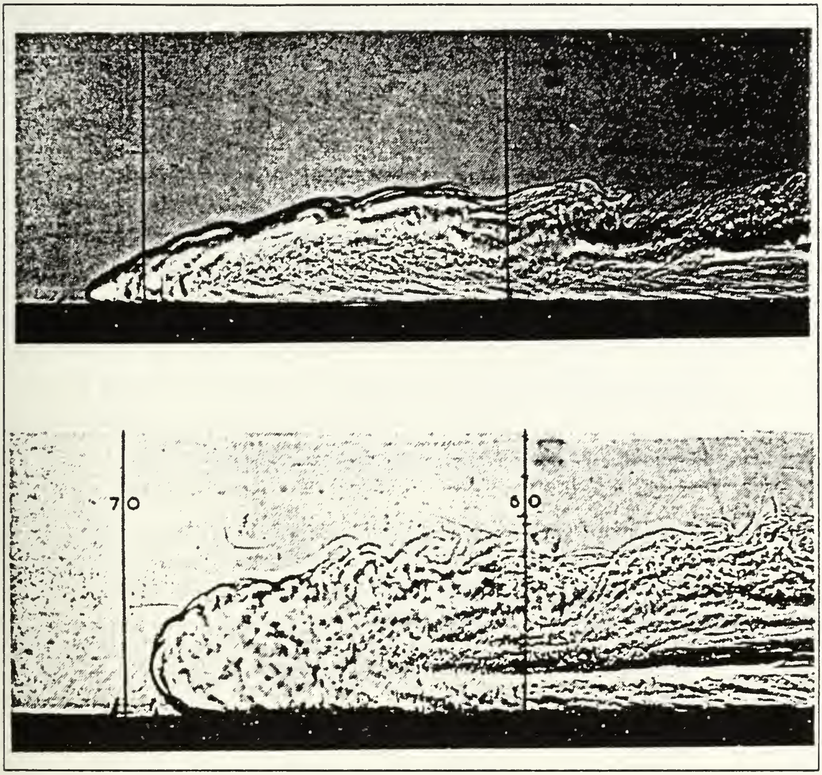

Fig. 5. Photographs of a Laboratory Gravity Head Structure in Prevailing Flows: The top photo is taken during opposing flow. The bottom is taken during accompanying flow. (from Simpson and Britter, 1980)

and the latest was at 1830 UTC. The time for the increase in wind speed and in vertical velocity were also tabulated from the sodar data.

Onset times were also determined from the surface data. Onset was indicated by a change in wind direction and speed, temperature and relative humidity. Shortly before sea breeze onset, the wind direction was very variable with the trend changing from offshore to onshore flow. Wind speeds before onset decreased to near zero, then rapidly increased as the sea breeze front passed. Air temperature gradually rose due to solar heating in the morning, peaked at frontal passage and then decreased as the sea breeze was established. Relative humidity at onset increased quickly with frontal passage and leveled off at the sea breeze continued. A typical surface record with sea breeze passage is shown in Fig. 6.

In most cases, the wind direction shift was consistent with the observed sodar wind change. The mean time of onset measured by the surface data was 1813 UTC. The earliest frontal passage occurred at 1715 UTC, while the latest passage occurred at 1945 UTC. The variability of wind direction shifts in the surface measurements and sodar as well as the absence of data on various days from both sources explains the difference between the surface and sodar mean values. In Table 3, the times of onset based on the surface data at the sodar site and the directional shift are shown, as well as the times when the speed and vertical velocity increases occurred.

Table 3. **TIMES OF ONSET FOR THE SEA BREEZE:** sfcso = Onset based on Surface Measurements at the Sodar, sdir = Onset of wind direction shift at Sodar, sspd = speed change at Sodar, svrt = Time of Maximum Updrafts at Sodar. All times in UTC.

Date	sfcso	sdir	sspd	svrt
16	n a	1745	1750	1750
17	1715	1714	1717	1715
18	1750	1748	1813	1750
19	1730	1800	1819	1820
20	n a	1644	1709	1659
21	n a	1729	1749	1750
22	n a	1715	1730	1730
23	1830	1830	1850	1850
25	1945	n a	n a	n a
26	1855	n a	n a	n a
27	1830	1818	1824	1819
29	1800	1756	1801	1801
30	1745	n a	n a	n a
μ	1813	1742	1757	1752

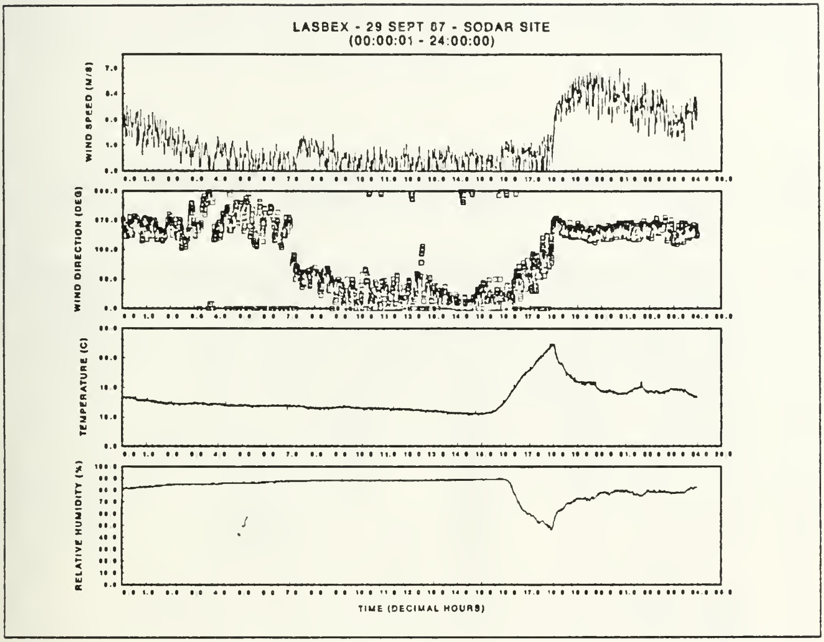

Fig. 6. Surface Data Record from 29 September 1987 at the Sodar Site

b. Height and Duration of the Sea Breeze

The directional gradient which indicates the boundary between the onshore and offshore flow could be followed in the 24-hour contour plots as the sea breeze deepened. The maximum vertical extent of the sea breeze was determined for the 10 cases and had a mean elevation of 659 meters, and ranged between 570 and 800 meters.

The cessation time of the sea breeze was indicated by a counter-clockwise turning of the winds, a decrease in the height of the sea breeze and the establishment of offshore flow. Duration of the sea breeze was the difference between the onset and cessation times determined from the directional data. The mean duration of the sea breeze was 10.7 hours. The longest duration was 13.4 hours and the shortest was 8.1 hours. The mean duration for the sea breeze was also determined using surface data measurements at the lidar and sodar sites. Using the surface data, cessation was when the wind direction was alongshore and the wind speed had dropped to 2 m/s. The mean durations calculated using surface data at the sodar and lidar were 10.2 and 11.4 hours respectively. A summary of maximum height and duration of the sea breeze is given in Table 4.

Table 4. **MAXIMUM HEIGHT AND DURATION OF THE SEA BREEZE**

Date	Maximum Height (meters)	Duration by Sodar (h)	Duration by Surface at Sodar (h)	Duration by Surface at Lidar (h)
16	600	8.1	n/a	n/a
17	725	9	13.0	n/a
18	640	13.4	13.0	12.0
19	800 (est)	13.0	n/a	n/a
20	600	11.3	n/a	11
21	570	n/a	n/a	10
22	680	11.5	n/a	n/a
23	650	8.5	12.0	12.0
25	n/a	n/a	10.0	12.0
26	n/a	n/a	n/a	8
27	625	11.8	11	9
28	n/a	n/a	n/a	8
29	700	12.2	10	10
μ	659	10.7	11.4	10.2

In Fig. 7 on page 25, the increasing height of the sea breeze is clearly shown, as well as the maximum height achieved and the decrease in the height with time.

c. *Slope of Sea Breeze Fronts*

The slope of the sea breeze front was determined for the first kilometer horizontally of the front and for the established sea breeze flow subsequent to the first kilometer. The slope for the first kilometer of the front was calculated by measuring the difference from the 50 meter level to the highest height of the onshore flow in the first kilometer and dividing by the horizontal distance between these points. The slope for the rest of the sea breeze was calculated by measuring the difference between the greatest height in the first kilometer and the greatest height of the onshore flow during rest of the sea breeze. Horizontal distance was calculated by multiplying the time difference be-

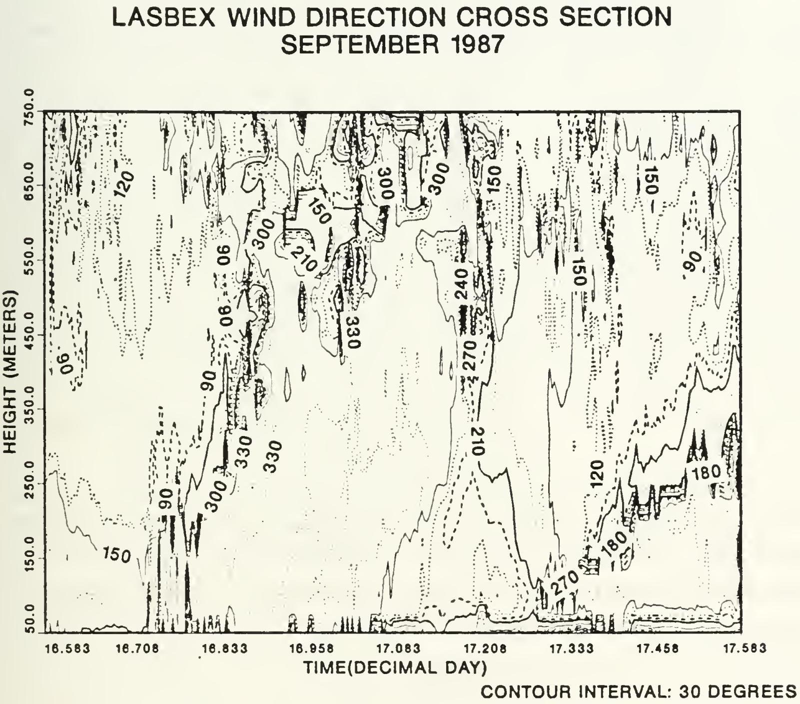

Fig. 7. 24 Hour Directional Plot for 16 September 1987

tween the two heights by the speed of advance of the front. Speeds of advance were found by taking the time difference between time of frontal passage based on the surface data at the lidar and the time of passage at the sodar. For those cases where a speed of advance could not be calculated, the mean speed of advance was used. The mean speed of advance during LASBEX was 2.5 m/s. These speeds are listed in Table 5.

Table 5. SPEED OF ADVANCE OF THE SEA BREEZE FRONT: Times of frontal passage are from the surface data, except in those marked *, which are based on sodar data.

Date	Lidar (UTC)	Sodar (UTC)	Δ t (h)	Speed of Advance (m/s)
18	1720	1750	0.5	3.1
19	1700	1730	0.5	3.1
20	1530	1644*	1.5	1.0
21	1700	1729*	.48	3.2
23	1700	1830	1.5	1.0
25	1915	1945	0.5	3.1
26	1815	1855	0.67	2.3
27	1800	1830	0.5	3.1
29	1708	1750	0.7	2.2
30	1730	1800	0.5	3.1
μ	1724	1806	0.74	2.5

In the first kilometer, the mean slope was 1:12 for strong offshore flow and 1:10 for weak flow. The typical slope after the first kilometer was 1:94 for strong offshore flow and 1:160 for weak offshore flow. All the values except the subsequent slope for the weak cases are similiar to ones cited in Simpson et al. (1977), which were 1:4 and 1:10 for the first kilometer and 1:100 for the subsequent portion of the sea breeze. However, there were no slopes on the order of the one reported by Helmis et al. (1987), which had a slope of 1:3 in the first kilometer. There appears to be no correlation between the degree of slope in the first kilometer and subsequent to passage. That is, a strong slope in the first kilometer did not mean that the rest of the sea breeze also had a sharp slope, and vice versa. This indicated that the sea breeze was very dynamic and its velocity and structure changed throughout its duration. The slopes for the sea breeze fronts during LASBEX are summarized in Table 6.

Table 6. SLOPE OF THE SEA BREEZE FRONT: μ_s = mean of strong offshore flows. μ_w = mean of weak offshore flows.

Date	Slope in first kilometer	Slope after first kilometer	Offshore Flow (Strong or Weak)
16	1:17	1:87	Strong
17	1:5	1:158	Weak
18	1:8	1:205	Weak
19	1:6	1:153	Strong
20	1:11	1:110	Strong
21	1:9	1:59	Strong
22	1:14	1:58	Weak
23	1:11	1:220	Weak
27	1:15	1:100	Strong
29	1:16	1:56	Strong
μ_s	1:12	1:94	n/a
μ_w	1:10	1:160	n/a

2. Wind Speed

a. Synopsis of Wind Speed Data During LASBEX

A characteristic of the sea breeze that was investigated during this study is the difference in time between the change of wind direction and the increase in wind speed and whether or not this time difference was affected by the previous offshore flow. The general structure of the wind speed field was also compared with the wind direction field to see whether features, such as shear zones, indicated in one agreed dimensionally with the other, that is if the height and width of the shear zone in one case was similar to the other.

The wind speed data were plotted with contour intervals of two meters per second for the 24 hour plots and one meter per second for the shorter plots. These plots were analyzed for a continuous increase of wind speed with time. The mean time of wind speed increase at the sodar site was 1757 UTC or 17 minutes after the shift in wind direction. The mean temporal gradient was a 1 m/s change over 55 minutes for strong offshore flow and 1 m/s over 21 minutes for a weak offshore flow. In this case, the findings do not agree with Pearson's (1983) model that shows no relation between the intensity of the mean flow and the intensity of the sea breeze circulation. The results from LASBEX point to the shortcomings that a model has in trying to represent a dynamic flow such as the sea breeze circulation.

There was a shear zone at the boundary between the sea breeze and the offshore flow. The vertical gradient of this shear zone was a 1 m/s change over 40 meters for the strong case and 1 m/s over 44 meters for the weak offshore flows. The level of the wind speed shear correlated with the level of the wind direction shear. Table 7 lists the gradients in speed.

Table 7. GRADIENTS OF WIND SPEED AT THE SEA BREEZE FRONT: μ_s = mean of strong offshore flow, μ_s = mean of weak offshore flows.

Date	Temporal Speed ∇(m/s/min)	Vert. Speed ∇(m/s/m)	Offshore Flow (Strong or Weak)
16	1/96	1/40	Strong
17	1/22	1/46	Weak
18	1/40	1/50	Weak
19	1/34	1/35	Strong
20	1/100	1/24	Strong
21	1/66	1/36	Strong
22	1/15	1/20	Weak
23	1/6	1/58	Weak
27	1/21	1/55	Strong
29	1/10	1/50	Strong
μ_s	1/55	1/40	n/a
μ_w	1/21	1/44	n/a

3. Wind speed after frontal passage

The mean wind speed within three hours after frontal passage during LASBEX was 5.3 m/s for strong offshore flows and ranged between 4 and 6 m/s. The mean for weak offshore flow was 7 m/s and was between 6 and 10 m/s. The wind speeds of the sea breeze reached maximum intensity about the same time as maximum height was achieved. The mean maximum speeds during the entire duration of the sea were 8.3 m/s for stong flows and 7 m/s for weak flows. The maximum speeds ranged between 6 and 10 m/s. Offshore flow was clearly present before the onset of the sea breeze. This flow was considered the established land breeze and was usually confined below 400 meters. The mean speed of the strong offshore flow was 6.3 m/s and the mean of the weak offshore flows was 2.0 m s. All the weak offshore flows were 2 m s or less, while the strong offshore flows were between 4 and 8 m s. Table 8 on page 29 gives the various maxima of wind speed.

Table 8. MAXIMUM WIND SPEEDS DURING THE SEA BREEZE AND MAXIMUM OFFSHORE FLOW: μ_s = mean of strong offshore flows. f.mu sub w = mean of weak offshore flows.

Date	Maximum Speed after onset (m's)	Maximum during Sea Breeze (m s)	Maximum Previous Offshore Flow (m s)	Offshore Flow (Strong or Weak)
16	6	10	8	Strong
17	6	6	2	Weak
18	6	6	2	Weak
19	4	10	6	Strong
20	6	10	6	Strong
21	4	6	4	Strong
22	10	10	2	Weak
23	6	6	2	Weak
27	6	6	8	Strong
29	6	10	6	Strong
μ_s	5.3	8.7	6.3	n a
μ_w	7	7	2	n a

As the sea breeze established itself, the top of the onshore breeze increased until it assumed a relatively constant elevation. Above the this level, the return flow which completes the sea breeze circulation was detectable by the sodar. Since the sodar signal had little data past 750 meters, the extent and characteristics of the return flow could not be determined. However, the information from the lidar clearly showed offshore flow on 16 September that began around 400 meters and extended vertically up to 1600 meters.

4. Vertical Velocity Structure

a. Vertical Velocity Maxima and Location of the Updraft Region

The vertical velocity was investigated in order to determine the strength and location of the updraft region in the sea breeze front. Vertical velocity cross-sections showed good correlation with both the wind direction and speed cross-sections. The maximum in upward vertical velocity occurred after the wind direction change and about the same time as the increase in wind speed (see Table 3 on page 22). The occurrence of the updraft region indicated the front of the longitudinal vortex which is the major current within the sea breeze frontal circulation. The mean maximum vertical velocity observed after frontal passage was 0.56 m/s, with the range of velocities between 0.2 and 1.0 m/s. This vertical velocity is much smaller than the maximum velocity observed by Ogawa et al. (1986) of 3.0 m/s; but similar to the values reported by Simpson et al. (1977) of 0.7 to 3.0 m/s and the average value that Helmis et al. (1987) observed of 0.5 m/s. A summary of the vertical characteristics of the sea breeze is contained in Table 9.

Table 9. VERTICAL MOTION CHARACTERISTICS OF THE SEA BREEZE

Date	Max. Vert. Extent (m)	Max. Vert. Velocity (m/s)	Location of Max. Velocity	Offshore Flow (Strong or Weak)
16	225	0.6	50-150	Strong
17	350	0.4	100-275	Weak
18	370	1.0	50-250	Weak
19	270	0.4	50-200	Strong
20	150	0.6	50-175	Strong
21	200	0.6	50-175	Strong
22	335	0.6	75-225	Weak
23	380	0.8	75-350	Weak
27	220	0.6	50-150	Strong
29	175	0.2	50-150	Strong
μ	207	0.5	50-167	n/a
μ_w	359	0.7	75-275	n/a

The location of the vertical velocity maximum within the sea breeze front/gravity head structure is shown in Fig. 8, where the longitudinal vortex turns upward.

The location of the updraft region was found to be related to the height of the sea breeze front, which in turn was related to the strength of the previous offshore flow. The mean location of the maximum vertical velocity was at 207 meters in strong offshore flow and 359 meters in weak offshore flows. When offshore winds were strong before the sea breeze, the updraft region started at a lower elevation and died out at an

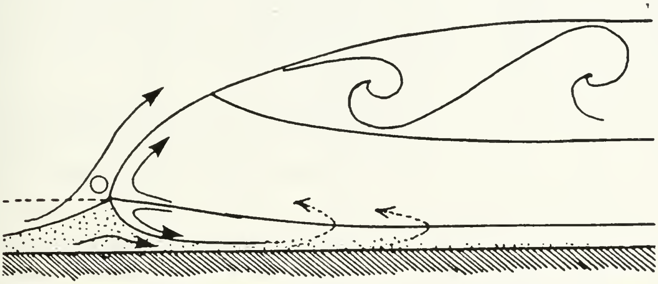

Fig. 8. Flow regions of the Gravity Head: The stippled region is where the opposing flow is being overrun by the gravity head current (from Simpson and Britter,1980)

average of of 183 meters, and when the winds were weak, the updraft began around 75 meters and died out around 250 meters. These conditions both agree with the gravity head structure in prevailing flow that was observed by Simpson and Britter (1980). In a strong opposing current, the gravity head is flatter with the flow constrained to a shallower region than in onshore or weak offshore flow. The leading edge of the onshore flow also tends to have a more pronounced "knee" where it is overriding the counter-flow. (see Fig. 5 on page 21) The updraft in the onshore flow is higher, indicating some influence from the counter-flow. Fig. 8 shows how the updraft is affected by the overrunning and elevated region at the front of the gravity head flow. The "knee" structure of the gravity head current was apparent in all the sea breeze fronts investigated during LASBEX.

5. Variations of the Vertical Velocity

The standard deviation of the vertical velocity was used to determine those areas of the sea breeze front that were the most turbulent. The standard deviation is higher in turbulent regions and near zero in non-turbulent stable layers. The values for σ_w were directly generated by the PSU sodar. These values were read and plotted in the same manner as the other parameters. Generally, the values of σ_w decreased with height, which indicated a reduction in the amount of turbulence. Vertical velocity fluctuations were damped by the boundary at the base of the inversion. Table 10 on page 33 shows the change of σ_w across the front at 80 meters.

The values of σ_w did not consistently decrease with time at the lower levels (i.e $<$ 100 m) after the passage of the sea breeze front. In the majority of the cases, the value of σ_w increased by an average of 0.17 m/s, with other maxima occurring at various time in the established sea breeze flow. The changes in σ_w were between -0.1 and + 0.4 m/s. Helmis et al. (1987) observed that the values of σ_w decreased after the passage of the sea breeze, whereas, Ogawa et al. (1986), found that the values increased across the front. The explanation given by Helmis was that the times of onset and the location are the governing factors in the degree of turbulence generated by the sea breeze. In the case of LASBEX, the onset of the sea breeze occurred early in the day. The variation in vertical velocity was mainly due to mechanical mixing at and within the front. Helmis observed sea breezes that passed in the early afternoon. The sea breeze in this case acted to decrease the amount of thermal activity caused by the heated land. There appeared to be no correlation between the strength of the previous offshore flow and the change of σ_w across the front. In the case study for 16 September, the behavior of σ_w will be investigated.

F. DERIVED DATA TIME-HEIGHT CROSS SECTIONS

1. Horizontal Divergence

Since the sea breeze front is an area of strong convergence, it was logical to calculate the intensity of the convergence from the velocity fields. The horizontal divergence was calculated using the vertical velocity field according to equation (3.6). The divergence calculation using the vertical velocity field was straight forward, since the sodar produced velocities as a function of z.

Table 10. STANDARD DEVIATION OF VERTICAL VELOCITY ACROSS THE SEA BREEZE FRONT

Date	σ_w Before	σ_w After	Increase or Decrease	Offshore Flow (Strong or Weak)
16	0.9	0.8	↓	Strong
17	0.8	0.8	no change	Weak
18	0.9	1.3	↑	Weak
19	1.0	0.9	↓	Strong
20	0.7	0.9	↑	Strong
21	1.0	0.8	↓	Strong
22	0.7	0.8	↑	Weak
23	0.7	0.8	↑	Weak
27	0.8	0.9	↑	Strong
29	0.6	0.7	↑	Strong
μ_i	0.73	0.90	0.17	n a
μ_u	0.97	0.83	0.14	n a

Lyons and Olsson (1973) calculated and plotted horizontal divergence in time-distance coordinates, using the u-component of velocity based on the assumption that all variations occurred along a two-dimensional axis (i.e. $\partial v/\partial y = 0$), according to the continuity equation. The maximum values for convergence that they calculated at the lake breeze front was on the order of $2 \times 10^{-3}s^{-1}$. The values of convergence calculated during LASBEX exceeded $4 \times 10^{-3}s^{-1}$ at the head of the front, and at times were as much as $12 \times 10^{-3}s^{-1}$. The values calculated from the vertical velocity field of the sodar are believed to be a better representation of the actual divergence along sea breeze front, because the values of vertical velocity were directly measured. The lake breeze studied by Lyons and Olsson had lower computed values of maximum vertical velocity, around 0.105 to 0.130 m s, whereas during LASBEX, maximum vertical velocities were almost an order of magnitude larger (i.e. 0.8 to 1.0 m's). This is further evidence that Lyons' and Olsson's calculations may have been low and that the assumption of two-dimensional flow was perhaps incorrect. Fig. 9 on page 35 shows the typical divergence plots from Lyons and Olsson. Fig. 10 on page 36 is an example of the horizontal divergence calculated from the vertical velocity field on 20 September 1987.

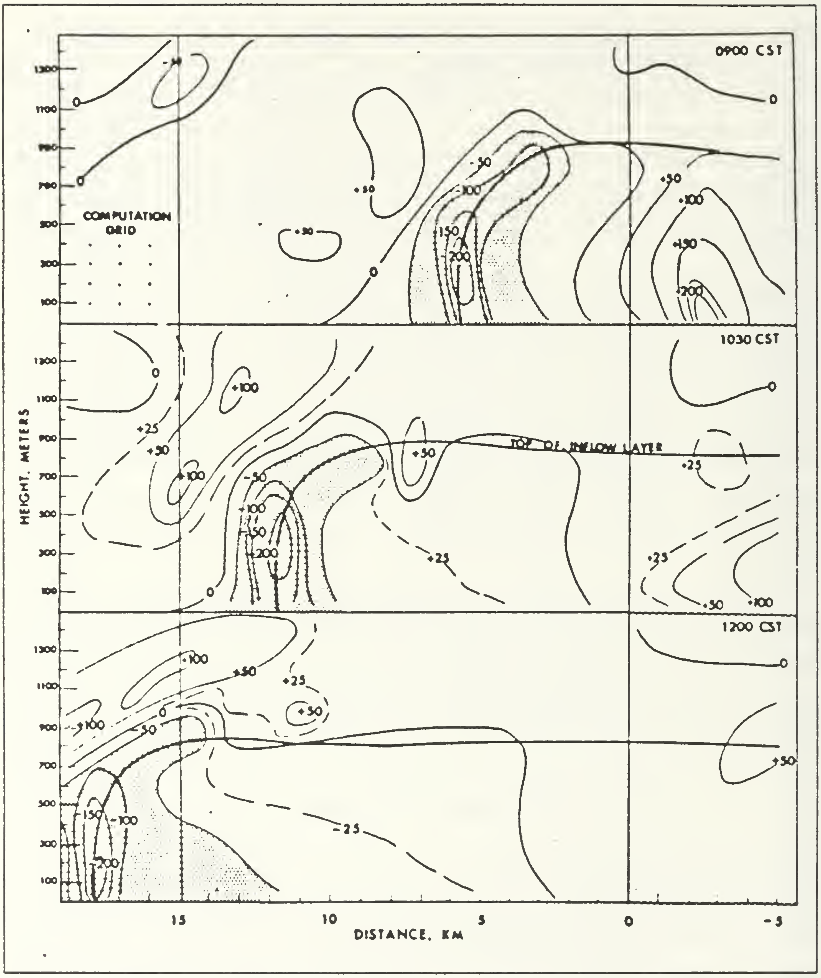

Fig. 9. Divergence values of the Chicago Lake Breeze Study: Contour interval is $50 \times 10^{-5} s^{-1}$. Shaded areas indicate convergence. (from Lyons and Olsson, 1973)

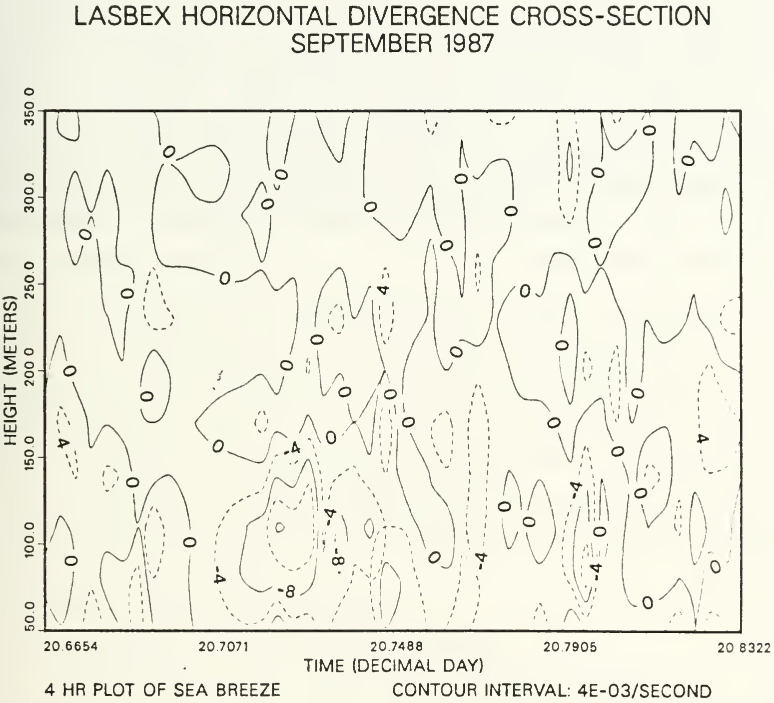

Fig. 10. Divergence values of the LASBEX Study: Convergence at the front occurs near 20.7071 decimal day.

2. Turbulent Kinetic Energy (TKE)

Since turbulence and mechanical mixing is highest within the head of the sea breeze front, the locations of maximum TKE should coincide with those regions of strong shear, strong convergence, or overturning flow that creates turbulent eddies. A general view of these regions was conducted using the standard deviations from the velocity fields. The contours for TKE were calculated by squaring the standard deviations from the three velocity components obtain their variance for substitution in equation (3.7). The values of TKE were then plotted in two hour format. TKE values were found to be highest at the base and top of the gravity head, where the longitudinal vortex is overturning and interacting with both the opposing flow and the vertical shear region above the gravity head, corresponding to the area where horizontal flow is directed upwards and into the shear zone within the gravity head. The case study for 16 September will show these characteristics.

IV. CASE STUDY OF THE SEA BREEZE ON 16 SEPTEMBER 1987

A. MOTIVATION FOR STUDY

September 16, 1987 proved to be an unusual day since the sodar detected the passage of two sea breeze fronts. The sea breeze front that passed in the morning is the subject of this case study. The late sea breeze is currently under further investigation. Since the 16th was unusual, WPL provided the lidar information gathered during the two sea breeze passages. Surface observations and radiosonde observations were not available, but were deemed unnecessary in the comparison of the wind field structure of the sea breeze that was detected by both the lidar and the sodar.

B. SYNOPTIC CONDITIONS

On 16 September, a sea level high pressure center of 1031 mb was located in the eastern North Pacific Ocean, northwest of California, along with a weaker high pressure over Arizona. A thermal trough was present in the Central Valley of California and intensified during the day, which led to alongshore flow in the afternoon. Winds were generally from the northwest along the coast, with a reported wind speed of 5 m/s from due west at Monterey in the morning. The wind shifted to the northwesterly in the afternoon. Skies were generally clear on the the 16th. The temperature was 56° F at 4 a.m. local and rose to a maximum of 76° F later in the day. Fig. 11 on page 38 shows the synoptic conditions for this day.

C. WIND FIELD DATA AND ANALYSIS

1. Wind Direction and the Onset of the Sea Breeze

The wind direction cross-section for 16 September was checked for a strong change in wind direction with time that indicated the passage of the sea breeze front. The onset of the sea breeze occurred at 1753 UTC (0953 PST). At onset, the wind direction veered from 180° to 300°. The temporal wind direction shift in this case was 90° in 12 minutes. The wind direction cross-section is shown in Fig. 13 on page 41. Following this directional shift, a perturbation in wind direction occurred directly behind the front. The wind direction in this pertubation at 50 meters was 120°, and was considered to be the offshore flow being overriden at the base of the sea breeze front. The presence of this pertubation may possibly be explained by the "lobe" and "cleft" structure that has been observed in the three-dimensional gravity head current. This pertubation

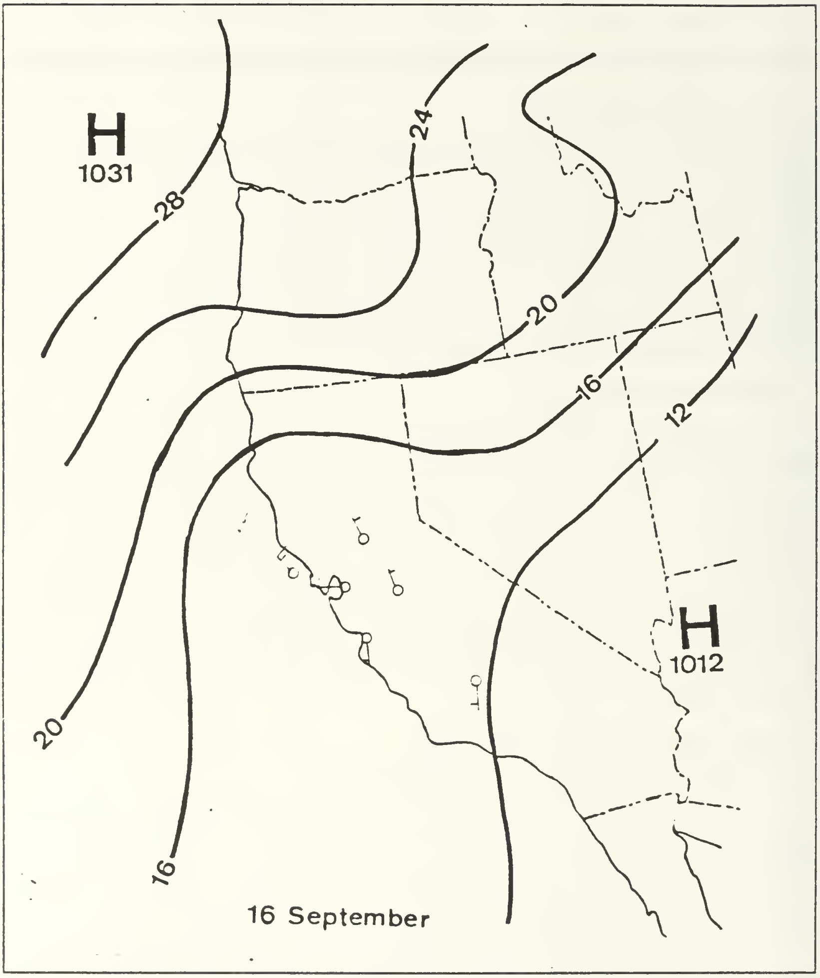

Fig. 11. Synoptic Situation on 16 September: Solid lines are isobars.

is the area where the opposing current penetrates the gravity current head and causes a "cleft" in frontal boundary. The "lobe" is the location of strongest flow at the front of the longitudinal vortex. If a "cleft" passed the sodar site, the wind direction would change rapidly as the onshore flow of the sea breeze was interrupted by the opposing flow and back to the onshore direction as the sea breeze is reestablished. The "lobe" and "cleft" structure is shown in Fig. 12.

A complete directional shift of larger scale occurred about 16.78 decimal day (1843 UTC). The wind direction backed with decreasing height, and reached 60° at 50 meters. This region was at the same location as a maximum in downward vertical velocity. A possible explanation for this area of directional shift with height is that the descending air from the overturning leg of the longitudinal vortex affected the horizontal integrity of the flow. The shift in wind direction occurred within the confines of sea breeze front which was defined by the directional shear region at its boundaries. The structure of the vertical velocity field which complements the wind shift region will be discussed later in section 4.3.

The height of the directional shear zone slowly increased with time. The gradient in the this zone was 180° over 83 meters and showed that the layer of marine air deepened as the sea breeze became well established.

2. Wind Speed

In Fig. 14 on page 42, the increase in wind speed began at 16.75 decimal day (1800 UTC). The wind speed slowly increased from 2 m/s to 3 m/s in about 30 minutes. The offshore flow on 16 September was above 8 m/s at 450 meters, with speeds greater than 4 m/s down to 250 meters. When cross-sections were compared, the change in wind speed occurred immediately after the change in wind direction. Helmis (1987) observed a wind speed change from 3 m/s to 5 m/s in about four minutes across a sea breeze front with offshore flow of 5 m/s and a change from 2 m/s to 3 m/s over 15 minutes with flow parallel to the shore.

The speed shear zone dividing the onshore and offshore flow was located between 250 and 350 meters. Helmis et al. (1987) found that the top of the inflow layer was between 100 and 200 meters; Simpson et al. (1977) observed that the speed shear zone was near 600 meters at the head of the sea breeze front and decreased to 300 meters after the front had passed; Lyons and Olsson (1973) observed average inflow layer heights of 500m, ranging between 100 and 1000 meters; and Ogawa et. al. (1986) observed that the speed shear layer was between 150 and 320 meters.

The strong offshore flow (> 4 m/s) was above 250 meters and decreased in intensity with time as the height of the sea breeze increased. In Fig. 15, the maximum

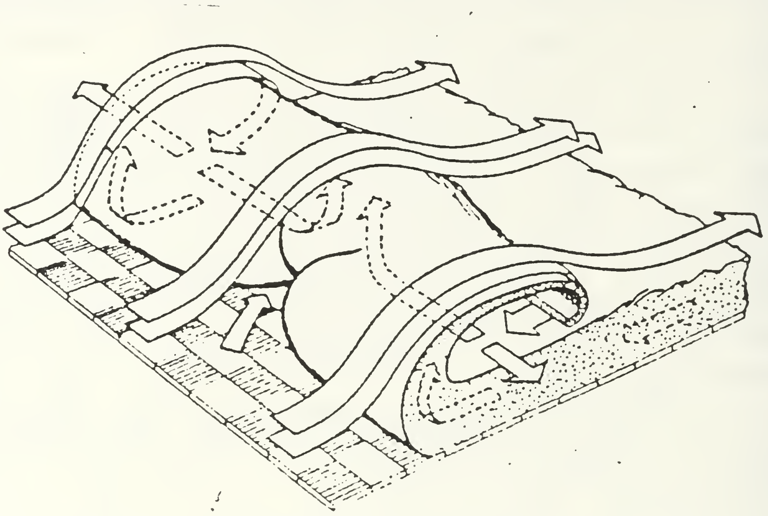

Fig. 12. Three Dimensional View of a Gravity Current Head: The "lobe" and "cleft" structure is shown. (from Simpson et. al.,1977)

wind speed after frontal passage was 10 m/s at 500 meters around 17.00 decimal day (2400 UTC). The maximum wind speed observed by Simpson et al. (1977) during a sea breeze was 5 m/s under 200 meters; by Johnson and O'Brien (1973) was 7.5 m/s at an elevation of 300 meters; by Lyons and Olsson (1973) was 6.5 m/s at 200 meters; and by Ogawa et al. (1986) was 5.5 m/s between 100 and 200 meters. The top boundary of the sea breeze flow was not as clearly evident in the wind speed cross-section as it was in the wind direction cross-section, but there was a wind speed transition around 550 meters. The wind maximum of 8 m/s above this level was associated with the offshore flow.

3. Vertical Velocity

In Fig. 16 on page 45, a maximum upward velocity of 0.6 m/s occurred shortly after 16.75 decimal day (1800 UTC) and coincided with a "bump" in the wind direction contour plot. This "bump" indicated the highest vertical extent of the gravity head structure and was present in all the sea breeze fronts that passed the sodar site.

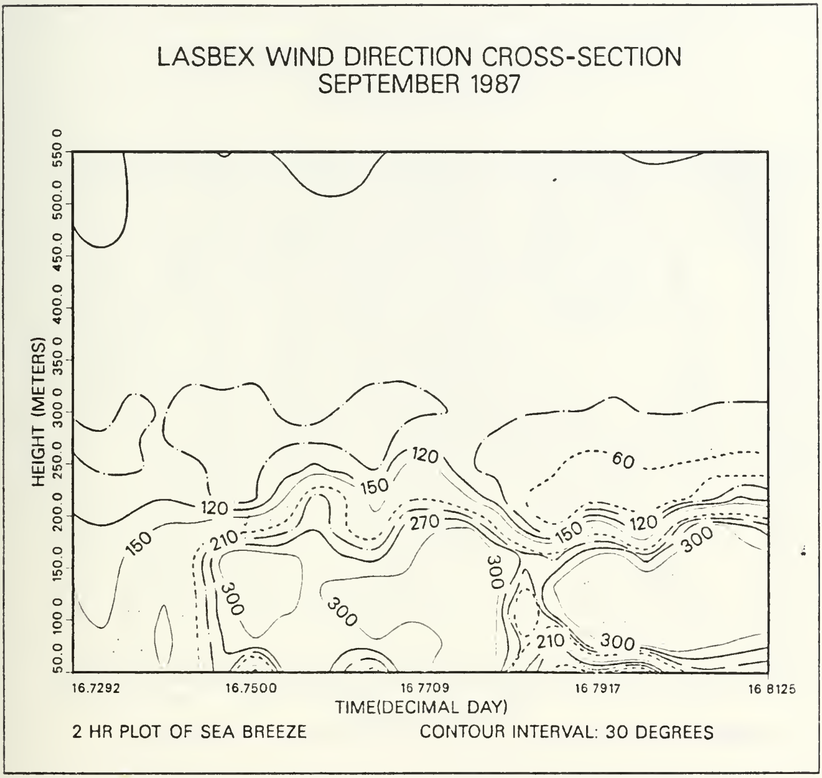

Fig. 13. Two-Hour Cross-Section of Wind Direction (16 September 1987): Plot begins at 1730 UTC through 1930 UTC.

Maximum upward vertical velocities of 3 m s were observed by Ogawa et al. (1986) and of 1.5 m s by Helmis et al. (1987). The top of the vertical velocity maximum, which is marked by the zero vertical velocity, coincided with the bottom of the shear zone in the direction and speed cross-sections. From the direction, speed and vertical velocity cross-sections, the elevation at the head of the sea breeze front on 16 September was between 180 and 220 meters. The depth of this same region observed by Simpson et. al. (1977) was approximately 600 meters. The updraft region was located between 50

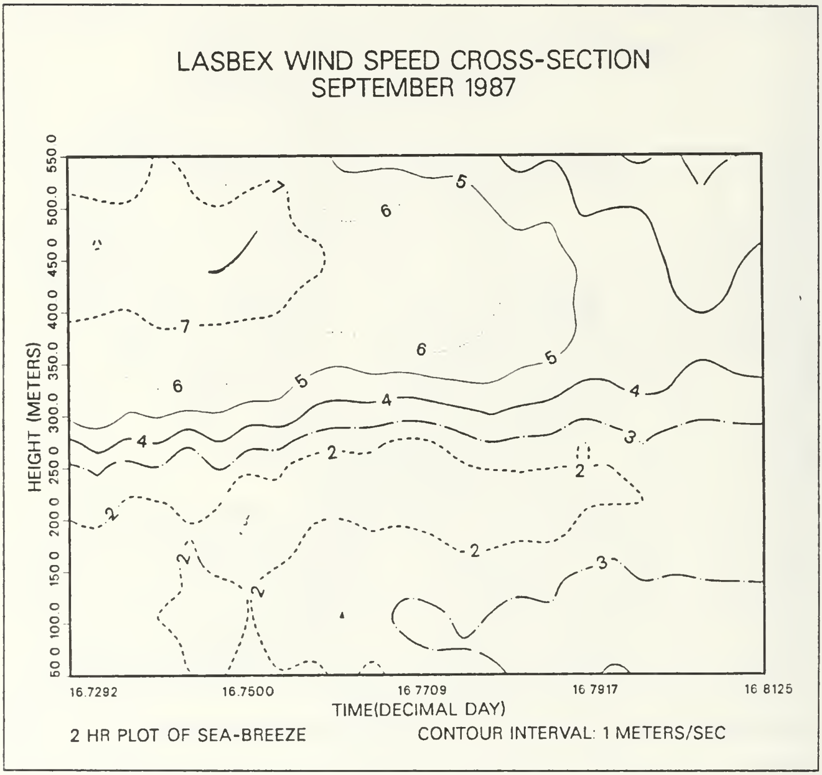

Fig. 14. Two-Hour Cross-Section of Wind Speed (16 September 1987)

and 150 meters. Helmis et al. (1987) observed an updraft region that was from the surface up to 150 meters.

A region of downward vertical velocity was present around 16.7917 decimal day (1900 UTC). The maximum downward velocity in this region was -0.4 m/s. This was consistent with descending flow in the rear leg of the longitudinal vortex within a gravity head current. Using a mean advance of 2.54 m/s for the sea breeze fronts during LASBEX, the horizontal extent of the longitudinal vortex on 16 September was 8.1 km. This dimension is similar to the 7 km longitudinal vortex described by Simpson et al.

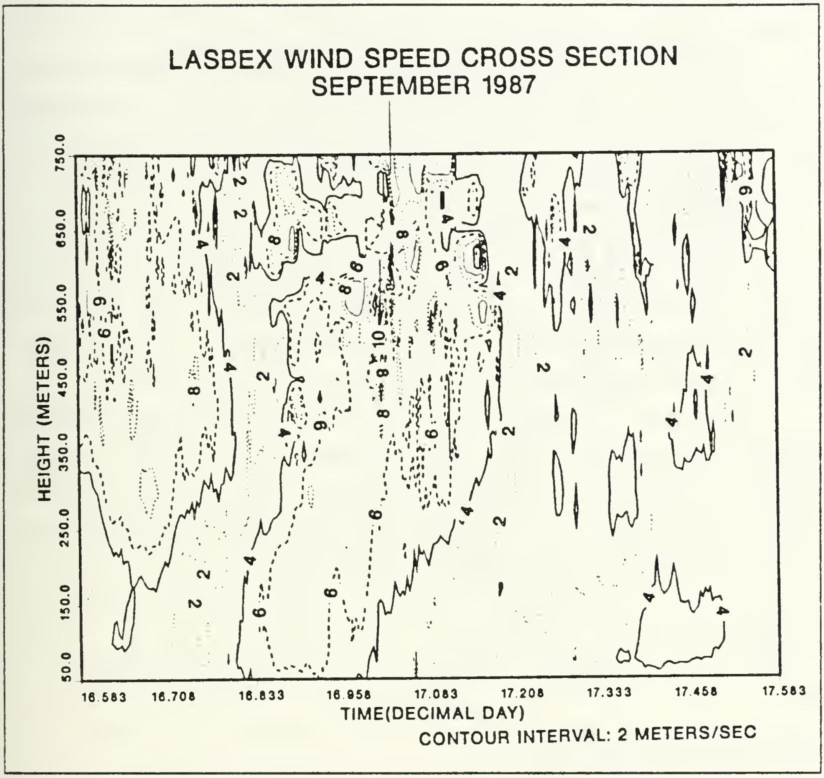

Fig. 15. 24-Hour Cross Section of Wind Speed (16 September 1987)

(1977). This vortex is an oblong circulation that is located fully within the the sea breeze front. The vortex observed on 16 September was a third as deep as the vortex observed by Simpson. This difference between the depths of the vortices was probably due to the strength of the offshore flow on 16 September, which was up to 8 m/s. This strong offshore flow flattened the front and restricted the depth of the onshore flow. The descending leg of the longitudinal vortex observed on 16 September also showed up in the wind direction cross section. In Fig. 13. there was a strong temporal gradient of the wind direction at 1850 UTC, in the region where the vertical velocity has a gradient of

0.4 m s over 5.6 minutes. This location is where vertical motion changed from ascent to descent.

About 16.7917 decimal day (1900 UTC), the vertical velocity contours indicated the area where the sea breeze was reestablished after the penetration of the descending leg of the longitudinal vortex. This evidence supports Simpson's theory that the gravity head current is a possible description of the actual sea breeze frontal structure.

4. Standard Deviation of Vertical Velocity

The location of the strongest fluctuations in the vertical velocity is shown in Fig. 17 on page 46. The highest standard deviations of vertical velocity occurred at the base of the sea breeze front and around the upward leg of the longitudinal vortex. In fact, the whole region of the sea breeze front showed the highest values of standard deviation, indicating strong turbulence and vertical velocity fluctuations in this area.

The behavior of σ_w within the boundary layer has been found to follow certain relationships (Caughey and Palmer, 1979). Since the σ_w field was available, this relationship was investigated. In Caughey and Palmer, σ_w was normalized using the scaling velocity w_*. Scaling velocity in the convective boundary layer is determined from the heat flux based on the following equation (Ogawa et al.,1986):

$$w_* = \left(\frac{g}{\bar{\theta}}\,\overline{w'\theta'}_0 z_i\right)^{1/3}, \tag{4.1}$$

where

g = acceleration due to gravity (ms^{-2}),

$\bar{\theta}$ = mean potential temperature in the boundary layer ($^\circ C$),

$\overline{w'\theta'}_0$ = sensible heat flux at surface ($ms^{-1}{}^\circ C$)and

z_i = depth of the mixed layer (m).

The value of w_*, could not be calculated since heat flux data were not available. However, over a period 30 minutes, the change in heat flux was considered to be negligible and, therefore, the value of w_* was also taken to be constant. The value of z_i was found as the height on the σ_w cross-section which was indicative of the base of the inversion (i.e. where the values are decreasing quickly towards 0).

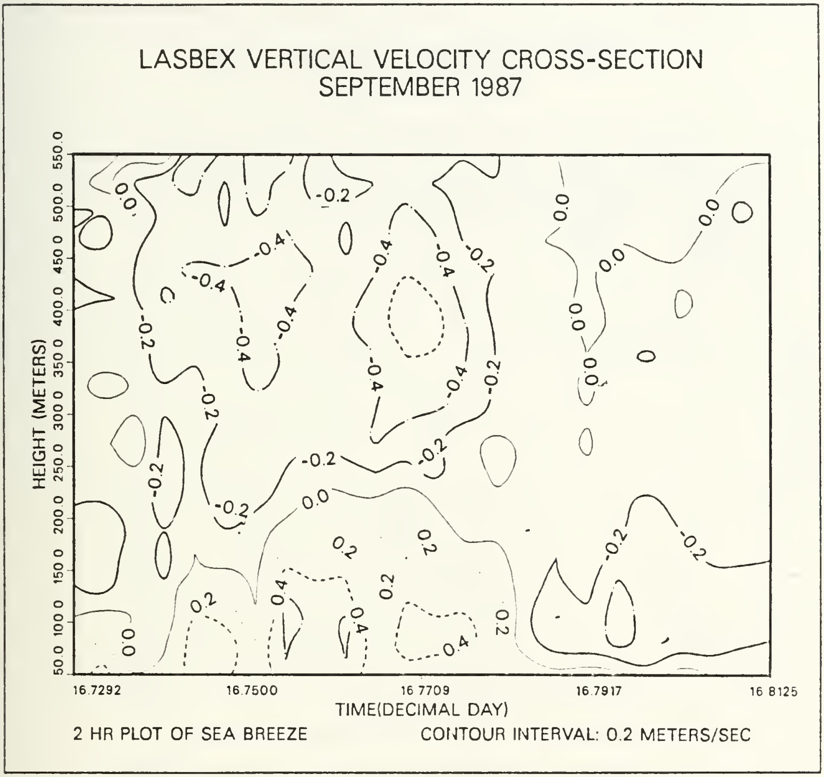

Fig. 16. Two-Hour Cross-Section of Vertical Velocity (16 September 1987)

The values of σ_w were plotted versus z/z_i to compare with Ogawa et al. (1986). The emphasis of this comparison was on the distribution of σ_w. In Fig. 18 on page 47 and Fig. 19 on page 48, the maximum value in σ_w occurred at $z/z_i = 0.25$ for the prefrontal case and at $z/z_i = 0.3$ for the postfrontal. The heat flux was allowed to vary, so that the maximum in Caughey and Palmer's (1979) curve matched the variance of the acoustic sounder values of σ_w are at a maximum in comparison with z/z_i. The plot by Ogawa et al. (1986) is shown in Fig. 20 on page 49.

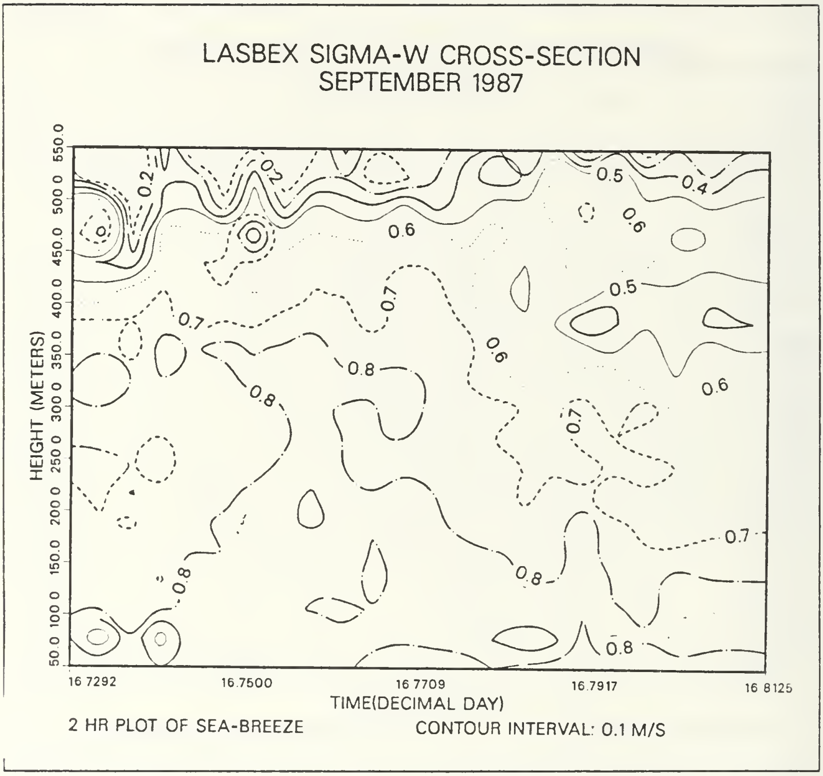

Fig. 17. Two-Hour Cross-Section - Standard Deviation of w (16 September 1987)

Ogawa observed that the maximum value of the normalized σ_w occurred at $z/z_i = 0.3$. The values of σ_w decrease with height as Fig. 20, which contains the free convection case as described by Caughey and Palmer (1979). Contrary to Ogawa, the values of σ_w in the LASBEX plots did not fall off as dramatically with height and at times actually increased with height. This was because of the strong offshore flow above 400 meters on 16 September caused more turbulence above the inversion. The wind profile that Ogawa observed decreased in intensity with height above the inversion, which gave lower values of σ_w.

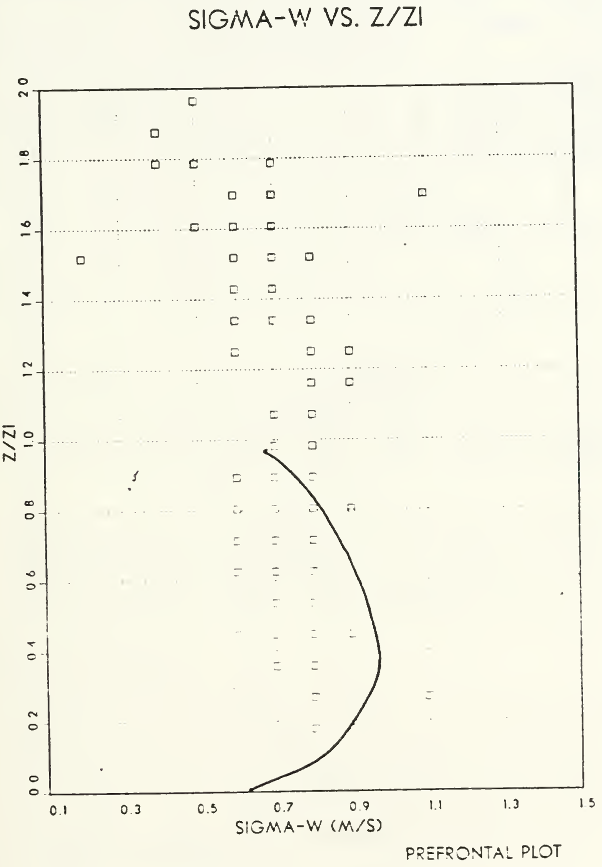

Fig. 18. Standard Deviation of w on 16 September: σ_w versus z/z_i for the Prefrontal Case. Solid curve = Caughey and Palmer (1979)

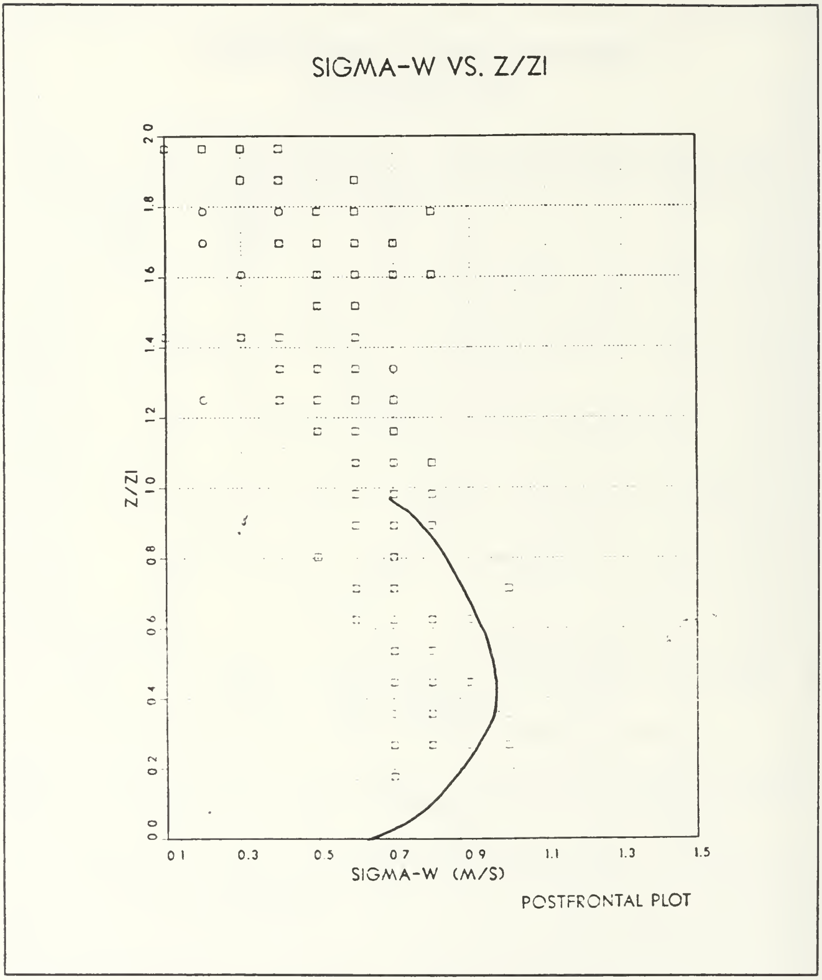

Fig. 19. **Standard Deviation of w on 16 September:** σ_w versus z/z_i for the Postfrontal Case. Solid curve = Caughey and Palmer (1979)

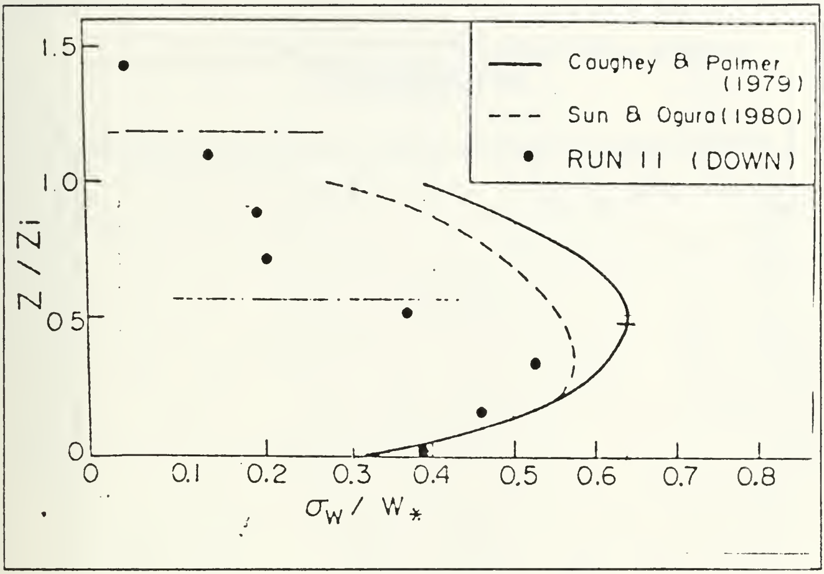

Fig. 20. Standard Deviation of w normalized: σ_w normalized versus z/z_i. Solid curve = Caughey and Palmer (1979). (from Ogawa, 1986) .

5. Horizontal Divergence

The divergence cross-section for the 16 September is shown in Fig. 21 on page 51. When compared with the wind direction cross-sections, the horizontal divergence cross-section showed an area of convergence at the head of sea breeze front. Fig. 21 shows that the maximum values of convergence occurred at the head of and within the sea breeze front. Values of convergence in these regions were up to $8 \times 10^{-3}s^{-1}$. The first region is located at the top of the maximum in vertical velocity and the second is located where the the longitudinal vortex is turning back into the foward flow. What is particularly notable is that this cross-section showed that the convergence followed the wind shift boundary of the sea breeze front outlining the boundary of the gravity head structure, similar to the divergence fields of Lyons and Olsson (1973).

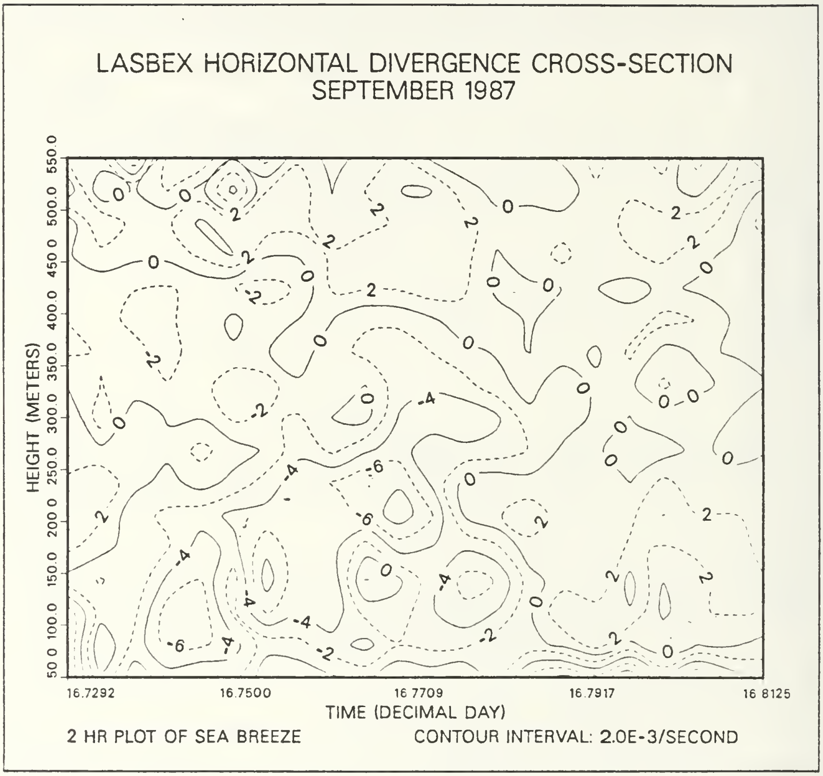

Fig. 21. Two-Hour Cross-Section of Horizontal Divergence (16 September 1987)

6. Turbulent Kinetic Energy

The cross-section of the TKE for 16 September showed that the highest values were located in the sea breeze front where mechanical mixing and vertical motion generated the greatest turbulence. The actual maxima in turbulent kinetic energy were located in the region where the overturning air turned back into the forward flow and at the strong shear zone near the base of the front. The TKE cross-section for this day is shown in Fig. 22 on page 52.

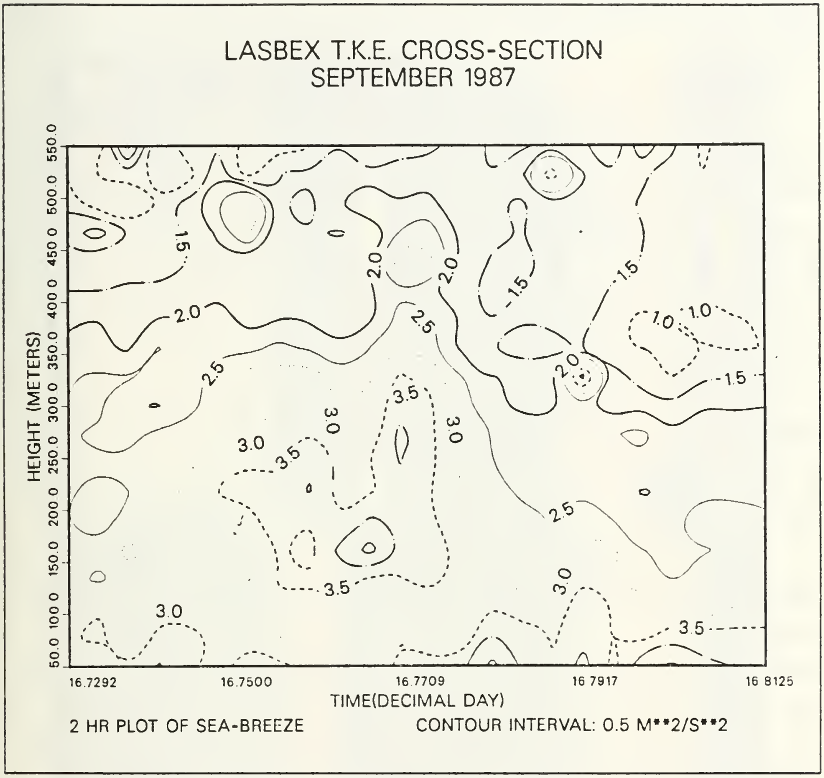

Fig. 22. Two-Hour Cross-Section of Turbulent Kinetic Energy (16 September 1987)

D. LIDAR DATA

1. Color Coding

Color coding was used on the WPL lidar plots to show the intensity and direction of the radial velocity field. "Cool" colors were used for velocities towards the lidar, whereas "warm" colors were used for velocities away from the site. The colors in each case were graduated with the "cool" velocities graduated from green to blue to purple, with green indicating slower speeds and purple indicating the highest speeds. The graduation for the "warm" colors was from tan to yellow to red, with tan being the slowest speeds and red the highest speeds. White was used to indicated zero radial velocities.

2. RHI Plots

The lidar information available for 16 September 1987 closely agreed with the wind field produced by the sodar. The RHI on this day was primarily oriented on a line of 90°. The separation between the low level sea breeze and the intense offshore flow was clearly indicated. The depth of this offshore flow started at 500 meters and had a depth of 1200 meters. The flow above 2 km was onshore. About 1722 UTC, there was an indication that the sea breeze front was moving away from the lidar site. This is shown in Fig. 23 as an increase in the speed of the flow moving away from the lidar to the east (right side of picture) at the lowest levels.

By 1735 UTC, the sea breeze had an estimated depth of about 200 meters, based on the height of the radial velocity field in the lowest layer. This agreed with the depth of the onshore flow determined by the sodar, which was between 200 and 250 meters. The actual location of the sea breeze front was not determined due to the spatial resolution of the output information.

There was one RHI view of the sea breeze oriented down the Salinas Valley of 140&degree; it is shown in Fig. 24. The onshore flow was easier to detect at this orientation because it showed up as a deeper and stronger flow both towards and away from the lidar. The speed of the offshore flow from the Salinas Valley was weaker, with a radial velocity of 4 m/s. The strong flow above the sea breeze (> 6 m/s) was believed to be due to the geography of the area and is explained in the next section.

3. PPI Plots

The PPI plots give a better indication of the offshore flow region and the progress of the sea breeze front. The 5° elevation angle plots show a velocity maximum at 520 meters of 8 m/s. This is shown in Fig. 25 as a velocity maximum towards the lidar from the northeast and the corresponding maximum away from the lidar towards the southwest. The elevation and orientation of this radial velocity maximum corresponded very well with the sodar wind direction and wind speed cross-sections. A region of wind speed of 7 m/s with a direction between 60° and 90° was present above the sodar site at the same time as the radial velocity maximum was above the lidar site. (Refer to Fig. 13 on page 41 for the wind direction and Fig. 14 on page 42 for the wind speed.)

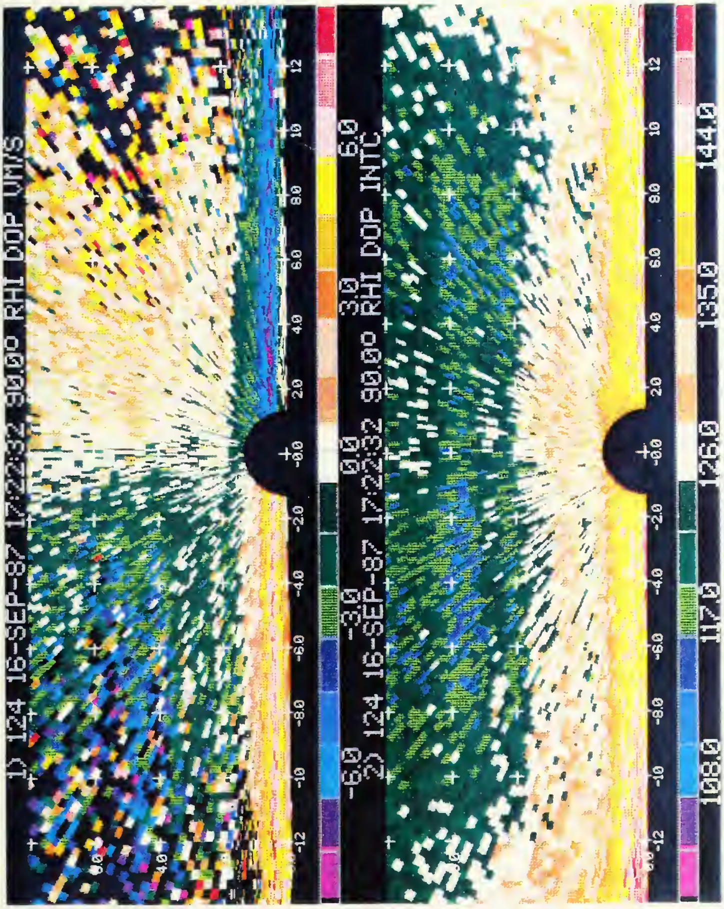

Fig. 23. **RHI Lidar Display at 1722 UTC, 16 September 1987:** Top picture is the RHI display. The lidar is at the center. Due east is to the right side of the picture. Distances and elevations are in kilometers. Velocities are in m s.

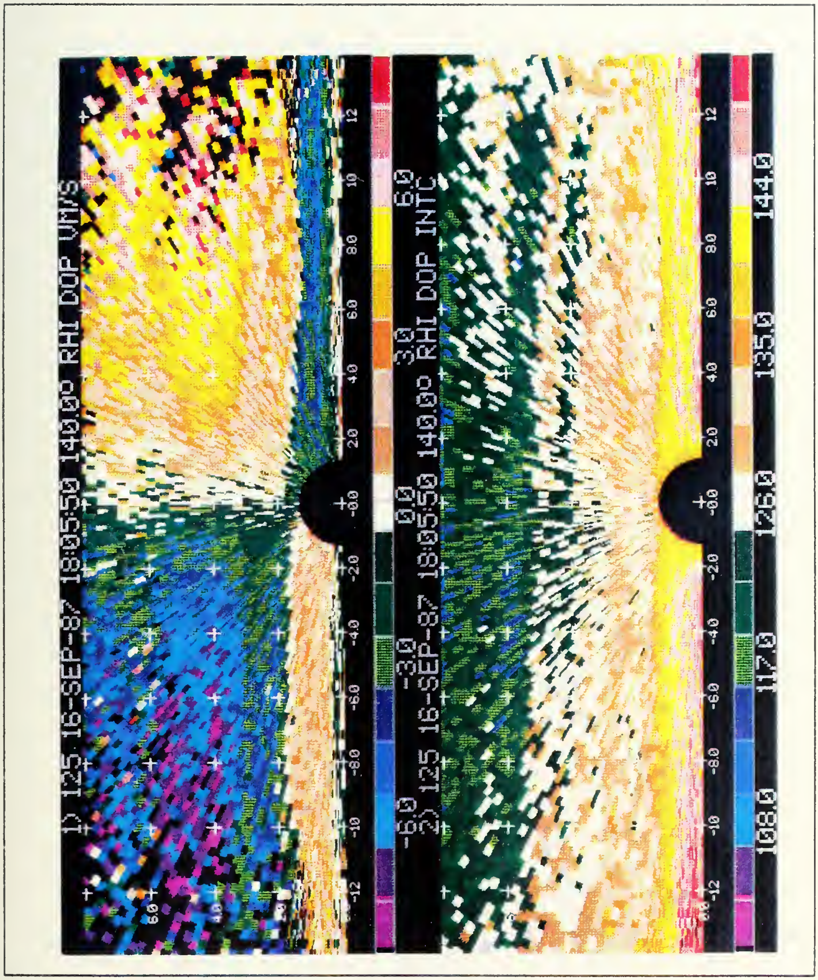

Fig. 24. **RHI Lidar Display at 1805 UTC, 16 September 1987:** Top picture is RHI display. Down valley is to the right of the picture. Distances and elevations are in km. Velocities are in m/s.

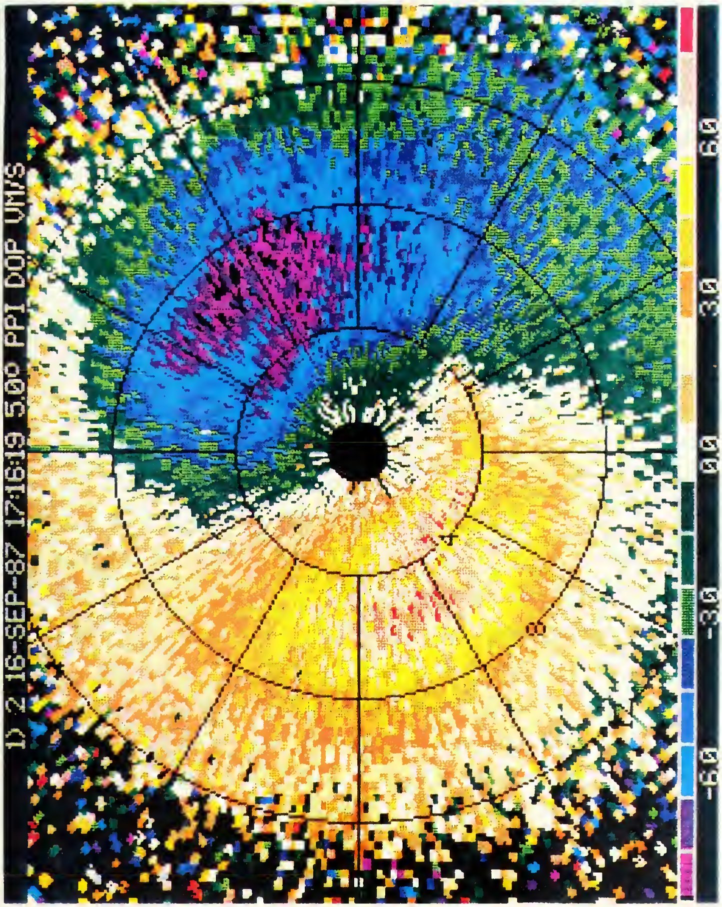

Fig. 25. PPI Lidar Display at 1716 UTC, 16 September 1987: Elevation Angle was 5°. True north is at the top of the picture. Rings are spaced 4 kilometers apart. Velocities are in m/s.

According to the lidar, the offshore flow was from the high terrain to the northeast and from the gap in the coastal ranges where the San Juan Valley is located. The strength of this offshore flow was attributed to the fact that the San Juan Valley is an outlet of airflow for the higher Santa Clara Valley which induced a strong offshore current.

The PPI plots at 1° elevation showed the progression of the sea breeze front. The convergence at the head of the front was detected as it moved in a general southeast direction away from the lidar site. The lidar showed that the sea breeze front was influenced by the surrounding terrain. At 1719, the sea breeze front was estimated to be located at or around the lidar site, since some weak convergence was approximately 1.5 km south. As shown in Fig. 26, the sea breeze flow advanced northeast up to the high terrain approximately 7 km due east of the lidar and north to the mouth of Elkhorn Slough. At this time, the sea breeze front had not advanced at all into the Salinas Valley.

The high terrain to the east effectively blocked the further advance of the sea breeze front at lower levels. The calculated height of the terrain at 7 km was about 120 meters. By 1743, the front had moved about 4.8 km south and southeast from the lidar and had began to move up Elkhorn Slough, north of the lidar. This is shown in Fig. 27 on page 58.

The estimated time of sea breeze frontal passage at the sodar site based upon the lidar data was around 1800 UTC and compared favorably with the time determined from the sodar wind field data , which was 1745 UTC. Using the lidar positions of the convergence zone at the sea breeze front, the calculated speed of advance was 2.09 m s. This compared well with average speed of 2.54 m s calculated from surface data. Fig. 28 on page 59 indicated that the sea breeze had completely filled the mouth of the Salinas Valley and all low terrain to the east of the lidar by 1827 UTC.

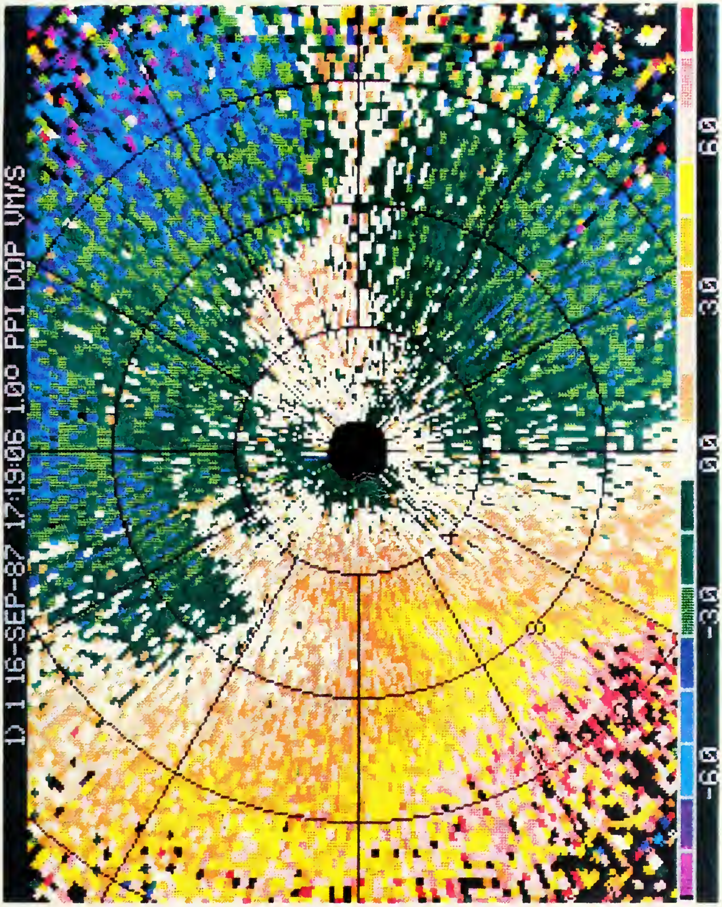

Fig. 26. **PPI Lidar Display for 1719 UTC, 16 September:** Elevation Angle was 1°. True north is at the top of the picture. Rings are spaced 4 kilometers apart. Velocities are in m/s.

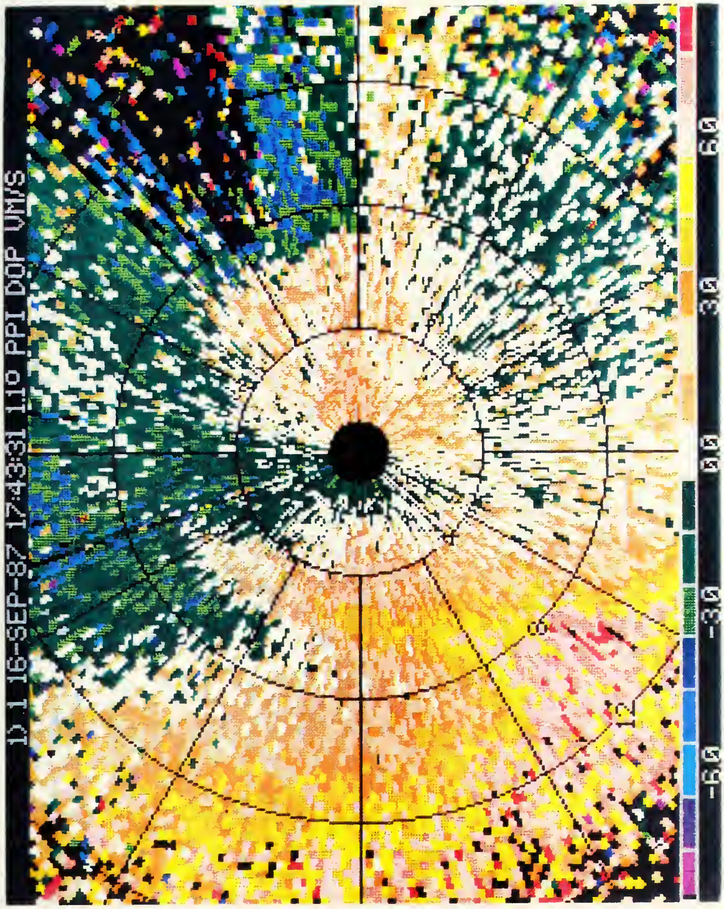

Fig. 27. **PPI Lidar Display for 1747 UTC, 16 September 1987:** Elevation Angle was 1°. True north is at the top of the picture. Rings are spaced 4 kilometers apart. Velocities are in m/s.

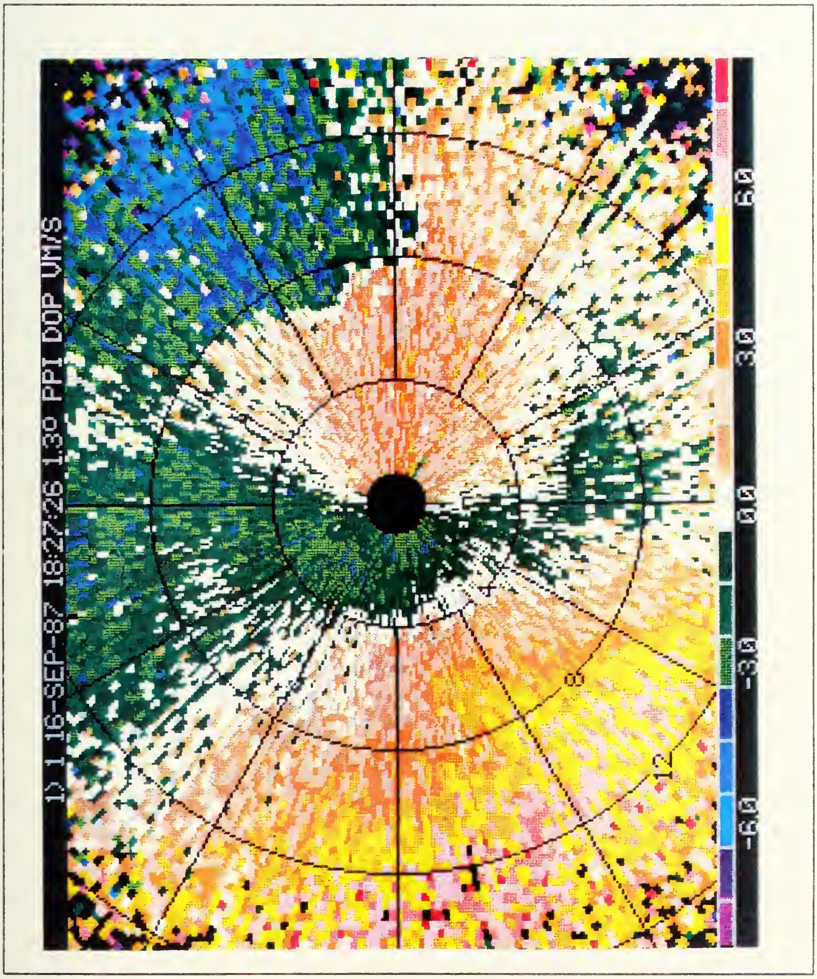

Fig. 28. PPI Lidar Display for 1827 UTC, 16 September 1987: Elevation Angle was 1°. True north is at the top of the picture. Rings are spaced 4 kilometers apart. Velocities are in m/s.

V. SUMMARY AND CONCLUSIONS

A. MAPPING THE SEA BREEZE CIRCULATION

1. Accuracy of the Sodar and Lidar

Various features that have been produced in laboratory experiments such as the flow regions of a gravity head current were observed during LASBEX, most notably the structure in the frontal region where turbulence and mechanical mixing produce large variations in velocity. This area is caused by the overturning of the longitudinal vortex that makes up the major flow within the frontal region and its interaction with the ambient flows surrounding it.

The unique combination of the lidar and the sodar proved to be an effective method to detail the structure of the sea breeze circulation. The instruments both performed well in a marine environment. The sodar detected and mapped the passage of the sea breeze front, whereas the lidar showed the separation between the onshore and offshore flow, as well as the progress of the convergence zone associated with the sea breeze front.

2. General Characteristics of the Sea Breeze Circulation

The general characteristics of the sea breezes that were observed during LASBEX on the Monterey Bay Salinas Valley in September 1987 were similar in many ways to those sea breezes seen in other studies.

The wind direction change over time was found to be an accurate indicator of sea breeze onset. The times of onset were consistent, occurring around 1742 UTC at the sodar station, which was 6.5 km inland. Differences in the relative slope, speed and general shape of the sea breeze flow was observed for each front as it passed the sodar. The directional shear in the vertical meausred by the sodar gave a good indication of the depth of the onshore flow. The lidar presented a similar depth in the RHI scan.

The observed sea breezes advanced onto land with a mean speed of 2.54 m/s, and lasted between 8 and 13 hours. The maximum height that the onshore flow achieved averaged about 659 meters vertically. The slope of the onshore flow measured using the height of the directional shear zone gave values that ranged between 1:5 and 1:17 in the first kilometer horizontally of the flow and between 1:56 and 1:220 in the established onshore flow. These values for the slope of the onshore flow compare favorably with those cited by Simpson et al. (1977).

The increase of wind speed and the maximum updraft region both occurred after the change in wind direction. This agreed well with the location of the longitudinal vortex within the sea breeze front. The maximum wind speeds of the sea breeze recorded at the sodar were from 6 to 10 m/s. Vertical velocities observed during the sea breeze in the mouth of the Salinas Valley ranged between 0.2 and 1.0 m/s and agreed with typical values recorded in previous studies, such as Ogawa et al. (1986). The correlation between depth of onshore flow and the vertical extent of the updraft region was observed. A larger area of upward flow was associated with weak offshore flow and a deeper front. The location of downdraft regions corresponded to the descending leg of the longitudinal vortex and gave a rough measure of the length of this current. On 16 September, the length of such a flow was found to be around 7 km long, and compares well with the vortex observed by Simpson et al. (1977).

The horizontal divergence calculations made using the vertical velocity field produced values of convergence that at times were up to $12x10^{-3}s^{-1}$. These were found to be twice as large as the values calculated by Lyons and Olsson (1973) in a Chicago lake breeze study. The convergence values calculated from the LASBEX vertical velocity field are believed to be the most accurate for the sea breeze front to date.

3. Tracking of the Sea Breeze Front

The lidar was able to detect and track the convergence zone associated with the leading edge of the sea breeze front. The derived mean speed of advance agreed favorably with speeds derived through surface measurements at both the lidar and sodar, as well with speeds seen in other studies. The depth of the offshore flow detected by the lidar was over twice as large as the onshore flow, which is the typical dimension seen in other studies. However, the speeds in this offshore flow were either the same of larger than the onshore flow. This observation is contrary to those studies which saw that the speed of the offshore flow was roughly half as fast as the onshore flow. In PPI, the lidar showed how terrain affected the movement of the sea breeze front, such as halting the advance of the sea breeze front and the movement of the onshore flow into Elkhorn Slough.

B. RECOMMENDATIONS

Since many of the features of the sea breeze flow have been observed by the sodar, further studies should concentrate using this versatile instrument to complete the dynamic structure of the sea breeze front, with concentration on the variations of the velocity components. These variations would help understand the dimensions and structure of the turbulence within the sea breeze front.

As far as improvements in the mapping of the sea breeze structure, there was another sodar which operated concurrently with the PSU sodar, but whose data was not available at the time of this study. The combination of this study and the data from the other sodar would give a better view of the sea breeze structure and refine the actual spatial dimensions of its associated flows.

APPENDIX A. TWO-HOUR WIND DIRECTION CROSS SECTIONS

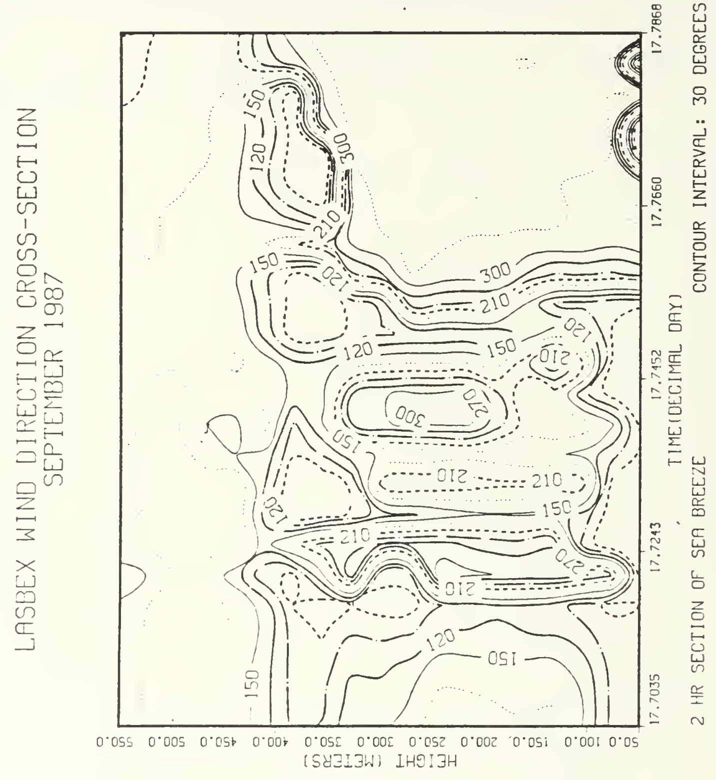

Fig. 29. Two-Hour Wind Direction Cross Section - 17 September 1987

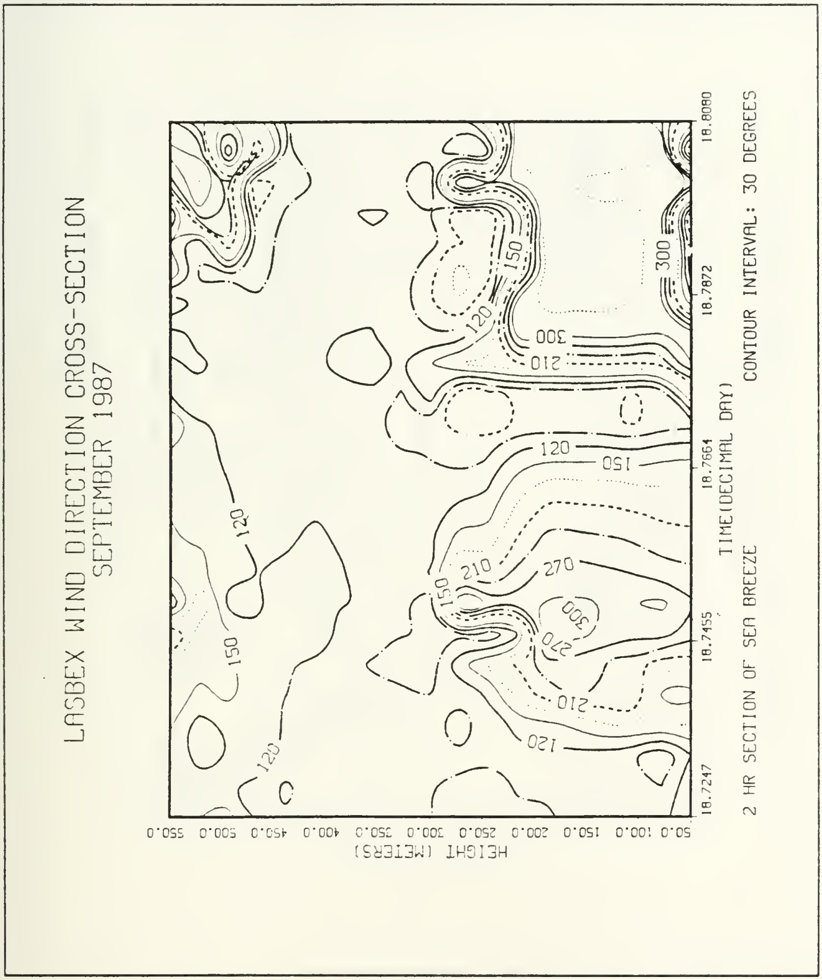

Fig. 30. Two-Hour Wind Direction Cross Section - 18 September 1987

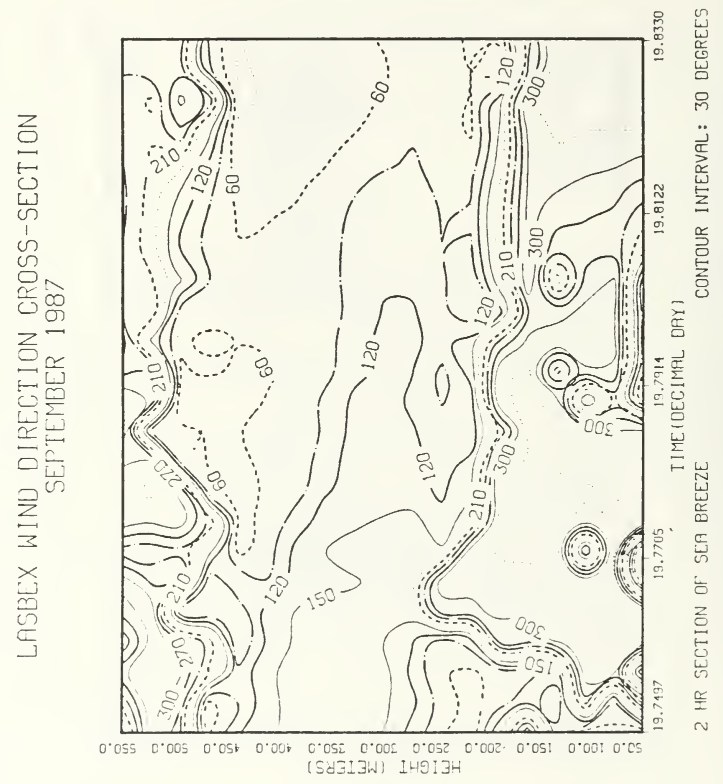

Fig. 31. Two-Hour Wind Direction Cross Section - 19 September 1987

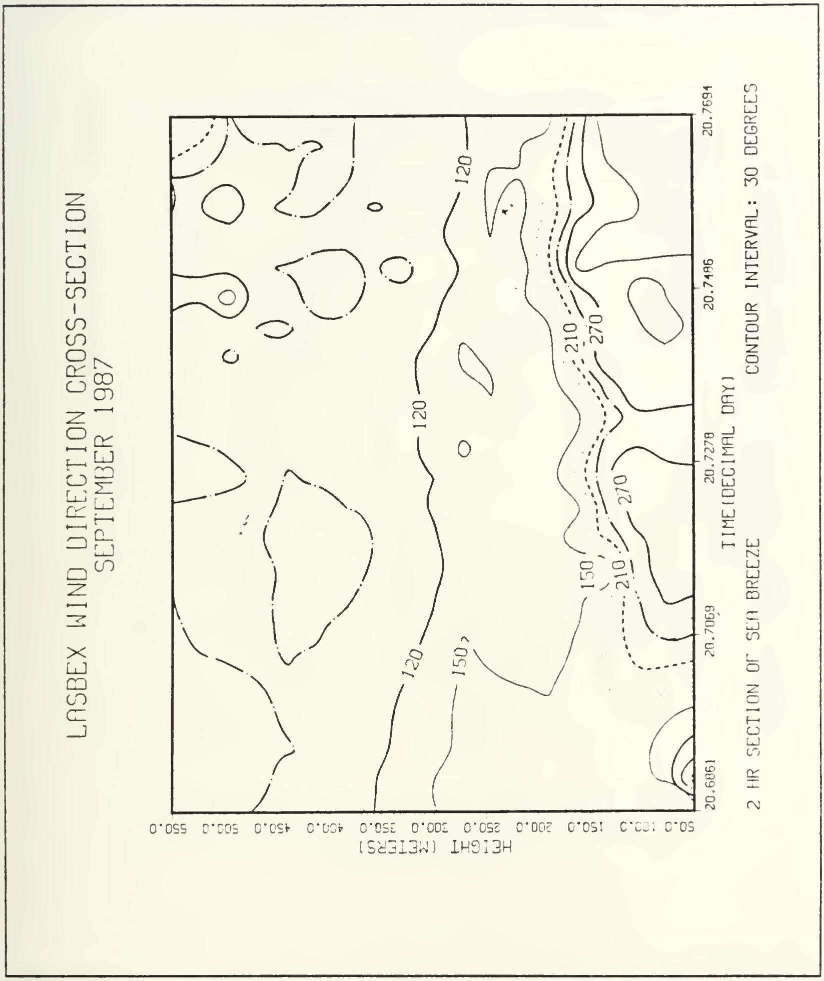

Fig. 32. Two-Hour Wind Direction Cross Section - 20 September 1987

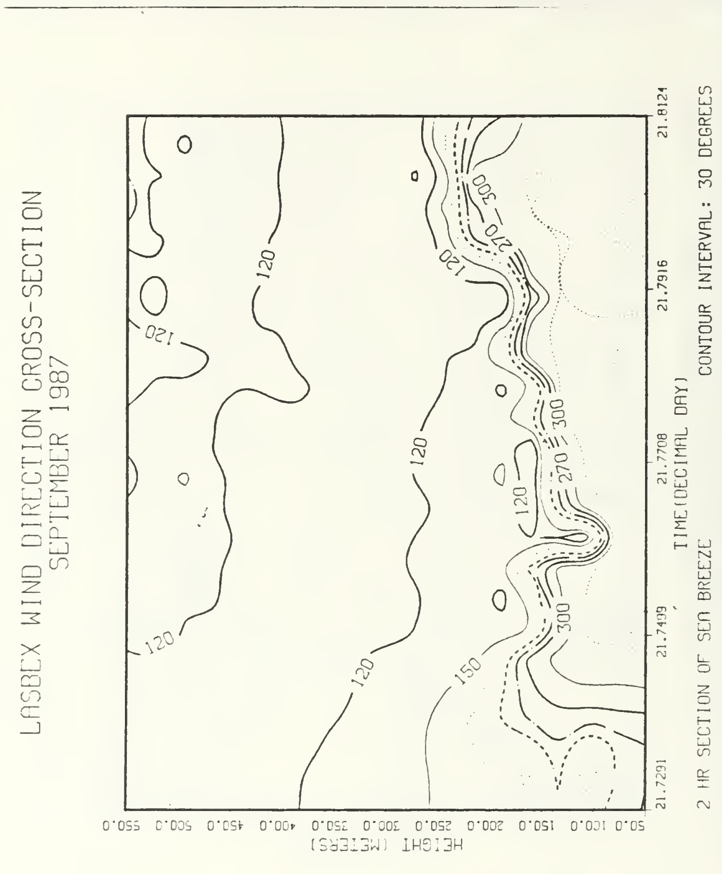

Fig. 33. Two-Hour Wind Direction Cross Section - 21 September 1987

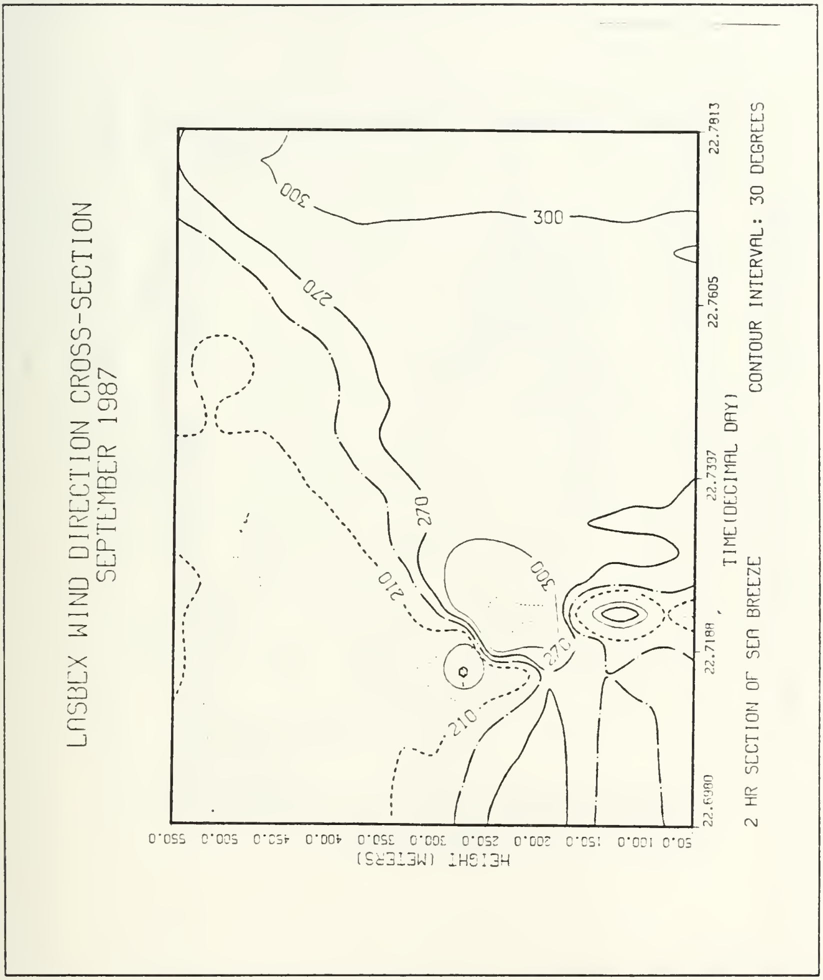

Fig. 34. Two-Hour Wind Direction Cross Section - 22 September 1987

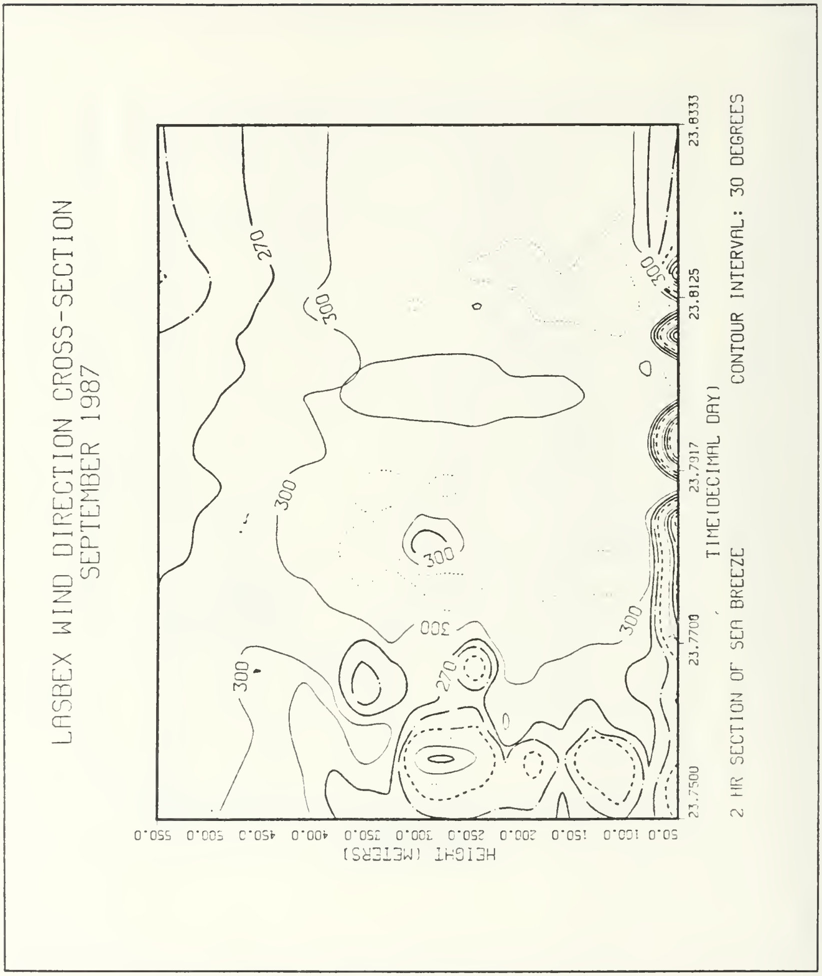

Fig. 35. Two-Hour Wind Direction Cross Section - 23 September 1987

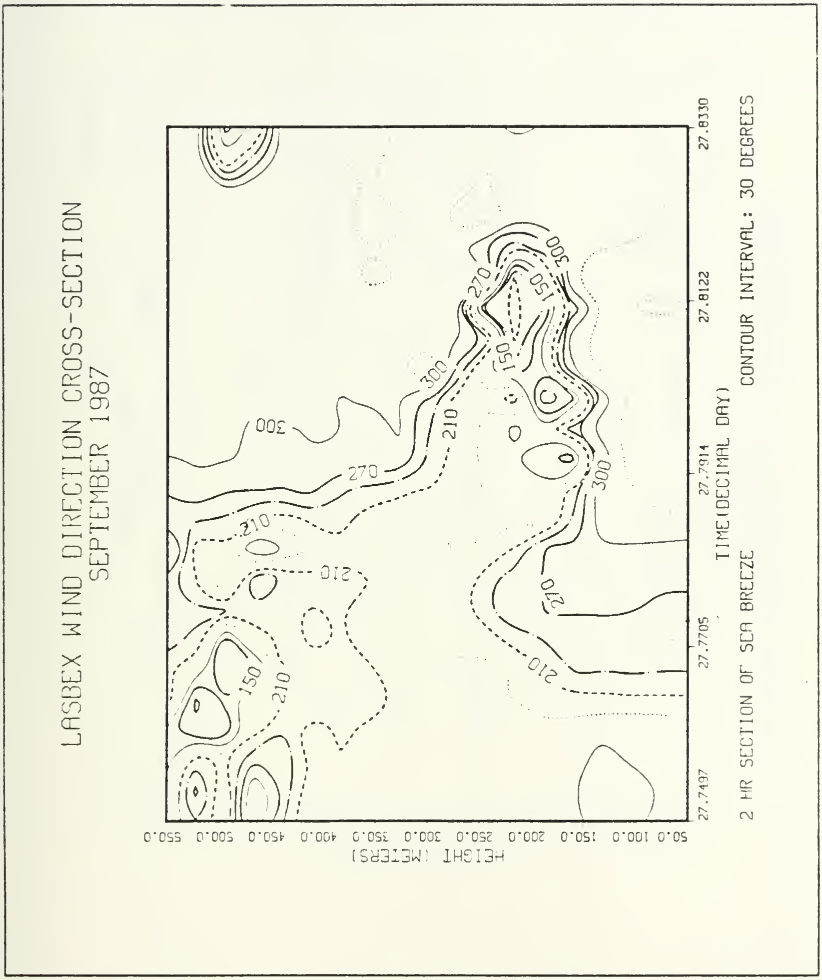

Fig. 36. Two-Hour Wind Direction Cross Section - 27 September 1987

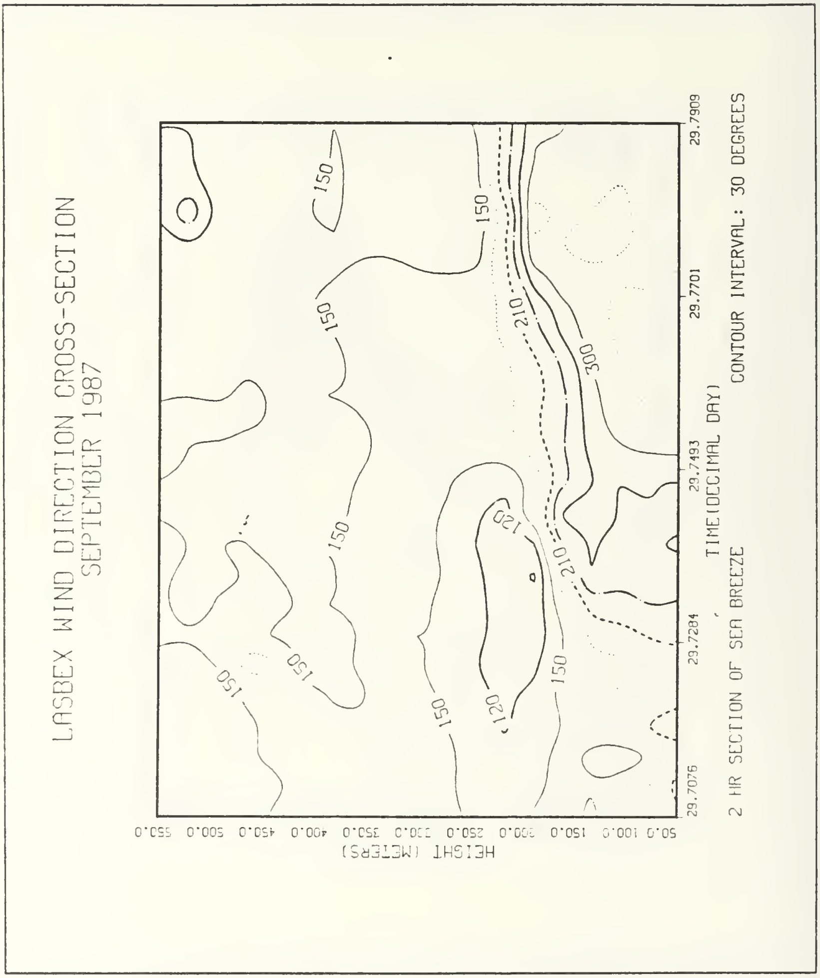

Fig. 37. Two-Hour Wind Direction Cross Section - 29 September 1987

APPENDIX B. TWO-HOUR WIND SPEED CROSS SECTIONS

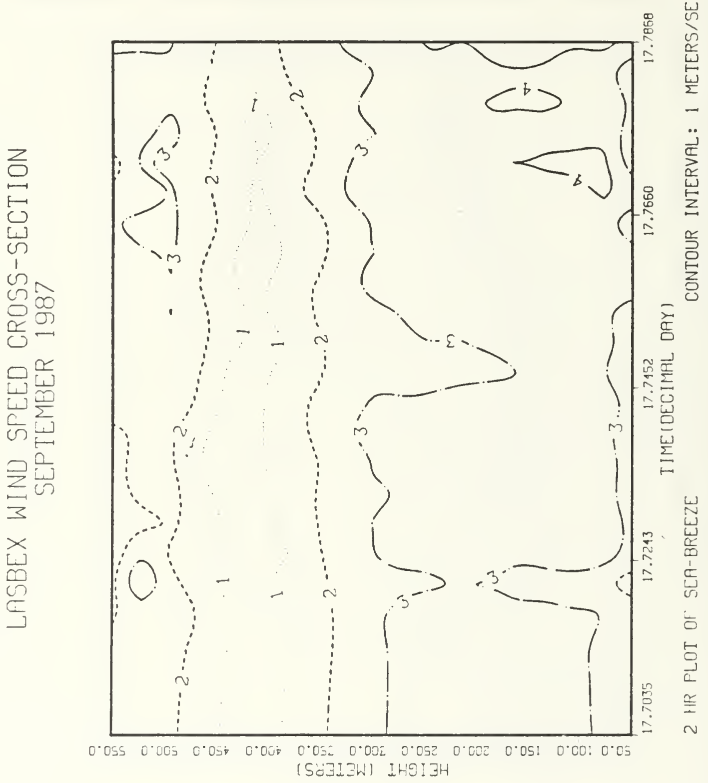

Fig. 38. Two-Hour Wind Speed Cross Section - 17 September 1987

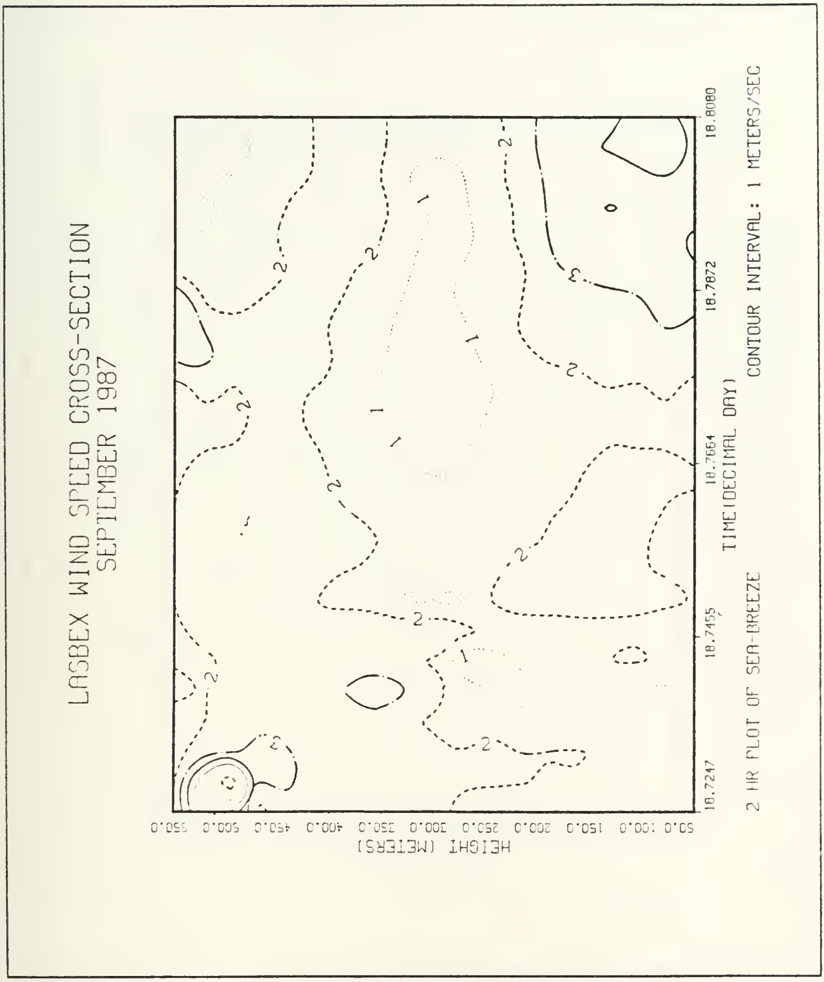

Fig. 39. Two-Hour Wind Speed Cross Section - 18 September 1987

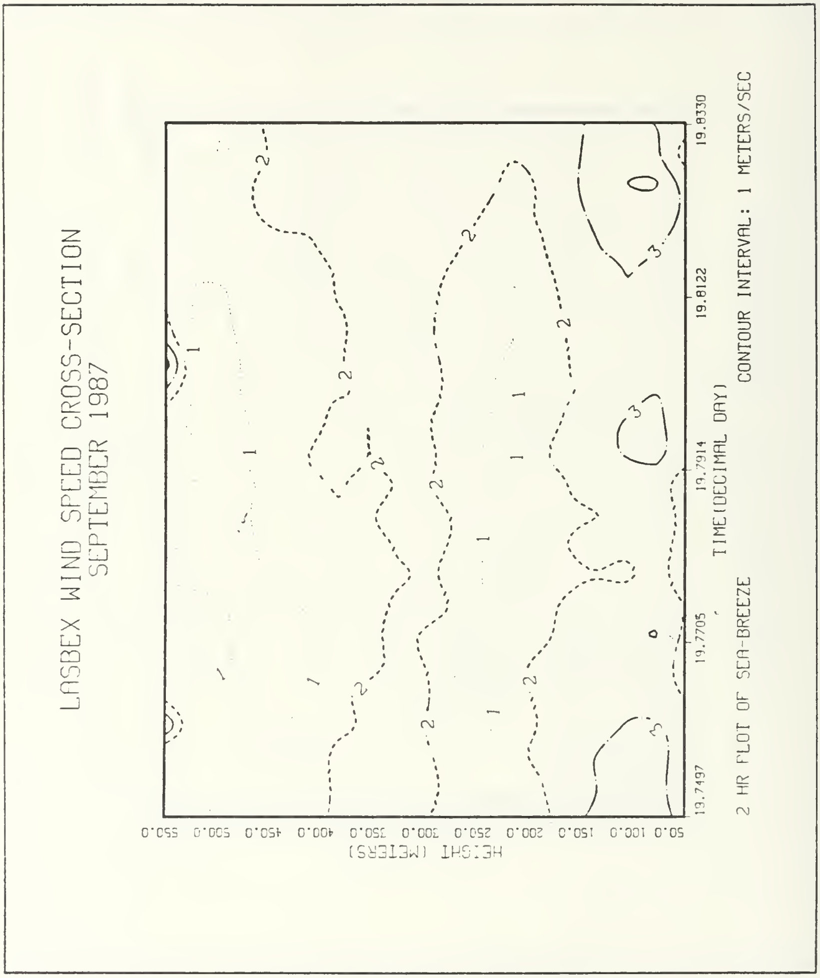

Fig. 40. Two-Hour Wind Speed Cross Section - 19 September 1987

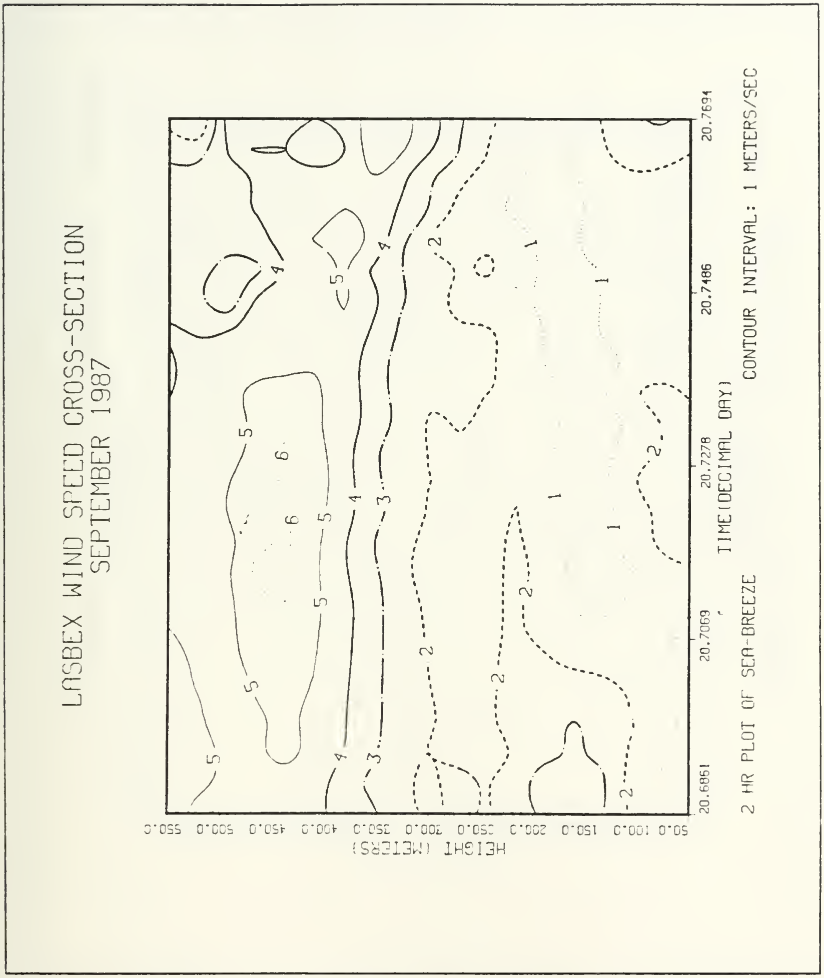

Fig. 41. Two-Hour Wind Speed Cross Section - 20 September 1987

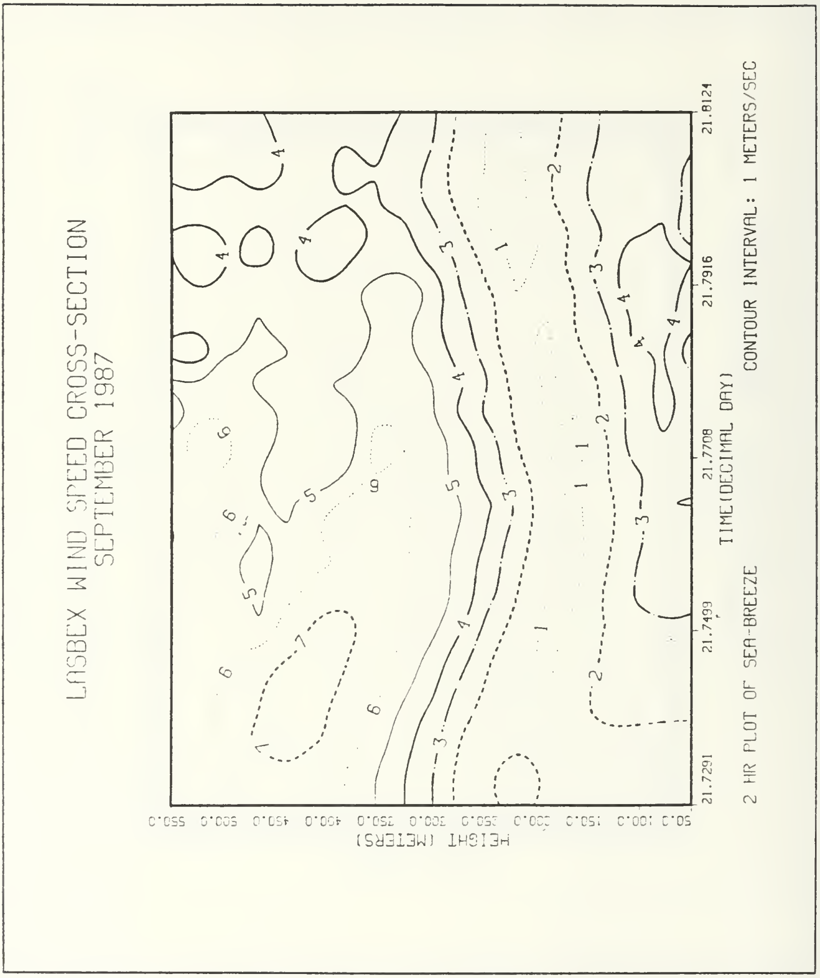

Fig. 42. Two-Hour Wind Speed Cross Section - 21 September 1987

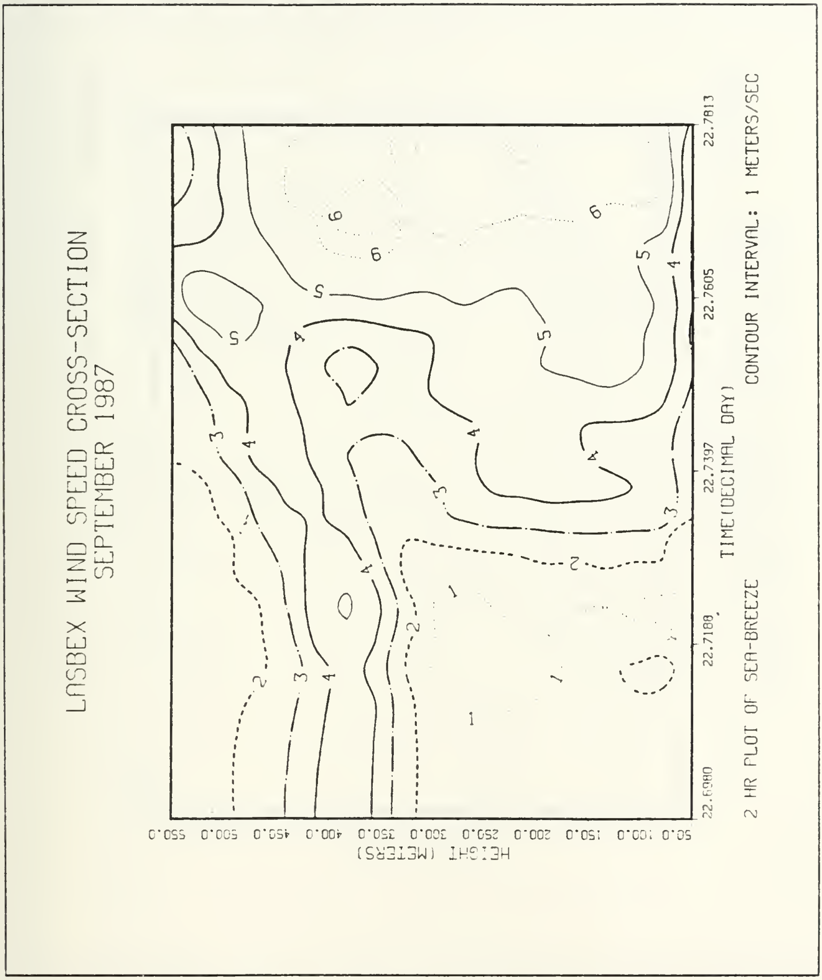

Fig. 43. Two-Hour Wind Speed Cross Section - 22 September 1987

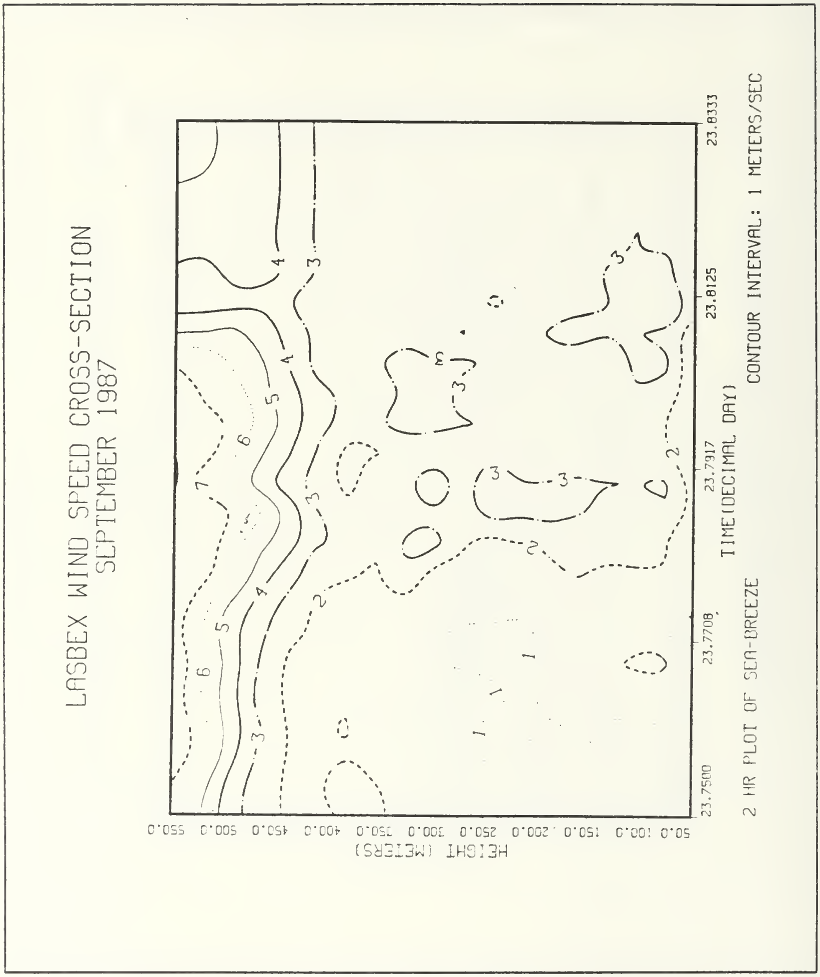

Fig. 44. Two-Hour Wind Speed Cross Section - 23 September 1987

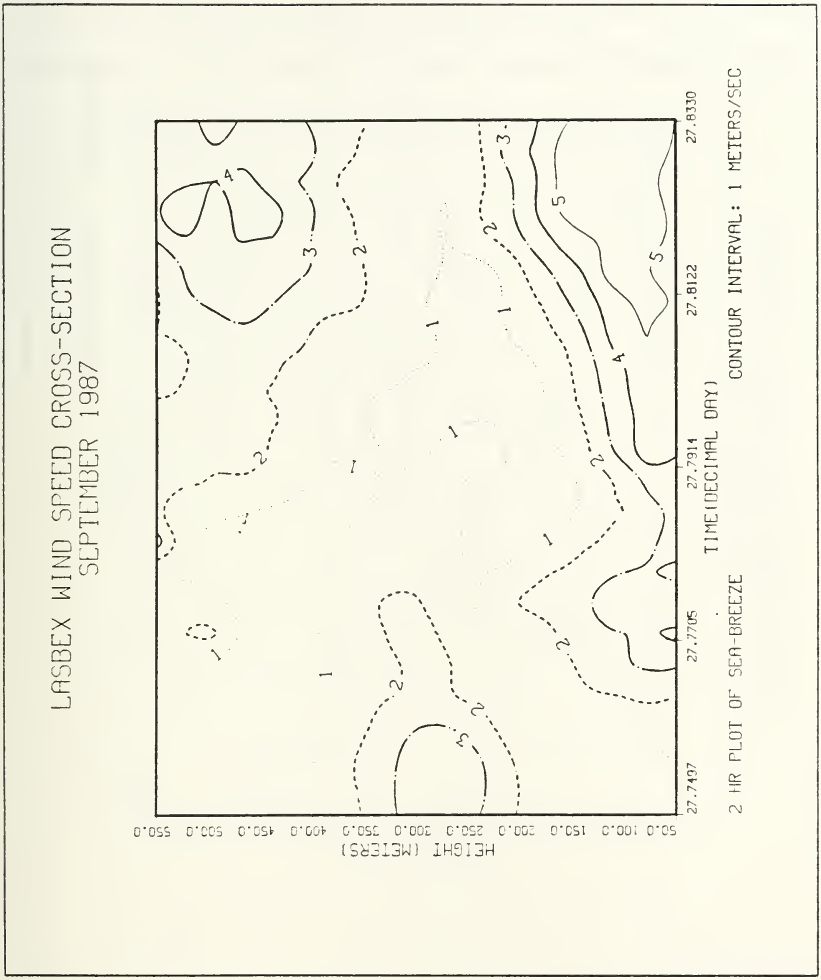

Fig. 45. Two-Hour Wind Speed Cross Section - 27 September 1987

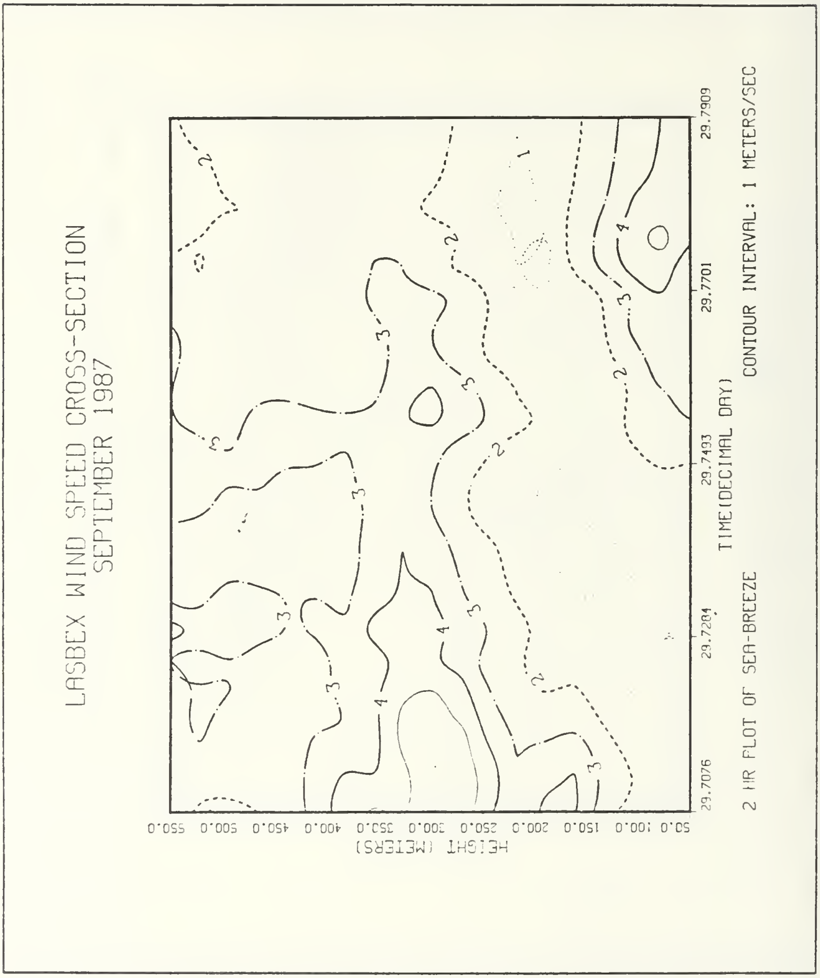

Fig. 46. Two-Hour Wind Speed Cross Section - 29 September 1987

APPENDIX C. TWO-HOUR VERTICAL VELOCITY CROSS SECTIONS

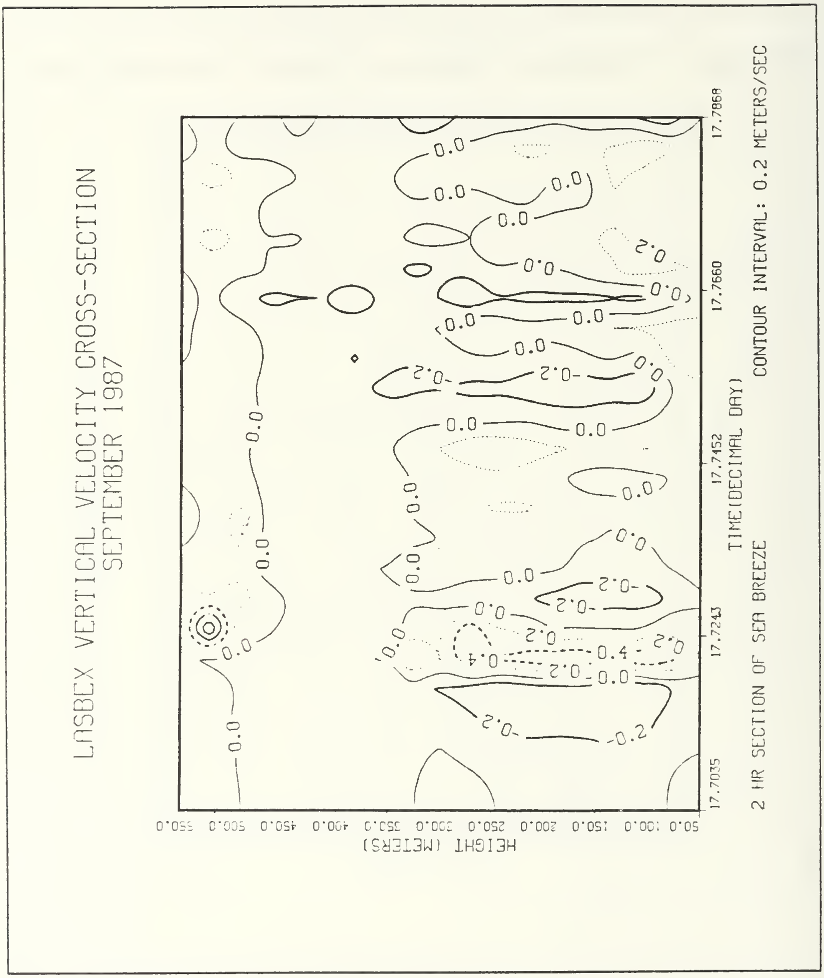

Fig. 47. Two-Hour Vertical Velocity Cross Section - 17 September 1987

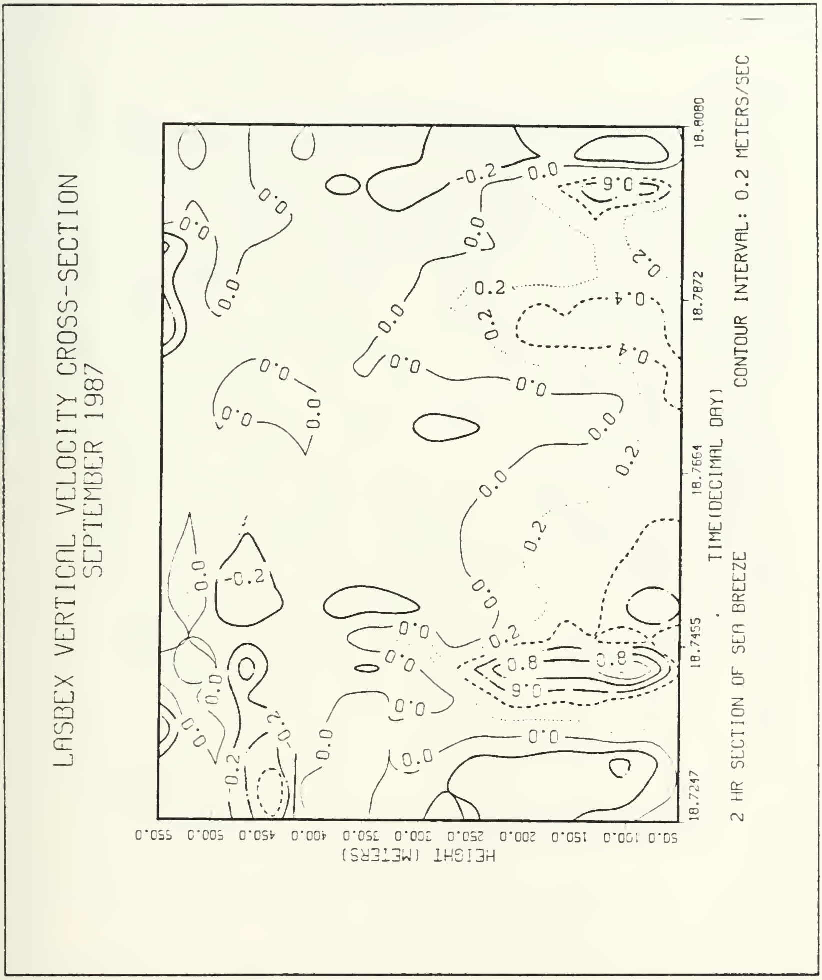

Fig. 48. Two-Hour Vertical Velocity Cross Section - 18 September 1987

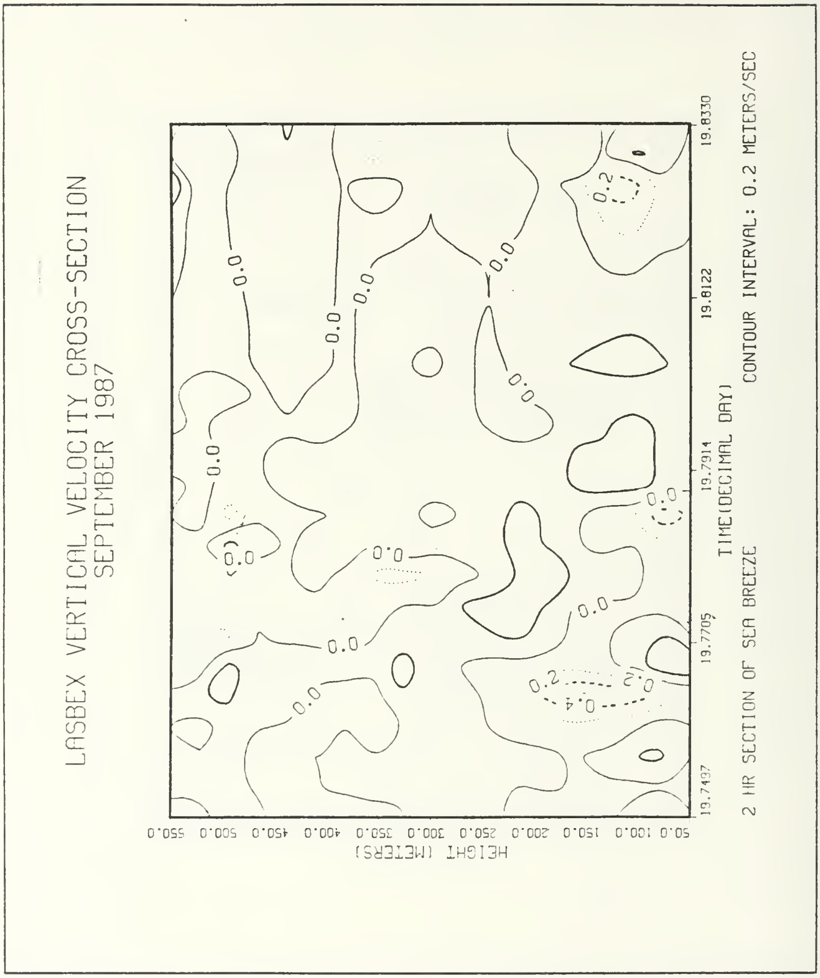

Fig. 49. Two-Hour Vertical Velocity Cross Section - 19 September 1987

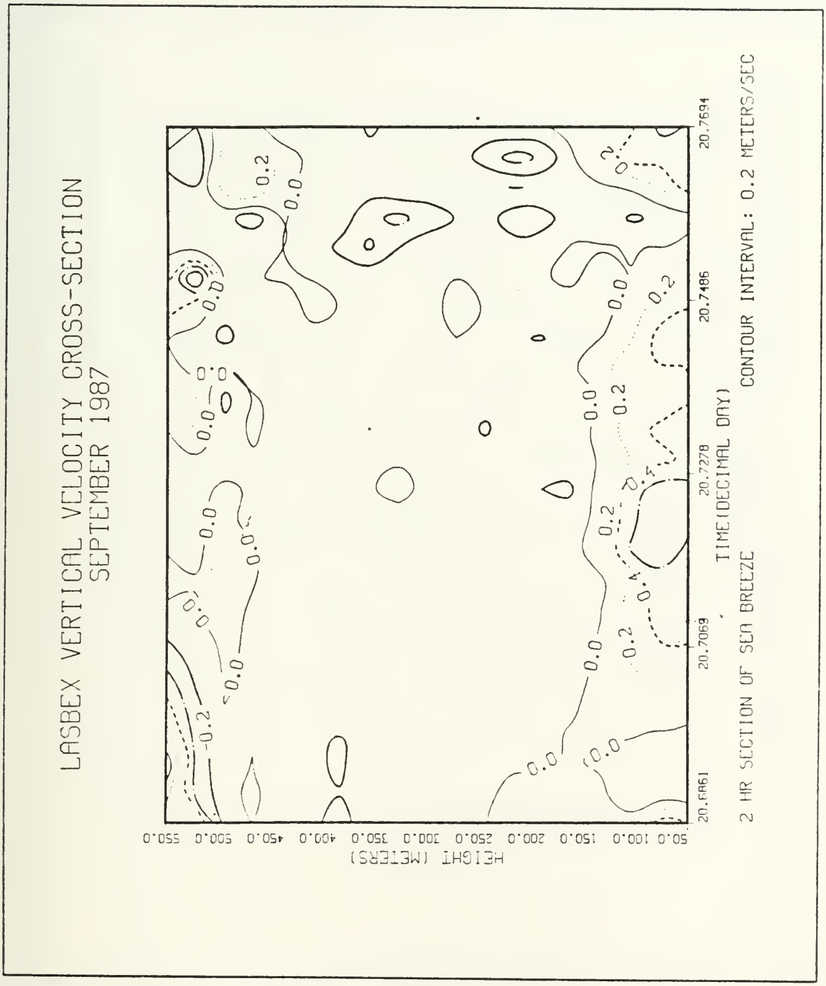

Fig. 50. Two-Hour Vertical Velocity Cross Section - 20 September 1987

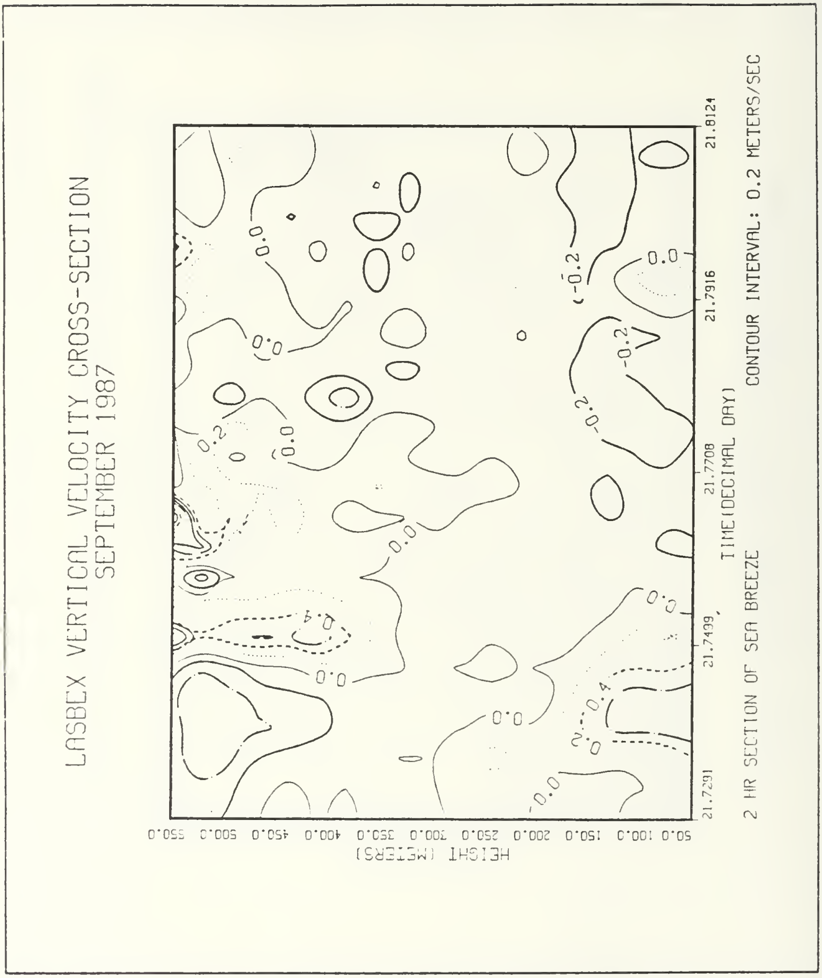

Fig. 51. Two-Hour Vertical Velocity Cross Section - 21 September 1987

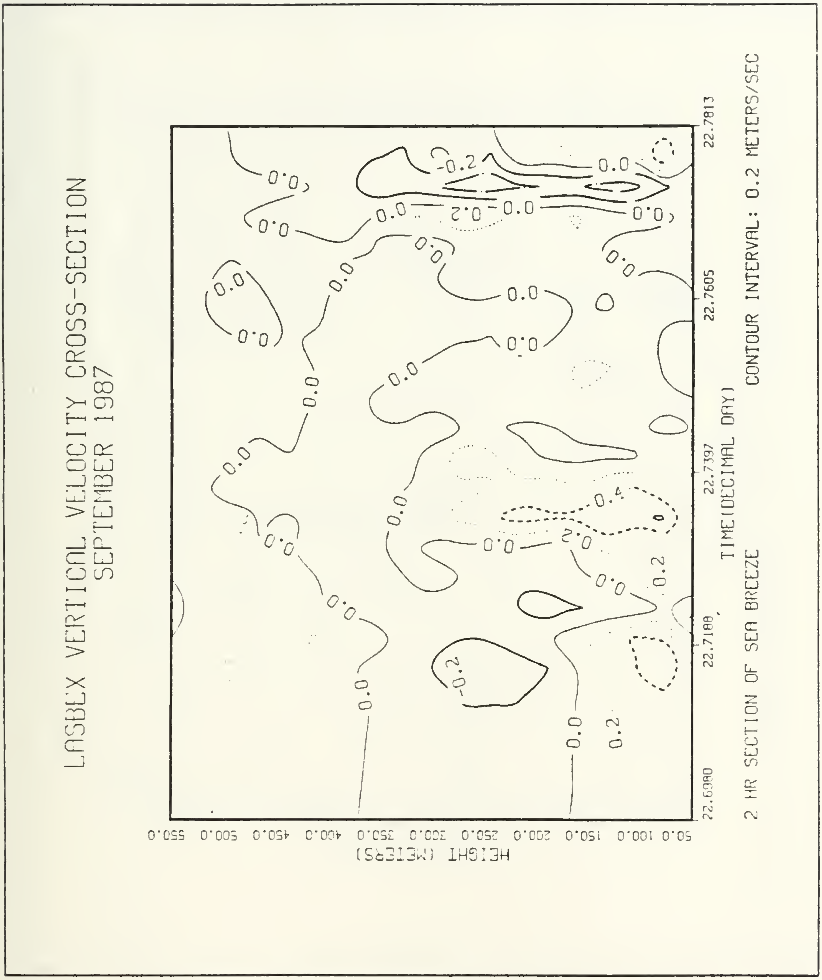

Fig. 52. Two-Hour Vertical Velocity Cross Section - 22 September 1987

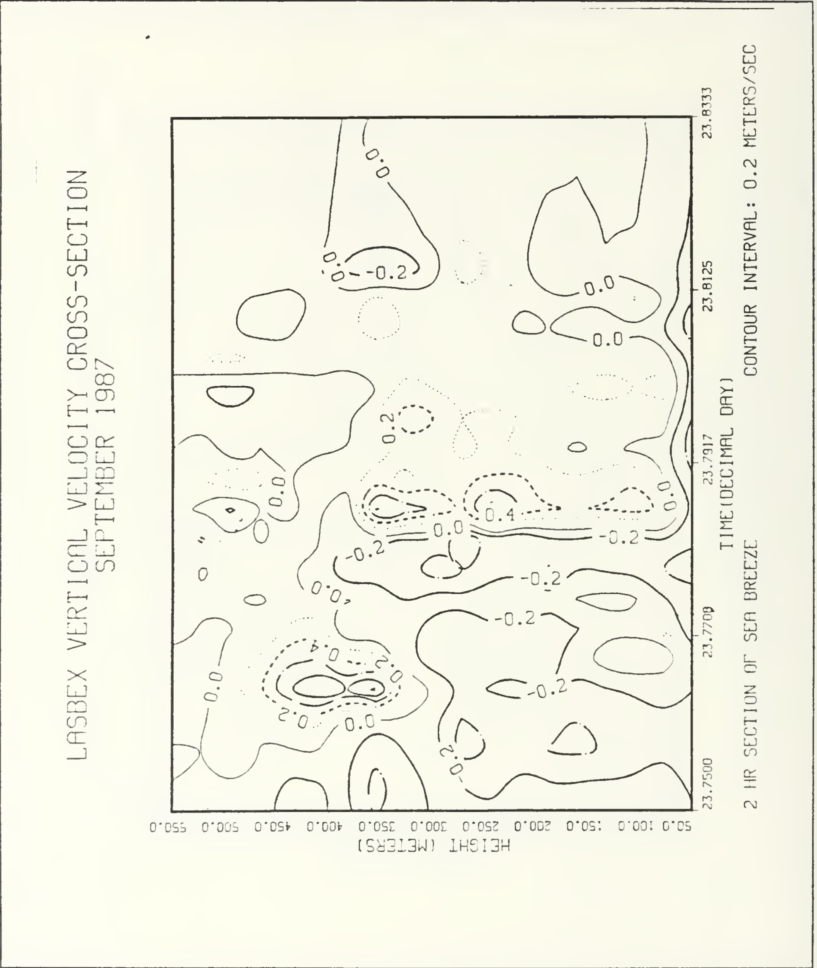

Fig. 53. Two-Hour Vertical Velocity Cross Section - 23 September 1987

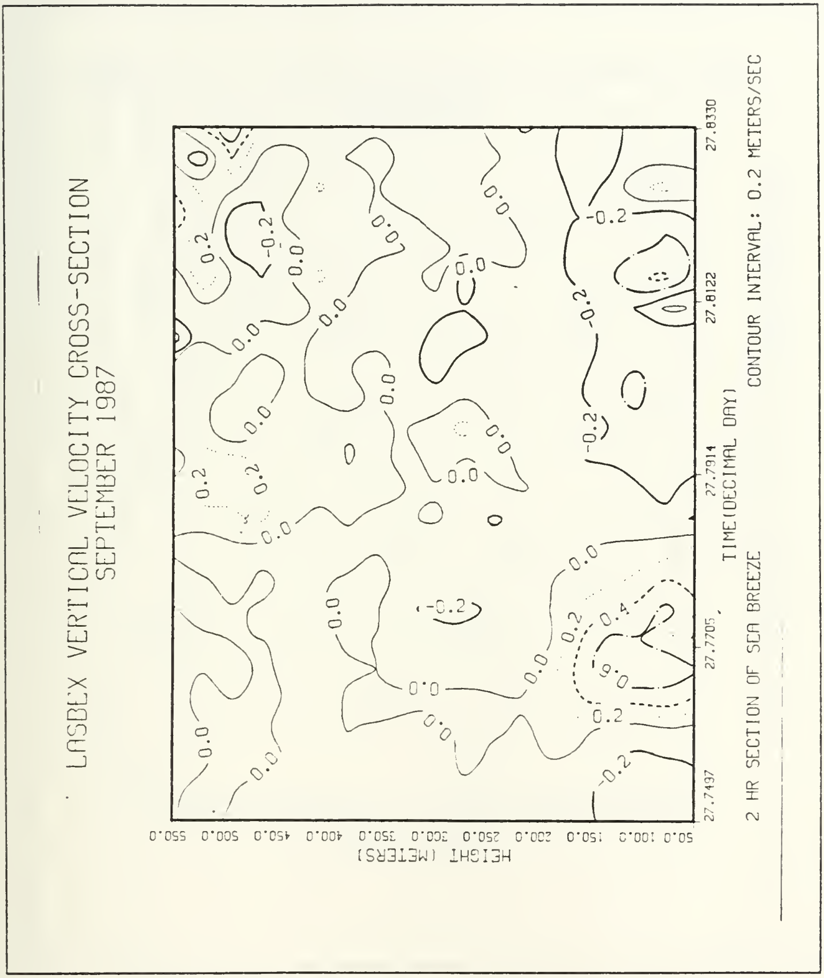

Fig. 54. Two-Hour Vertical Velocity Cross Section - 27 September 1987

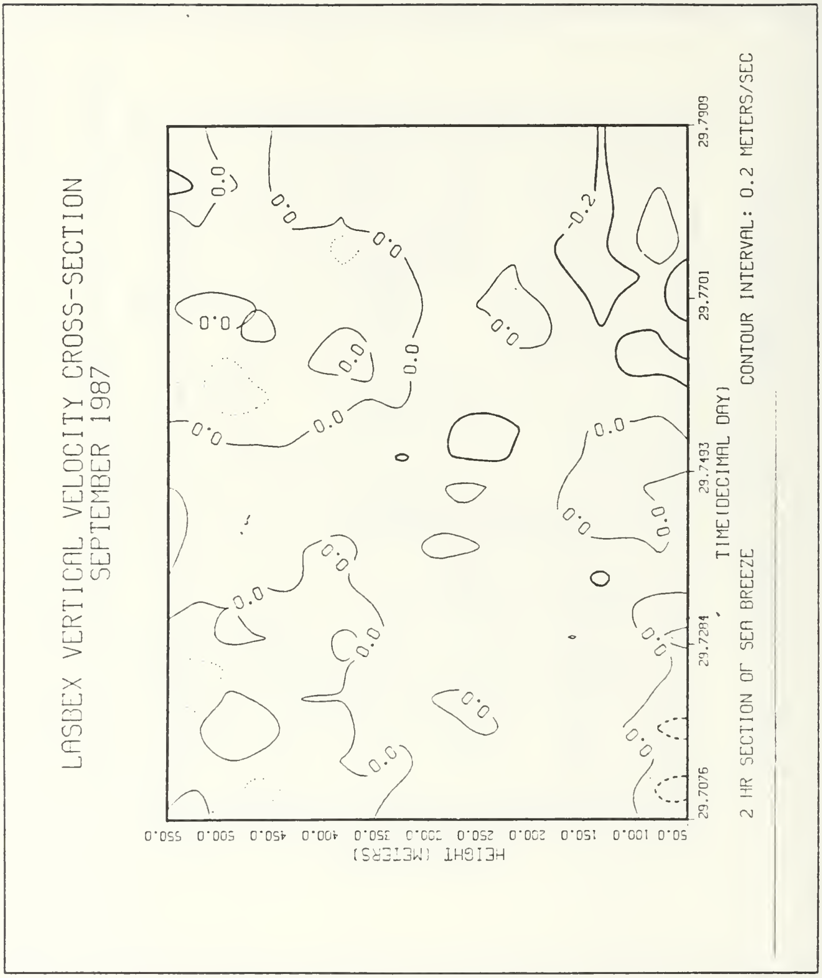

Fig. 55. Two-Hour Vertical Velocity Cross Section - 29 September 1987

APPENDIX D. TWO-HOUR STANDARD DEVIATION CROSS SECTIONS

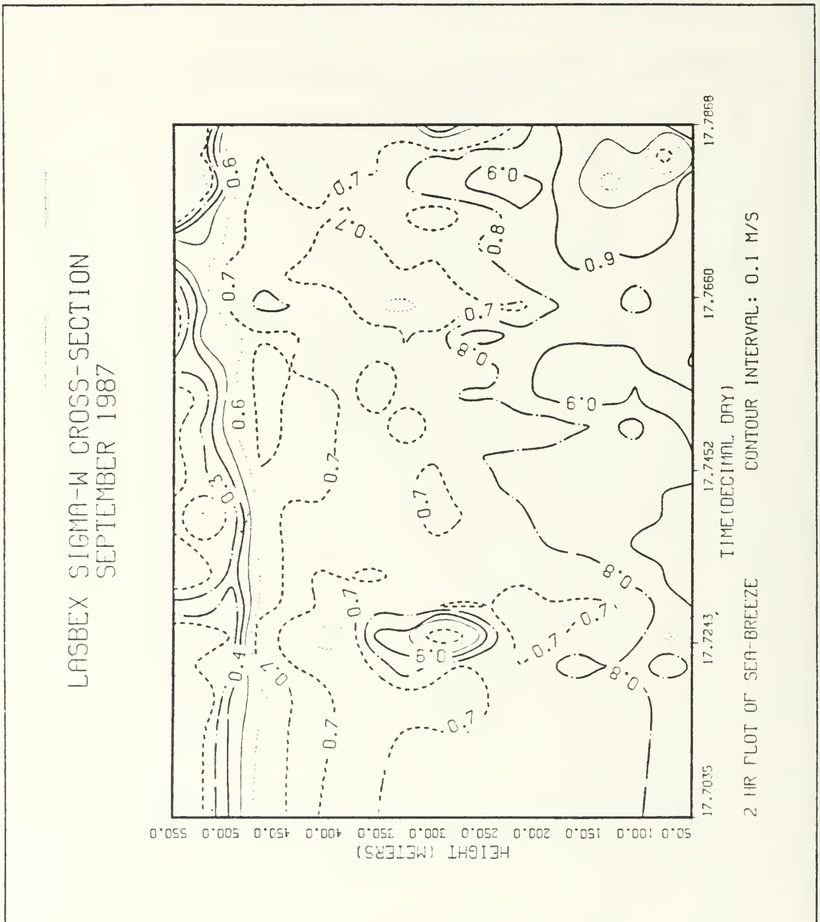

Fig. 56. Two-Hour Standard Deviation Cross Section - 17 September 1987

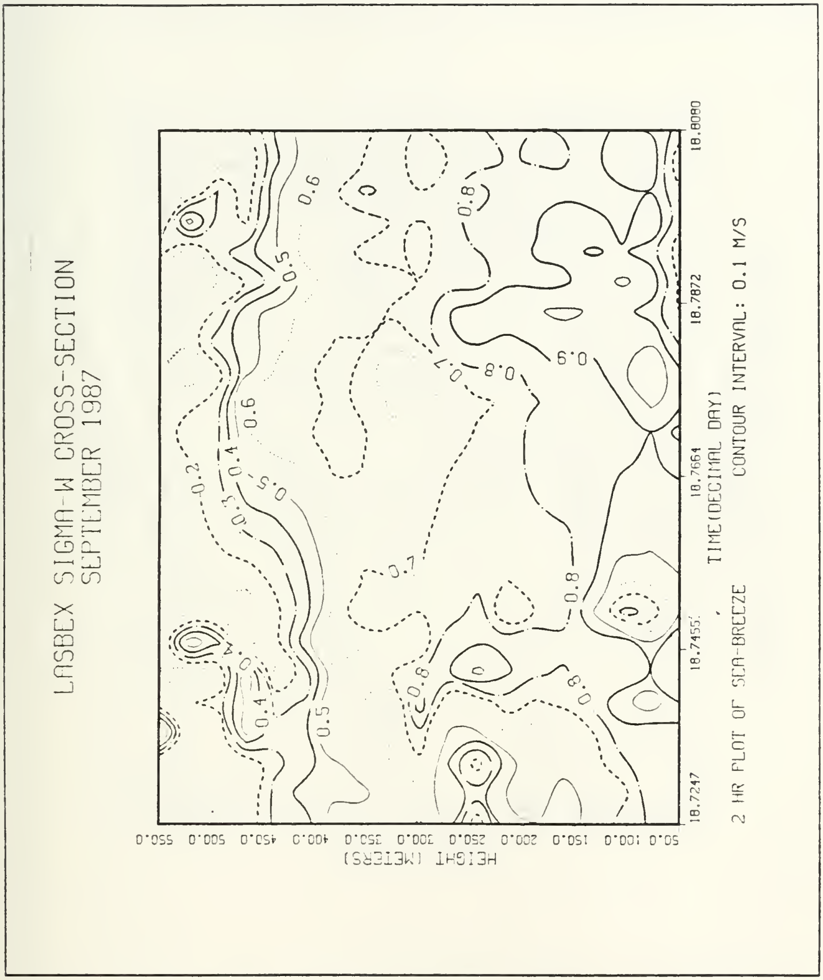

Fig. 57. Two-Hour Standard Deviation Cross Section - 18 September 1987

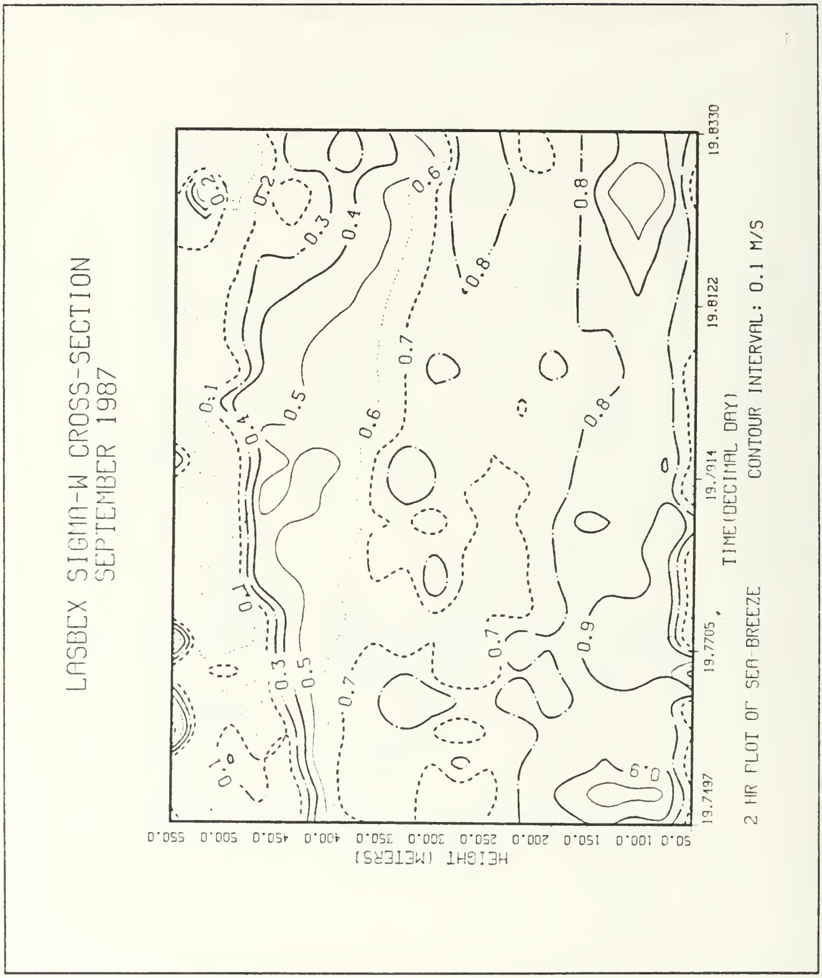

Fig. 58. Two-Hour Standard Deviation Cross Section - 19 September 1987

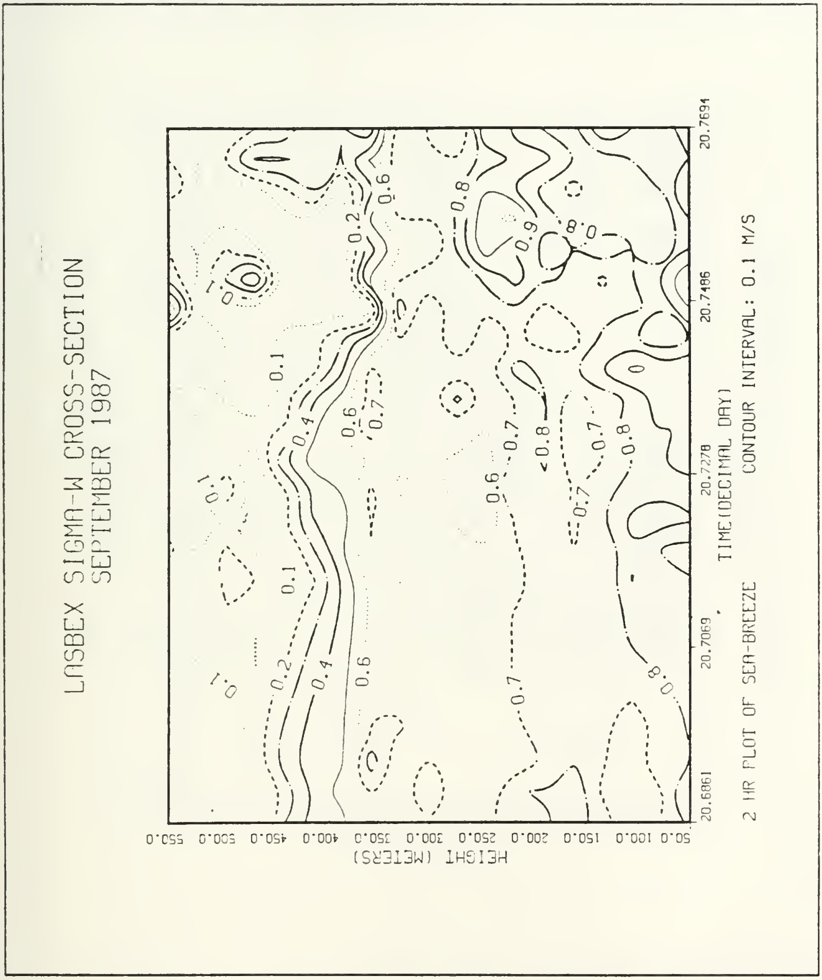

Fig. 59. Two-Hour Standard Deviation Cross Section - 20 September 1987

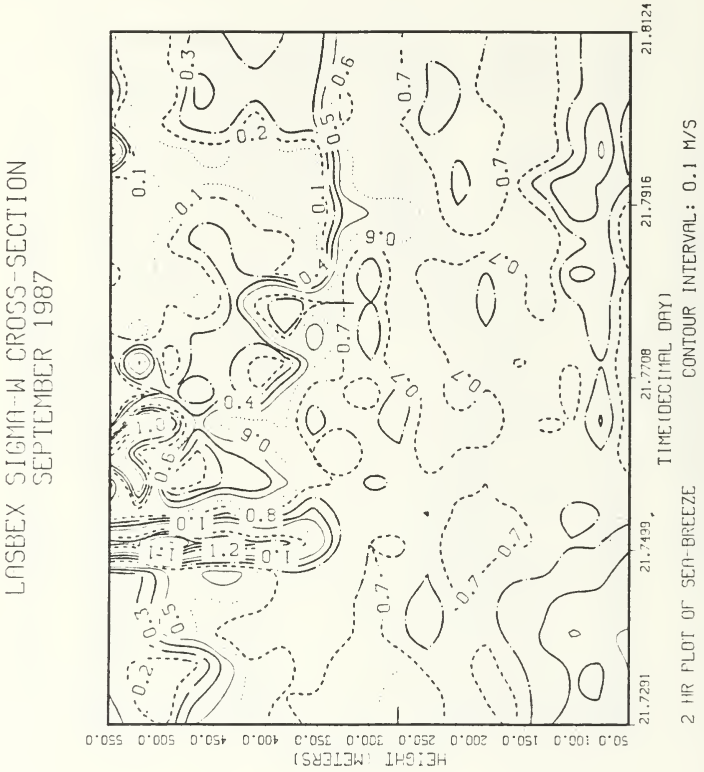

Fig. 60. Two-Hour Standard Deviation Cross Section - 21 September 1987

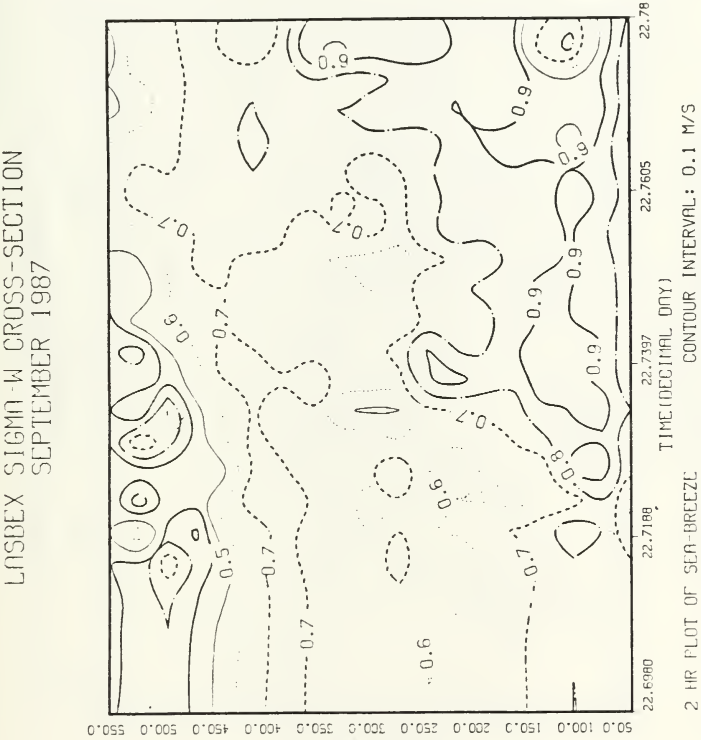

Fig. 61. Two-Hour Standard Deviation Cross Section - 22 September 1987

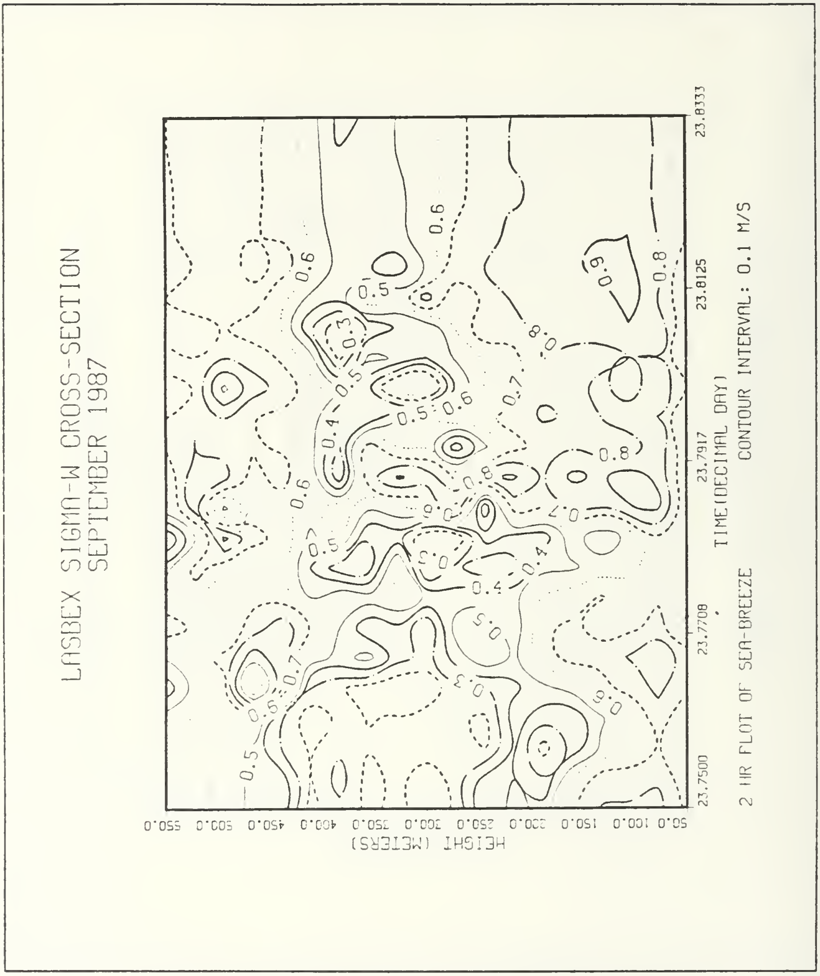

Fig. 62. Two-Hour Standard Deviation Cross Section - 23 September 1987

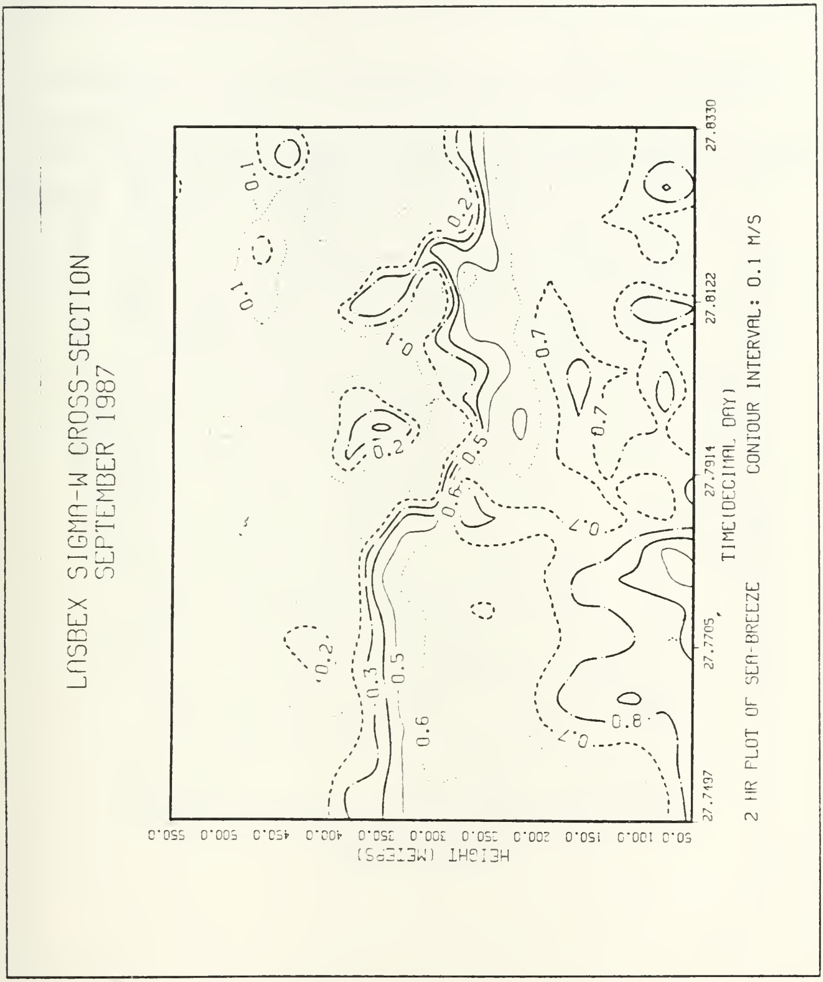

Fig. 63. Two-Hour Standard Deviation Cross Section - 27 September 1987

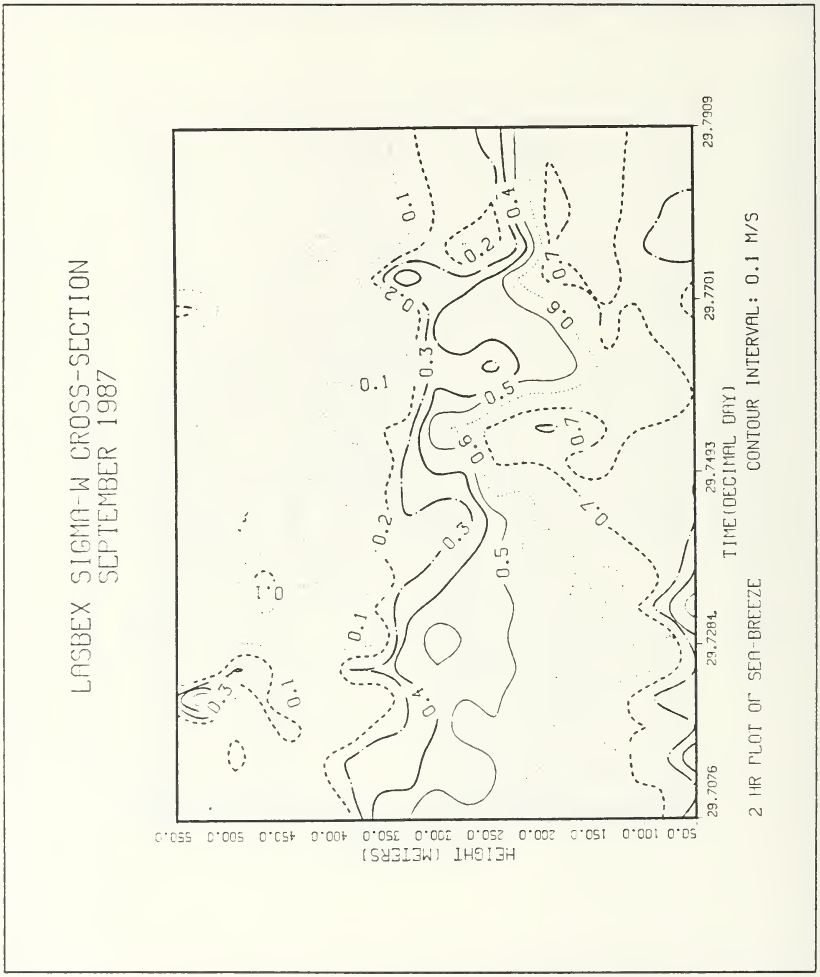

Fig. 64. Two-Hour Standard Deviation Cross Section - 29 September 1987

APPENDIX E. 24-HOUR WIND DIRECTION CROSS SECTIONS

A. NOTES

The cross-section for 23 September 1987 was too noisy between 23.958 and 24.208 decimal day. Data in this region were considered unusable.

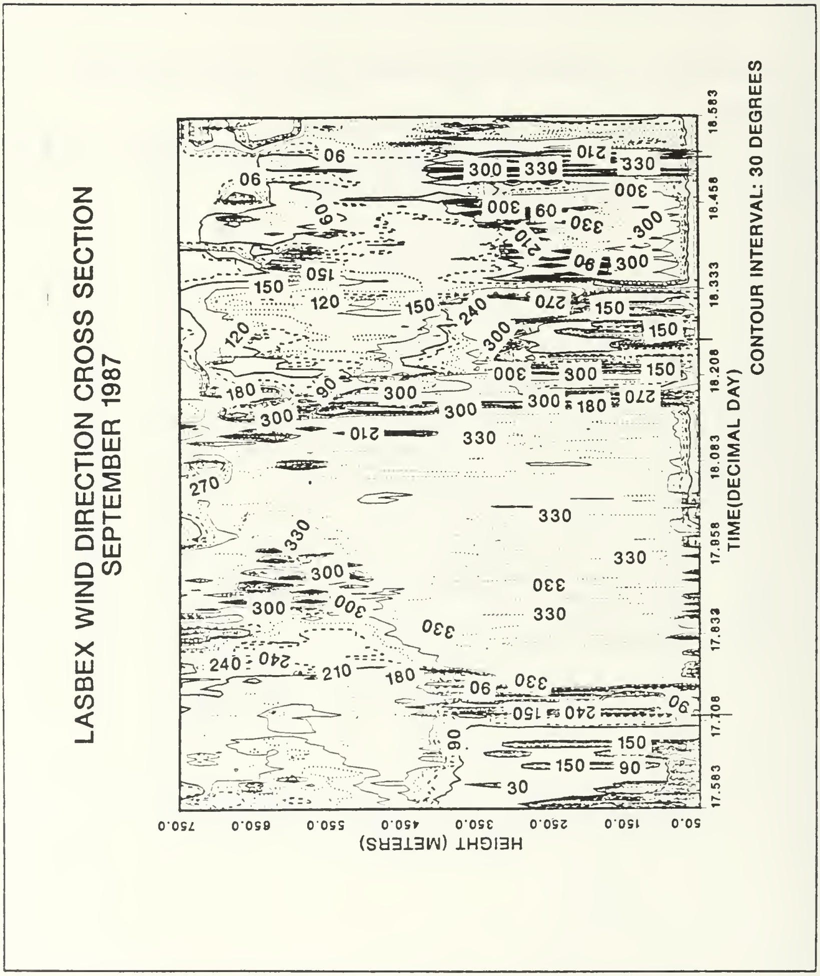

Fig. 65. 24-Hour Wind Direction Cross Section - 17 September 1987

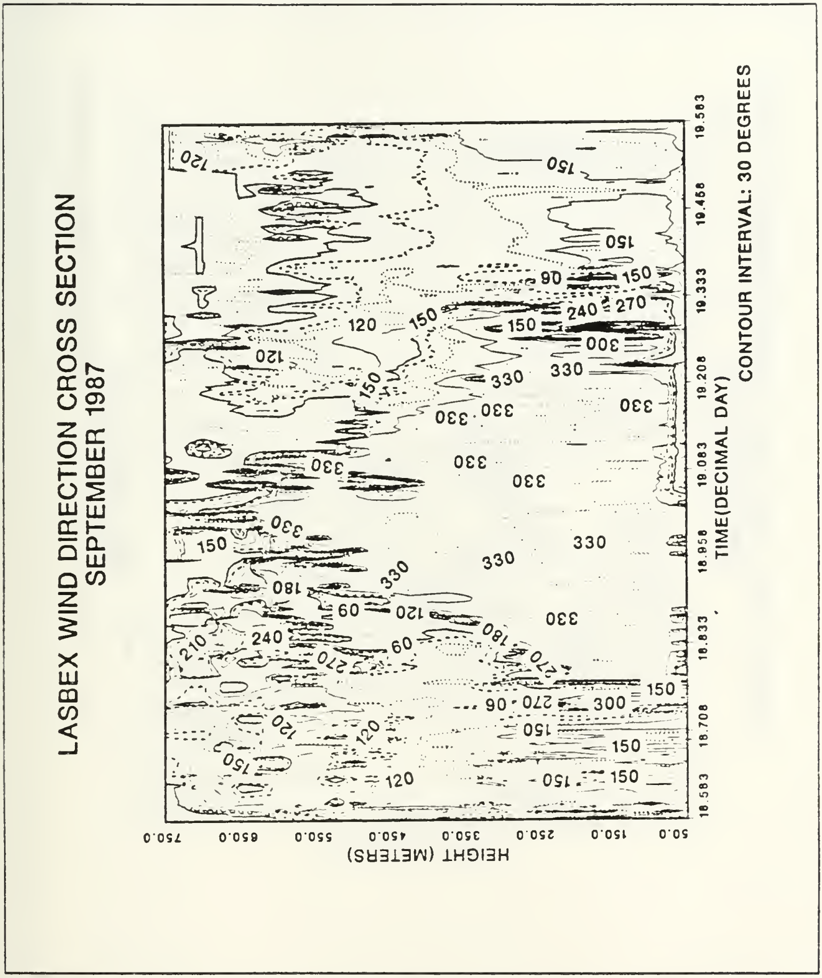

Fig. 66. 24-Hour Wind Direction Cross Section - 18 September 1987

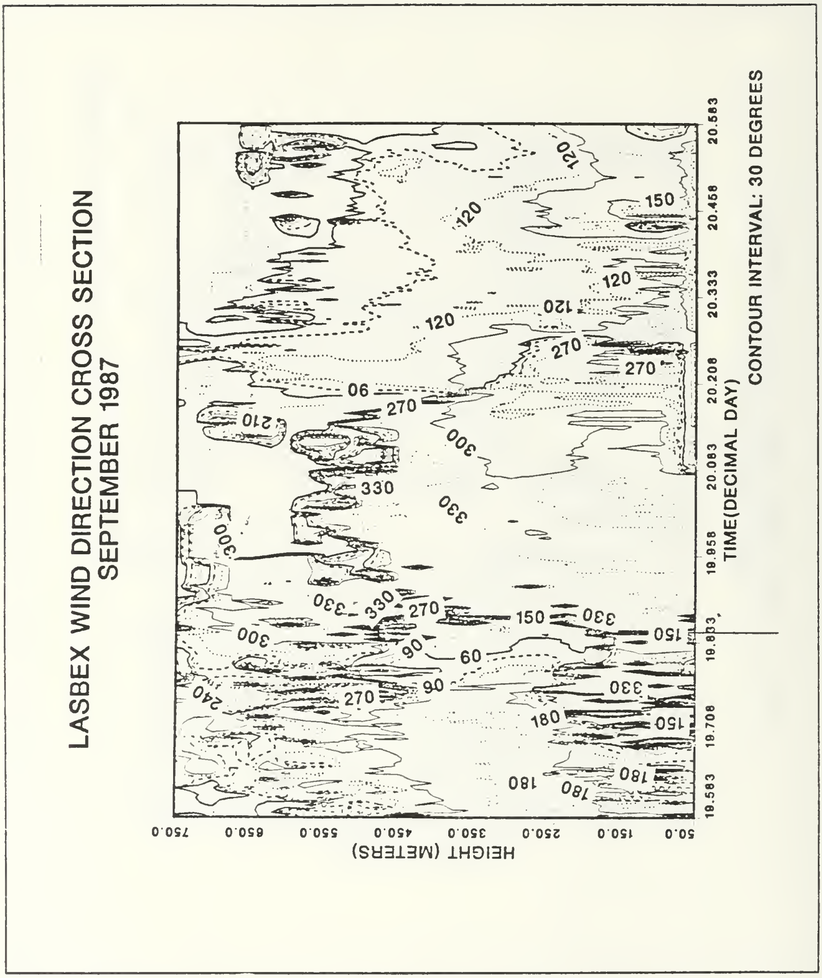

Fig. 67. 24-Hour Wind Direction Cross Section - 19 September 1987

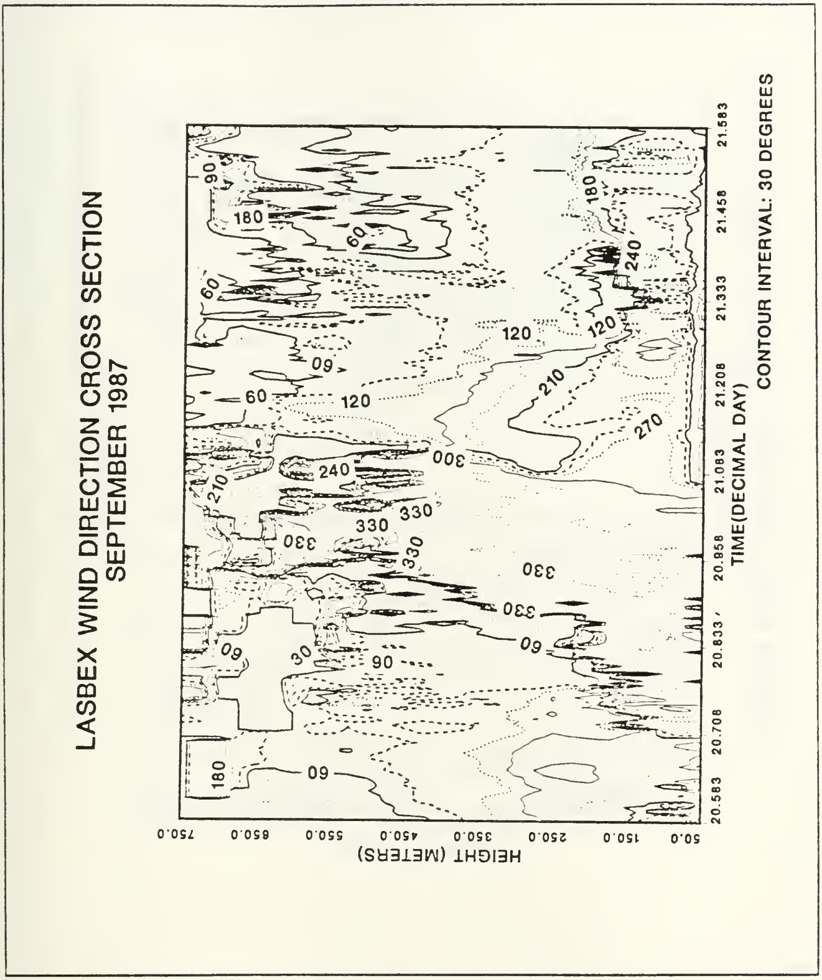

Fig. 68. 24-Hour Wind Direction Cross Section - 20 September 1987

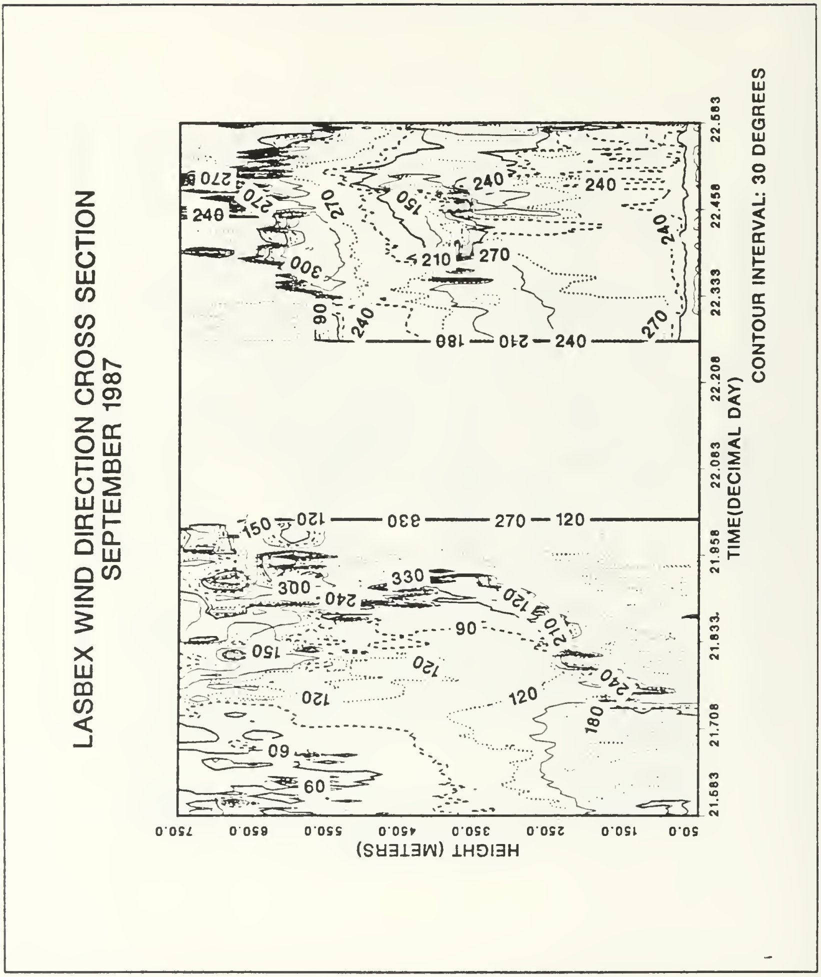

Fig. 69. 24-Hour Wind Direction Cross Section - 21 September 1987

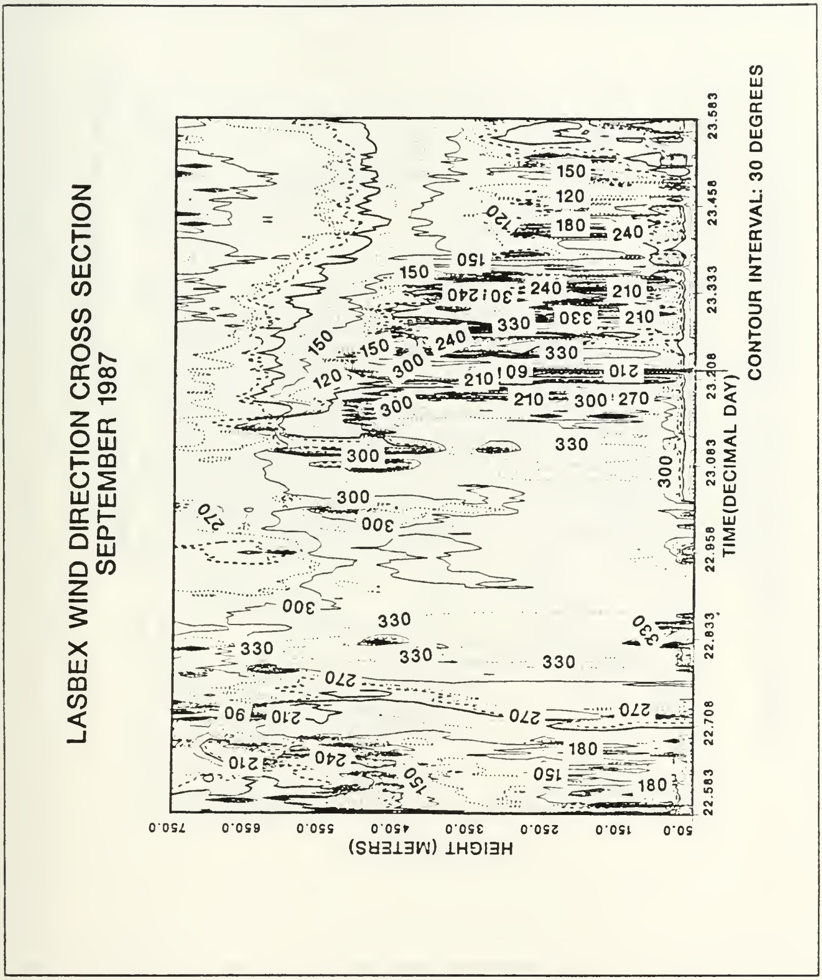

Fig. 70. 24-Hour Wind Direction Cross Section - 22 September 1987

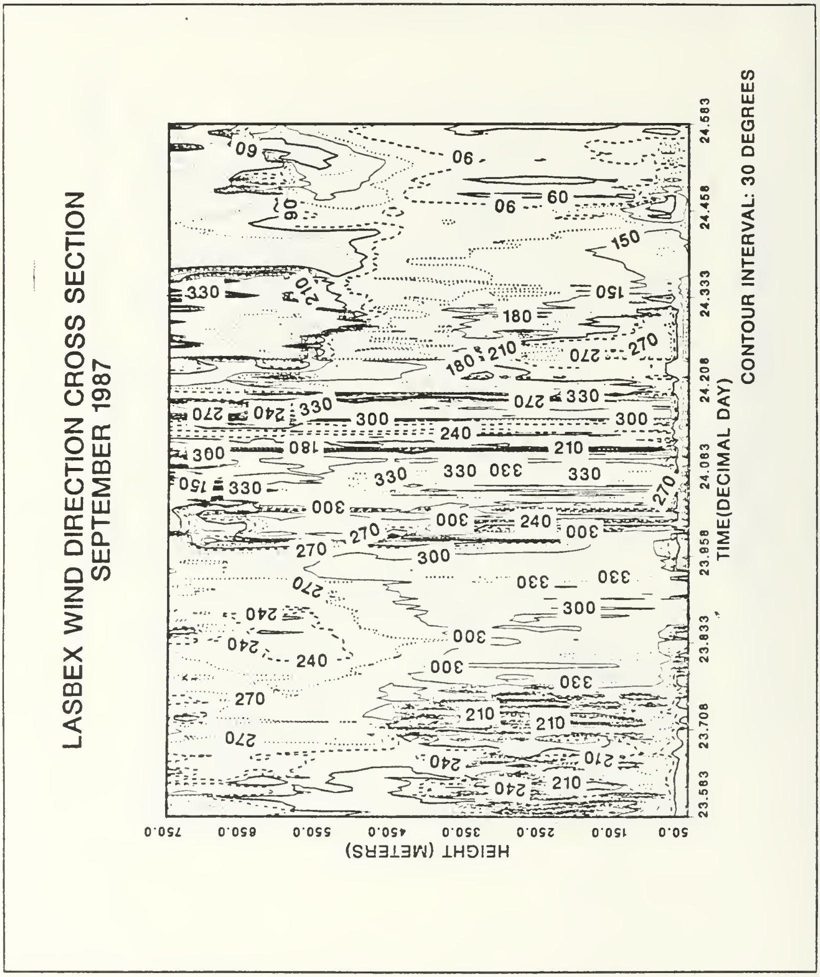

Fig. 71. 24-Hour Wind Direction Cross Section - 23 September 1987

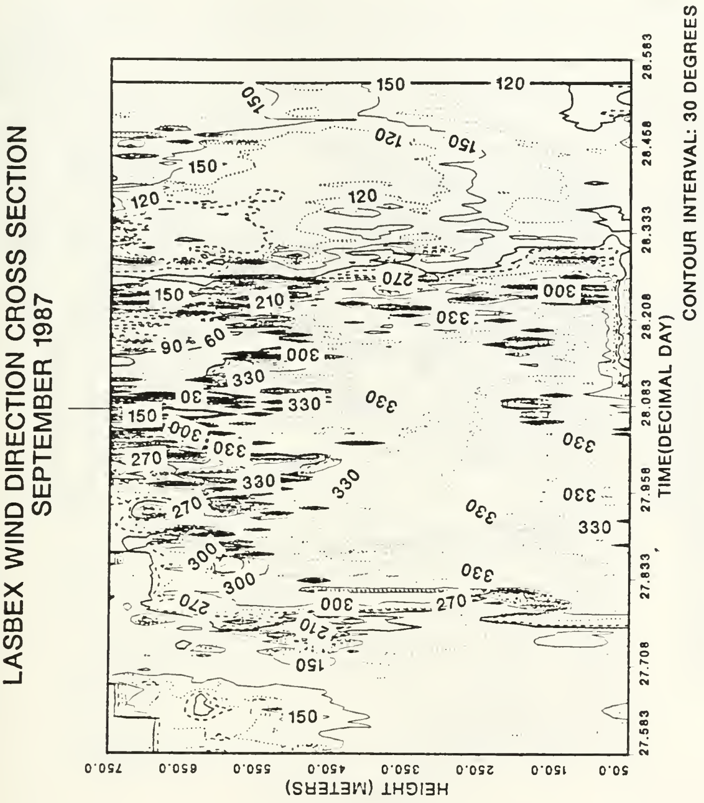

Fig. 72. 24-Hour Wind Direction Cross Section - 27 September 1987

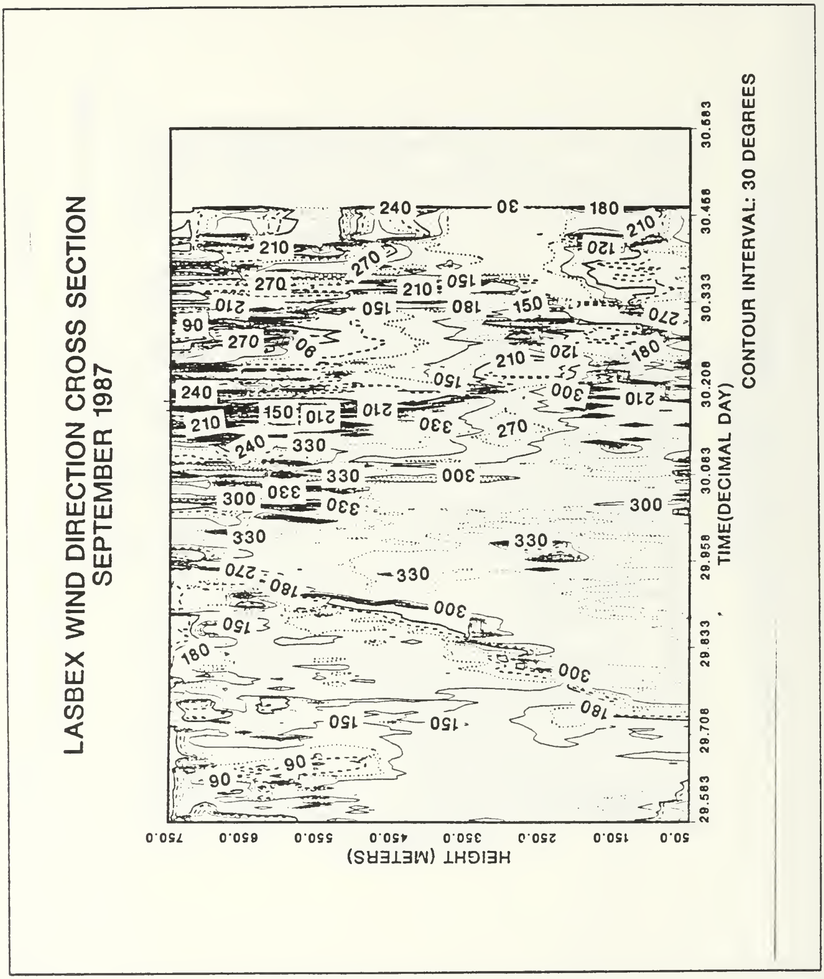

Fig. 73. 24-Hour Wind Direction Cross Section - 29 September 1987

APPENDIX F. 24-HOUR WIND SPEED CROSS SECTIONS

A. NOTES

The cross-section for 22 September 1987 was too noisy between 23.958 and 24.083 decimal day, where the speeds are greater than 10 m/s. Data in this region were considered unusable.

The cross-section for 23 September 1987 was too noisy between 23.958 and 24.208 decimal day. Data in this region were considered unusable.

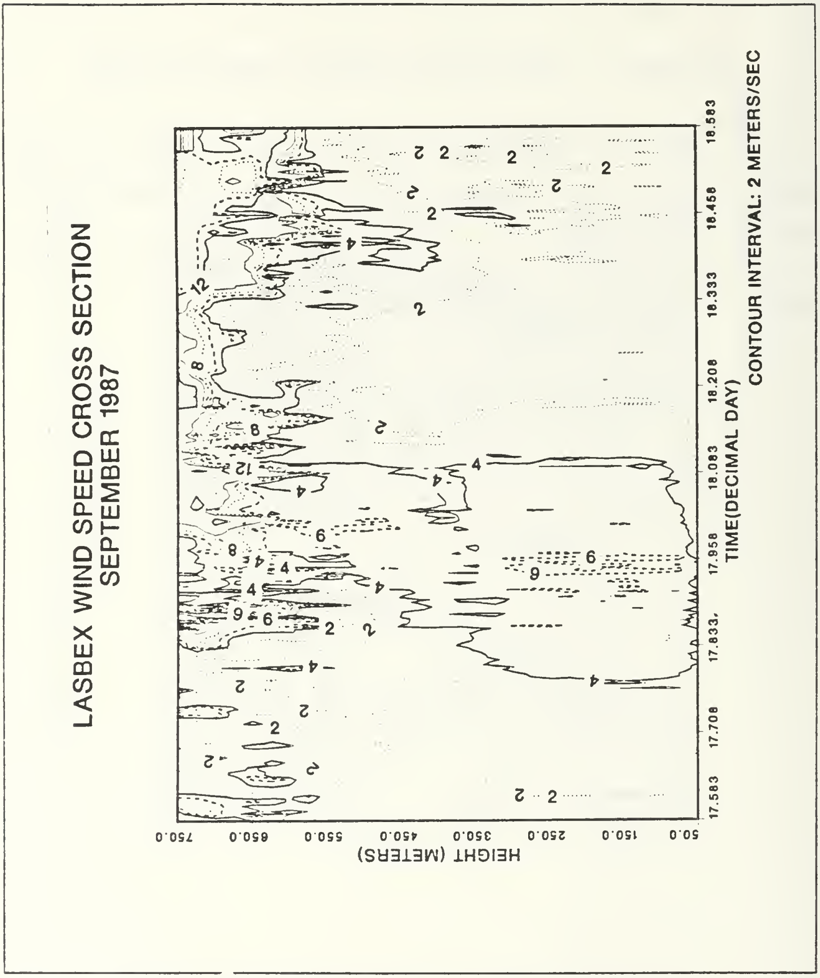

Fig. 74. 24-Hour Wind Speed Cross Section - 17 September 1987

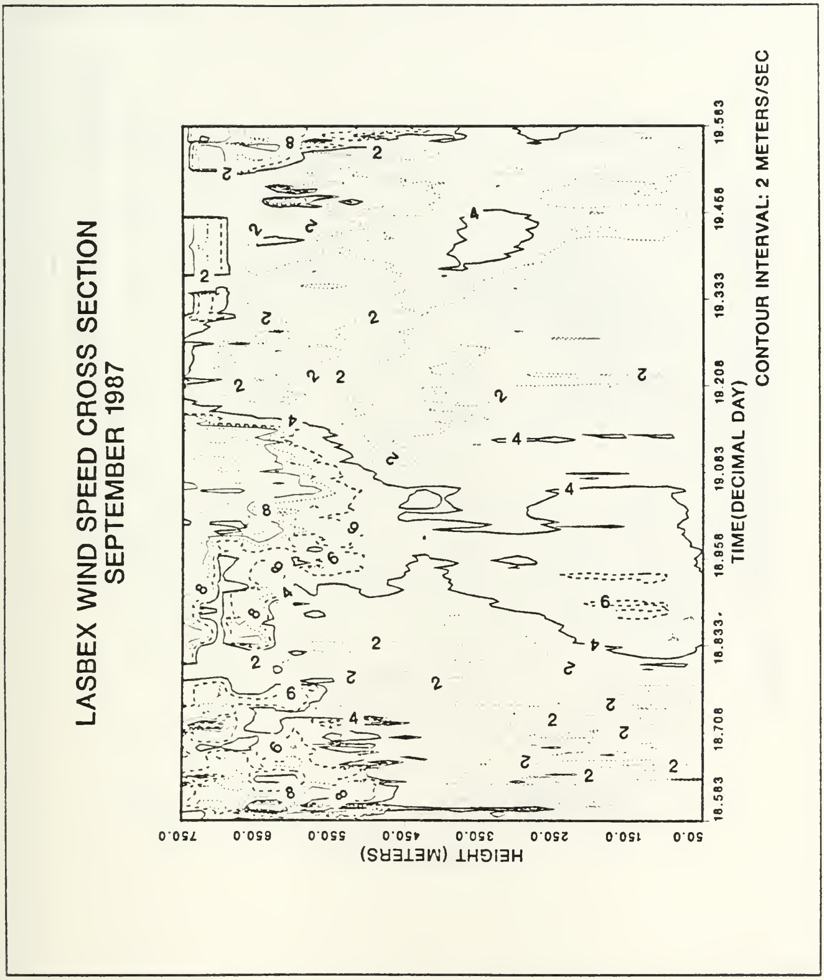

Fig. 75. 24-Hour Wind Speed Cross Section - 18 September 1987

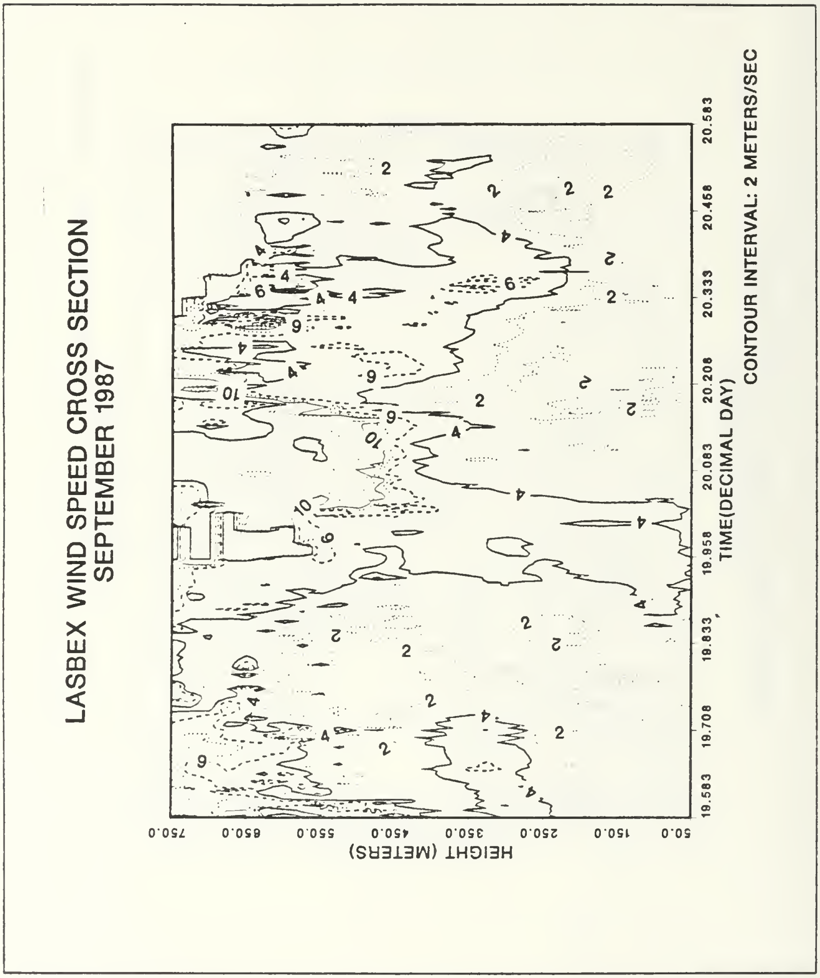

Fig. 76. 24-Hour Wind Speed Cross Section - 19 September 1987

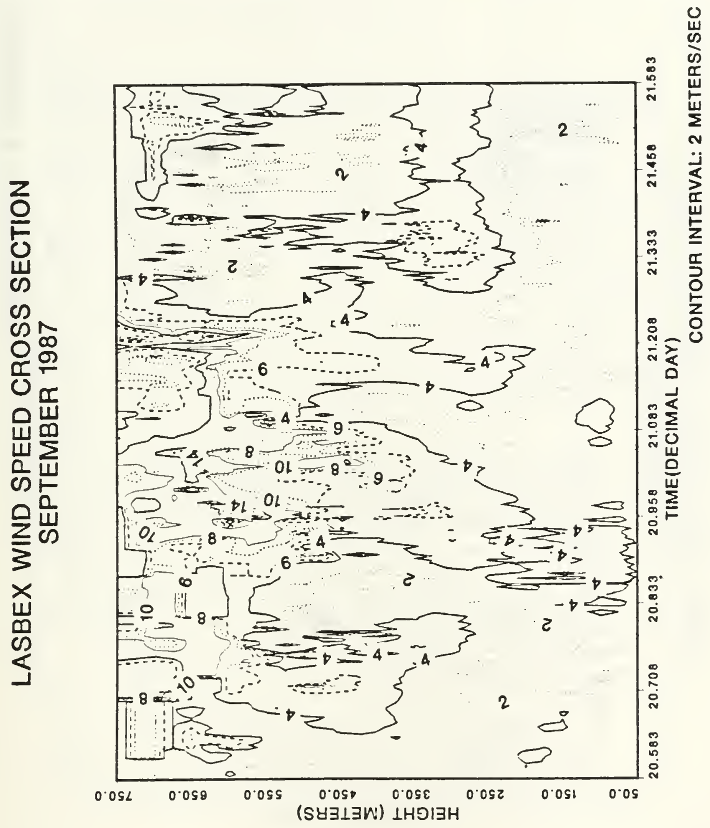

Fig. 77. 24-Hour Wind Speed Cross Section - 20 September 1987

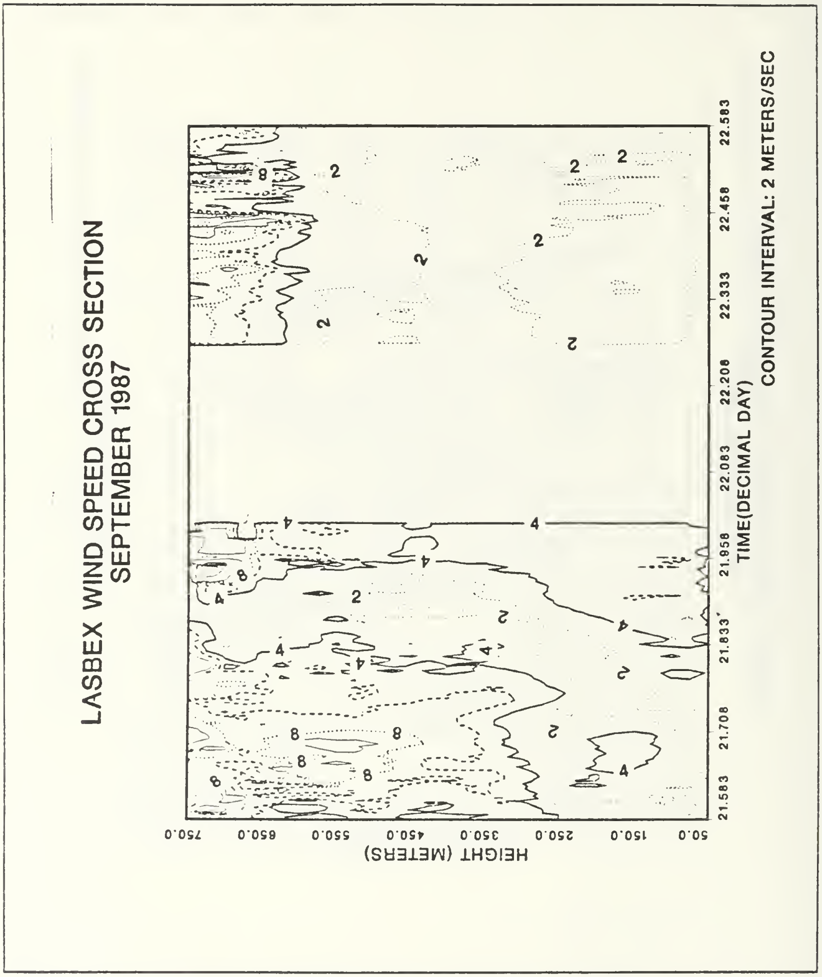

Fig. 78. 24-Hour Wind Speed Cross Section - 21 September 1987

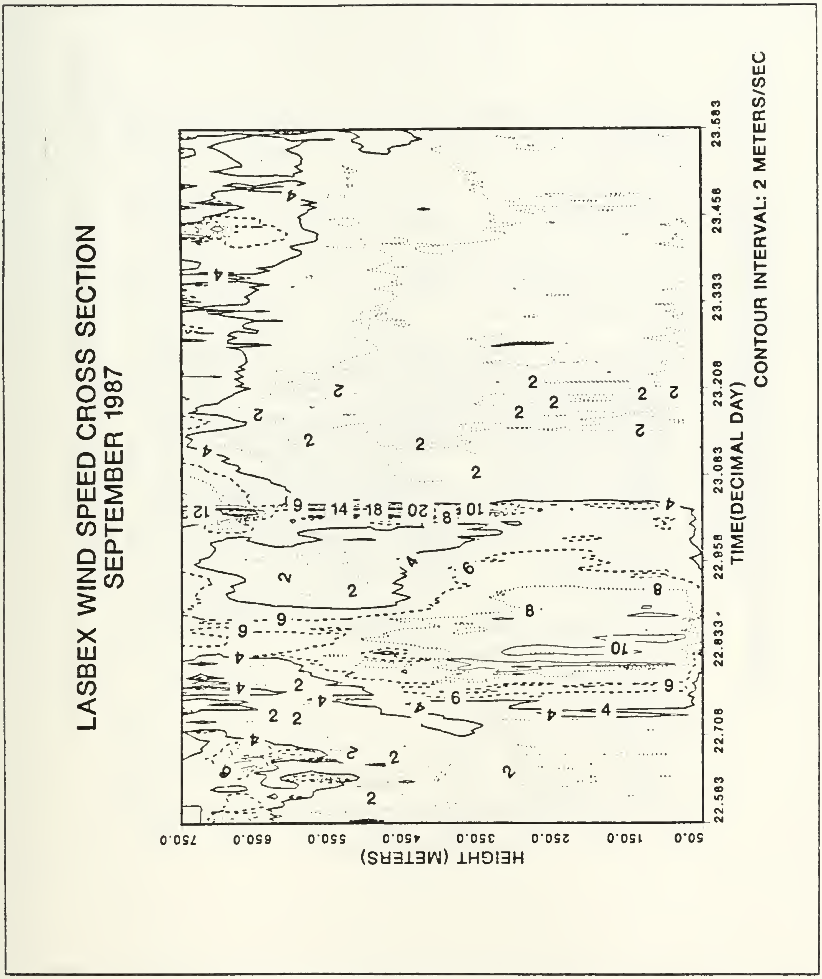

Fig. 79. 24-Hour Wind Speed Cross Section - 22 September 1987

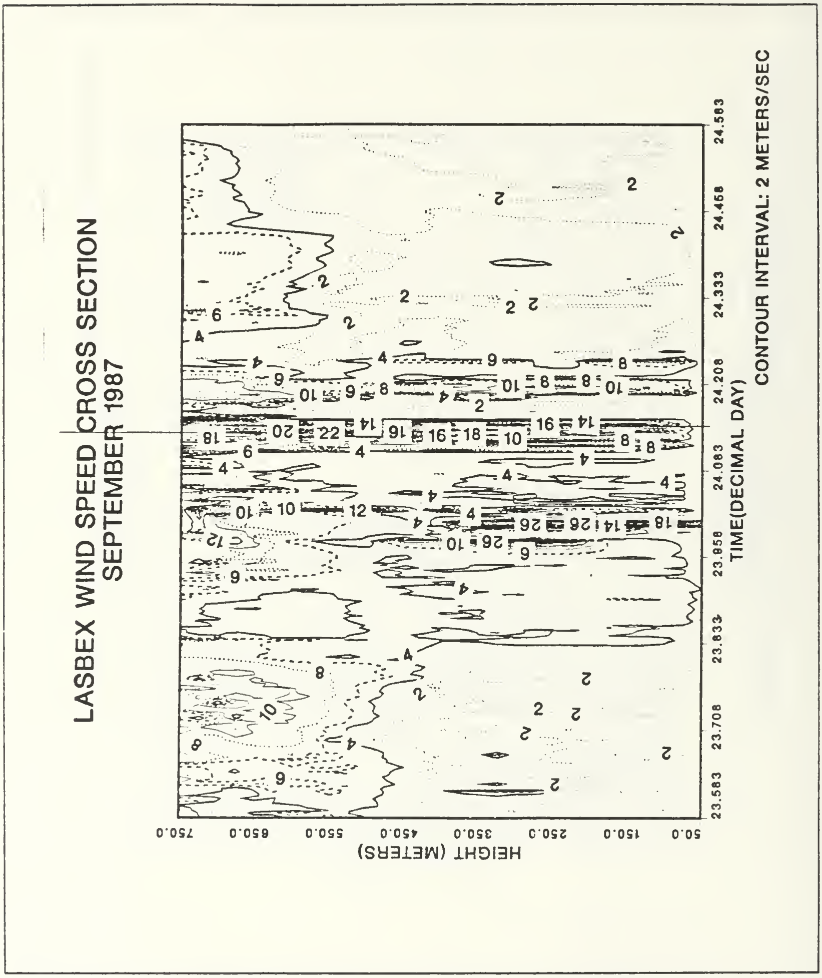

Fig. 80. 24-Hour Wind Speed Cross Section - 23 September 1987

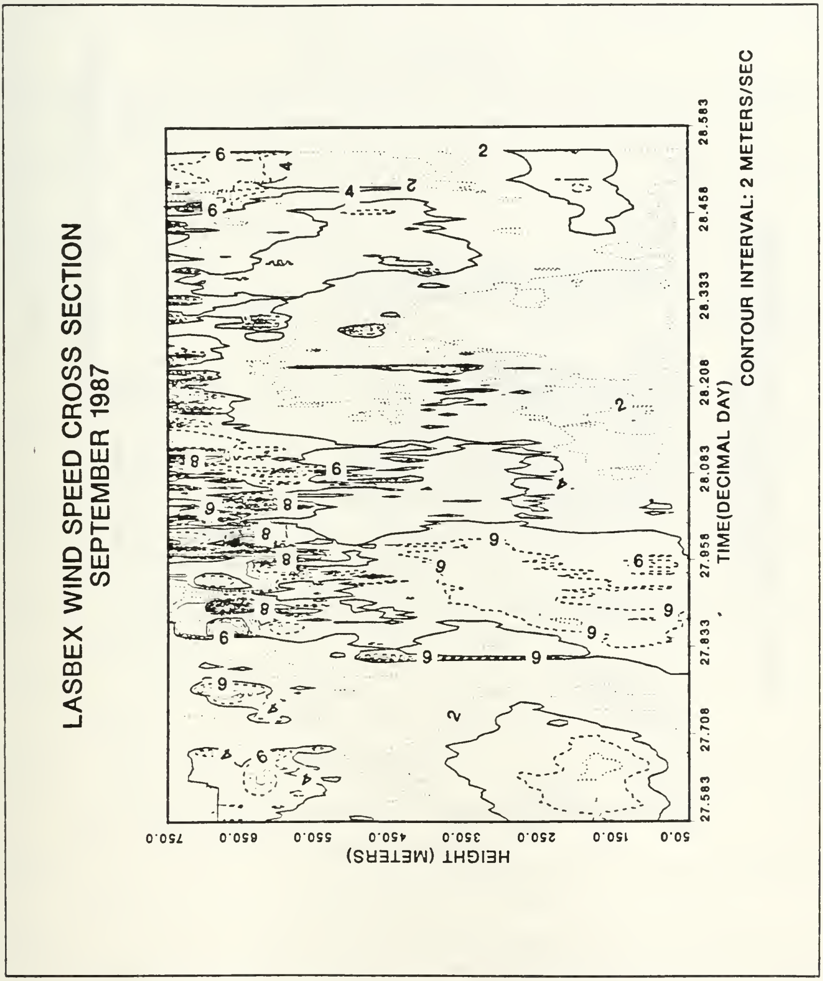

Fig. 81. 24-Hour Wind Speed Cross Section - 27 September 1987

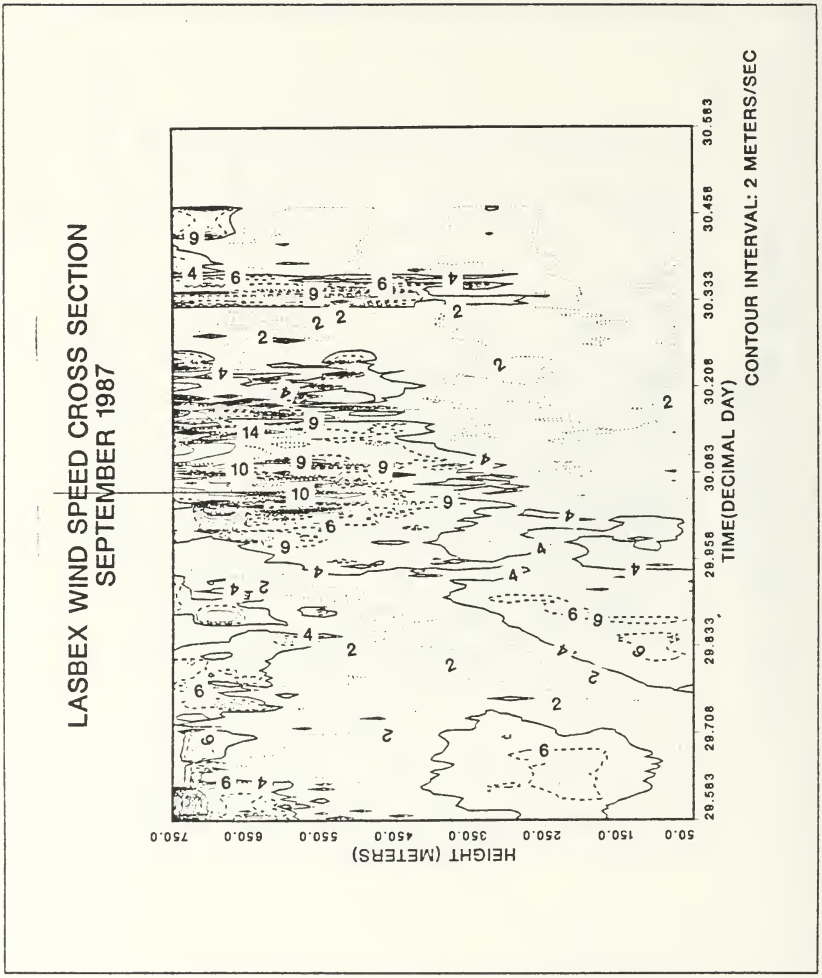

Fig. 82. 24-Hour Wind Speed Cross Section - 29 September 1987

LIST OF REFERENCES

Anthes, R.A., 1978: The height of the planetary boundary layer and the production of circulation in a sea breeze model. *J. Atmos. Sci.* **35**, 1231-1239.

Atkinson,B.W., 1981: *Mesoscale Atmospheric Circulations.* Academic Press, 495 pp. (see pp. 125-209)

Brown, E.H. and S.F. Clifford, 1976: On the attenuation of sound by turbulence. *J. Acoust. Soc. Amer.,* **60**, 788-794.

Caughey, S.J. and S.G. Palmer, 1979: Some aspects of turbulence structure through the depth of the convective boundary layer. *Quart. J. Roy. Meteor. Soc.,* **105**, 811-827.

Collis, R.T.H. and P.B. Russell, 1976: *Laser Monitoring of the Atmosphere.* ed. by E.D. Hinkley., Springer-Verlag, 380 pp. (see pp. 71-145)

Crease, B.A., S.J. Caughey and D.T. Tribble, 1977: Information on the Thermal Structure of the Atmospheric Boundary Layer. *Meteorological Magazine,* **106**, 42-52.

Defant, F., 1951: *Compendium of Meteorology.* Amer. Meteor. Soc., 658-672.

Estoque, M.A., 1962: The sea breeze as a function of the prevailing synoptic situation. *J. Atmos. Sci.,* **19**, 244-250.

Gaynor, J.E., 1977: Acoustic doppler measurement of atmospheric boundary layer velocity structure functions and energy dissipation rates. *J. Appl. Meteor.,* **16**, 148-155.

Helmis, C.G., D.N. Asimakopoulos, and D.G Deligiorgi, 1987: Observations of sea-breeze fronts near the shoreline. *Bound. Layer Meteor.,* **38**, 395-410.

John, J.I., 1980: A Sea Breeze front near Aberdeen, 7 July 1979. *Weather.,* **35**, 284-288.

Johnson Jr., A. and J.J. O'Brien, 1973: A study of an Oregon sea breeze event. *J. Appl. Meteor.,* **12**, 1267-1283.

Kaimal, J.C., J.C. Wyngaard, D.A. Haugen, O.R. Cote and Y. Izumi, 1976: Turbulence structure in the convective boundary layer. *J. Atmos. Sci.,* **33**, 2152-2169.

Kaimal, J.C. and D.A. Haugen, 1977: An acoustic doppler sounder for measuring wind profiles in the lower boundary layer. *J. Appl. Meteor.,* **16**, 1298-1305.

Keen, C.S. and W.A. Lyons, 1978: Lake Land breeze circulations on the western shore of Lake Michigan. *J. Appl. Meteor.,* **17**, 1843-1855.

Kitada, T., K. Igarashi and M. Owada, 1986: Numerical analysis of air pollution in combined field of land sea breeze and mountain/valley wind. *J. Clim. and Appl. Meteor.,* **25**, 767-784.

Kondo, H. and K. Gambo, 1979: The effect of the mixing layer on the sea breeze circulation and the diffusion of pollutants associated with land-sea breezes. *J. Meteor. Soc. Japan.,* **57**, 560-574.

Koracin, D. and R. Berkowicz, 1988: Nocturnal boundary-layer height: Observations by acoustic sounders and predictions in terms of surface-layer parameters. *Bound. Layer Meteor.,* **43,** 65-83.

Little, C.G., 1969: Acoustic methods for the remote probing of the lower atmosphere. *Proc. IEEE,* **57,** 571-578.

Lopez, R.E., 1977: Some properties of convective plume and small fair-weather cumulus fields as measured by acoustic and lidar sounders. *J. Appl. Meteor.,* **16,** 861-865.

Lyons, W.A., 1972: The climatology and prediction of the Chicago lake breeze. *J. Appl. Meteor.,* **11,** 1259-1270.

Lyons, W.A. and L.E. Olsson, 1973: Detailed Mesometerological studies of air pollution dispersion in the Chicage lake breeze. *Mon. Wea. Rev.,* **101,** 387-403.

Measures, R.M., 1984: *Laser Remote Sensing, Fundamentals and Applications.* John Wiley and Sons, Inc. 510 pp. (see pp. 281-413)

Mitsumoto, S., H. Ueda and H. Ozoe, 1983: A laboratory experiment on the dynamics of the land and sea breeze. *J. Atmos. Sci.,* **40,** 1228-1240.

Neff, W.D. and C.W King, 1988: Observations of complex terrain flows using acoustic sounders: Drainage flow structure and evolution. *Bound. Layer Meteor.,* **43,** 15-41.

Noonkester, V.R., D.R. Jensen, J.H. Richter, W. Viezee and R.T.H. Collis, 1974: Concurrent FM-CW radar and lidar observations of the boundary layer. *J. Appl. Meteor.,* **13,** 249-256.

Ogawa, Y., T. Ohara, S. Wakamatsu, P.G. Diosey and I. Uno, 1986: Observation of lake breeze penetration and subsequent development of the thermal internal boundary layer for the Nanticoke II shore-line diffusion experiment. *Boundary-Layer Meteor.,* **35**, 207-230.

Pearson, R.A., G. Carboni and G. Brusasca, 1983: The sea breeze with mean flow. *Quart. J. R. Met. Soc.,* **109,** 809-830.

Peterson, V.L., 1988: *The History, Principles, and Applications of Clear-Air Doppler Radar* Tycho Technology, Inc., Boulder, CO., 50 pp.

Pielke, R.A., 1974: A three-dimensional numerical model of the sea breeze over south Florida. *Mon. Wea. Rev.,* **102,** 115-139.

Piercy, J.E., T.F.W. Embleton, and L.C. Sutherland, 1977: Review of noise propagation in the atmosphere. *J. Acoust. Soc. Am.* **Vol. 61(6),** 1403-1418.

Richiardone, R. and R.A. Pearson, 1983: Inland convection and energy transfers in a sea breeze model. *Quart. J. Roy. Meteor. Soc.,* **109,** 325-338.

Russell, P.B., E.E. Uthe and F.L. Ludwig, and N.A. Shaw, 1974: A comparison of atmospheric structure as observed with monostatic acoustic sounder and lidar techniques. *J. Geophysical Research*, **79**, 5555-5566.

Simpson, J.E., D.A. Mansfield and J.R. Milford, 1977: Inland penetration of sea breeze fronts. *Quart. J. Roy. Meteor. Soc.*, **103**, 47-76.

Simpson, J.E. and R.E. Britter, 1980: A laboratory model of a atmospheric mesofront. *Quart. J. Roy. Meteor. Soc.*, **106**, 485-500.

Stunder, M. and S. Sethurman, 1985: A comparative evaluation of the coastal internal boundary layer equations. *Bound. Layer Meteor.*, **32**, 177-204.

Sutherland, L.C., 1975: Review of experimental data in support of a proposed new method for computing atmospheric absorption losses. *Rep. TST-75-87,* Dept. of Transportation, Washington, D.C.

Underwood, K.H., 1981: Sodar Signal Processing Methods and the Riso 78 Experiment. Ph.D. Thesis, Department of Meteorology, The Pennsylvania State University, University Station, PA. November 1981, 175 pp.

Walsh, J.E., 1974: Sea breeze theory and applications. *J. Atmos. Sci.*, **31**, 2012-2026.

Weseley, M.L., 1976: The combined effect of temperature and humidity fluctuations on refractive index. *J. Appl. Meteor.*, **15**, 43-49.

Wood, V.T. and R.A. Brown, 1983: Single Doppler velocity signatures: an atlas of patterns in clear air widespread precipitation and convective storms. *NOAA Tech. Memo.*, **ERL NSSL-95**, Environmental Research Laboratories (NTIS-#PB84-155779), 71 pp.

Wyckoff, R.J., D.W. Beran and F.F. Hall, Jr., 1973: A comparison of low-level radiosonde and the acoustic echo sounder for monitoring atmospheric stability. *J. Appl. Meteor.*, **12**, 1196-1204.

INITIAL DISTRIBUTION LIST

		No. Copies
1.	Defense Technical Information Center Cameron Station Alexandria, VA 22304-6145	2
2.	Library, Code 0142 Naval Postgraduate School Monterey, CA 93943-5002	2
3.	Chairman (Code 63Rd) Department of Meteorology Naval Postgraduate School Monterey, CA 93943-5000	1
4.	Chairman (Code 68Co) Department of Oceanography Naval Postgraduate School Monterey, CA 93943-5000	1
5.	Professor William J. Shaw (Code 63Sr) Department of Meteorology Naval Postgraduate School Monterey, CA 93943-5000	5
6.	Professor John W. Glendening (Code 63Gn) Department of Meteorology Naval Postgraduate School Monterey, CA 93943-5000	1
7.	Lt. Michael Fagan, USN USS Nimitz CVN-68 FPO Seattle, WA 98780	1
8.	Director Naval Oceanography Division Naval Observatory 34th and Massachusetts Avenue NW Washington, DC 20390	1
9.	Commander Naval Oceanography Command NSTL Station Bay St. Louis, MS 39522	1
10.	Commanding Officer Naval Oceanographic Office NSTL Station Bay St. Louis, MS 39522	1

11.	Commanding Officer Fleet Numerical Oceanography Center Monterey, CA 93943	1
12.	Commanding Officer Naval Environmental Prediction Research Facility Monterey, CA 93943-5006	1
13.	Chairman, Oceanography Department U. S. Naval Academy Annapolis, MD 21402	1
14.	Chief of Naval Research 800 North Quincy Street Arlington, VA 22217	1
15.	Office of Naval Research (Code 420) Naval Ocean Research and Development Activity 800 North Quincy Street Arlington, VA 22217	1
16.	Professor Dennis Thomson Department of Meteorology Pennsylvania State University University Station, PA 16802	1
17.	Professor Michael Hardesty NOAA Wave Propagation Laboratory 325 Broadway Boulder, CO 80303	1

Fagan

The sea breeze circulation during the Land Sea Breeze Experiment (LASBEX) in central California.